Spatial-temporal modelling of liver damage as well as regeneration and its influence on metabolic liver function

INAUGURAL–DISSERTATION

zur Erlangung des Grades eines

Dr. med. Vet.

beim Fachbereich Veterinärmedizin
der Justus-Liebig- Universität Gießen

Eingereicht von

Ahmed M. Ghallab

Aus dem Institut für Pharmakologie und Toxikologie
des Fachbereiches veterinärmedizin
der Justus-Liebig- Universität Gießen
Betreuer: Prof. Dr. Joachim Geyer

und

dem Leibniz-Institut für Arbeitsforschung an der TU Dortmund (IfADo)
Betreuer: Prof. Dr. med. Jan G. Hengstler

Spatial-temporal modelling of liver damage as well as regeneration and its influence on metabolic liver function

INAUGURAL–DISSERTATION
zur Erlangung des Grades eines

Dr. med. Vet.

beim Fachbereich Veterinärmedizin
der Justus-Liebig- Universität Gießen

Eingereicht von

Ahmed M. Ghallab
Tierarzt aus South Valley Universität
Qena, Ägypten

Gießen (2013)

Mit Genehmigung des Fachbereich Veterinärmedizin
der Justus-Liebig- Universität Gießen

Dekan: Prof. Dr. h.c. Martin Kramer

Gutachter:

Prof. Dr. Joachim Geyer

Prof. Dr. med. Jan G. Hengstler

Tag der Disputation: 10.04.2013

Table of contents

Abbreviations

ADP	Adenosine diphosphate
ALT	Alanine transaminase
AST	Aspartate transaminase
APC	Adenomatous polyposis coli
Arg1	Arginase1
ASL	Argininosuccinate lyase
ASS1	Argininosuccinate synthetase1
ATP	Adenosine 5-triphosphate
CPS1	Carbamoyl phosphate synthetase 1
d	Day
DAB	Diaminobenzidine
DEPC	Diethylpyrocarbonate
DMEM	Dulbecco´s Modified Eagle Medium
EDTA	Ethyline diamine tetra acetic acid
EGF	Epidermal growth factor
EGTA	Egtazic acid
FCS	Fetal calf serum
GDH	Glutamate dehydrogenase
GS	Glutamine synthetase
H&E	Hematoxylin and eosin
h/min/s	Hour/ minutes / seconds

HEPES	4-(2-Hydroxyethyl)piperazine-1-ethanesulfonic acid
HGF	Hepatocyte growth factor
kg/ g/ mg	Kilogram/ gram/ milligram
l/ ml/ µl	Liter/ milliliter/ micro liter
M/mM/µM	Mole/ millimole/ micromole
mm	Millimeter
OD	Optical density
PBS	Phosphate buffer saline
PDAC	2,6-Pyridinedicarboxylic acid
PFA	Paraformaldehyde
RNA	Ribonucleic acid
SD/SE	Standard deviation/ Standard error
TBS	Tris Buffered Saline
TGF-β	Transforming growth factor beta
U/l	Unit/liter
α-KG	Alpha-ketoglutarate

List of Figures

List of tables

1 Introduction

The liver is the central organ of metabolism. It serves as a filter against drugs and toxicants absorbed from the intestinal tract before passing to the systemic circulation (Michalopoulos and De Frances, 1997).

1.1 Architectures of the liver

1.1.1 External anatomy

Mouse liver weighs 1.3 -1.5 g forming approximately 5-6% of the total body weight. It occupies the cranial third of the abdominal cavity just caudal to the diaphragm and surrounded by a thin capsule (Glisson's capsule) (Piper and Suzanne, 2012). Similarly as for other mammals, the mouse liver is a multi-lobar organ. It consists of four lobes: the right, left, median and caudate lobe (Fig.1.1). The left lobe is the largest liver lobe in mice located at the peritoneal surface of the liver. However, the caudate lobe is small has two segments and located at the visceral surface of the liver. The right lobe is sub-divided horizontally into anterior and posterior portion. The median lobe has an incomplete fissure where the falciform ligament attaches. This fissure divides the median lobes into two segments where the gall is bladder located in between (Thoolen et al., 2010).

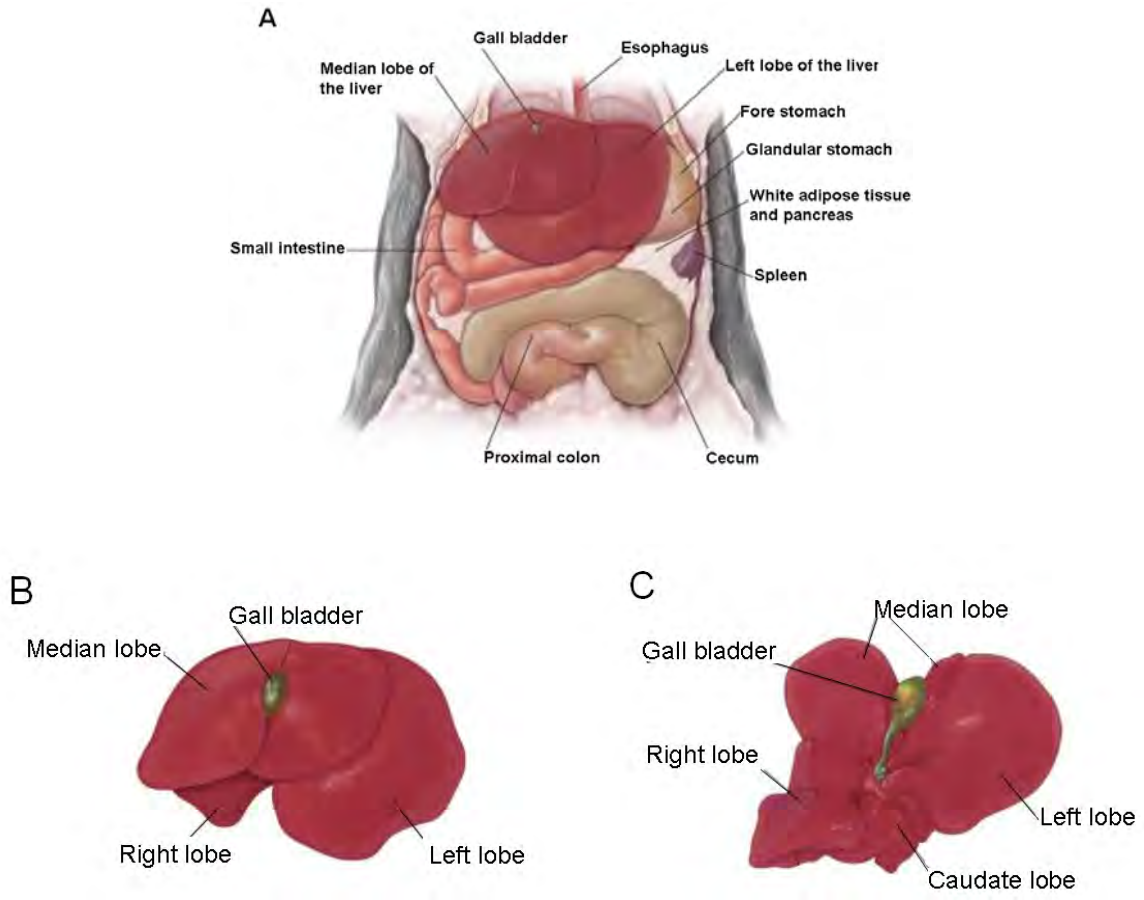

Fig. 1.1: Anatomy of the mouse liver. (A) The mouse liver is located just caudal to the diaphragm. It occupies the entire cranial third of the abdominal cavity. The mouse liver has four lobes: left, right, median and caudate. **(B)** The peritoneal surface of the mouse liver showing the left, right and median lobe. The gall bladder protrudes between the two segments of the median lobe. **(C)** The visceral surface of the mouse liver showing the caudate lobe in addition to the left, right, median lobes and the gall bladder (source: Elsevier Inc., WWW.Netterimages.com).

1.1.2 The hepatic vascular system

The liver receives its blood supply via two sources, the portal vein and the hepatic artery. The portal vein serves as a drainage system for the capillaries of the gastrointestinal tract, spleen and pancreas. It contributes with 75% of the total blood supply of the liver. However, the hepatic artery participates by the remaining 25% and supplies the liver with arterial blood. Both vessels enter the liver through the hilus where they branch to guide the blood to the periportal regions of the liver lobules. From there the blood flows through the hepatic

sinusoids and drains into the central vein at the center of the lobule (Fig. 1.2). The central veins collect into hepatic veins which leave the liver and drain into the inferior vena cava (Vollmer and Menger, 2009; Hoehme et al., 2010).

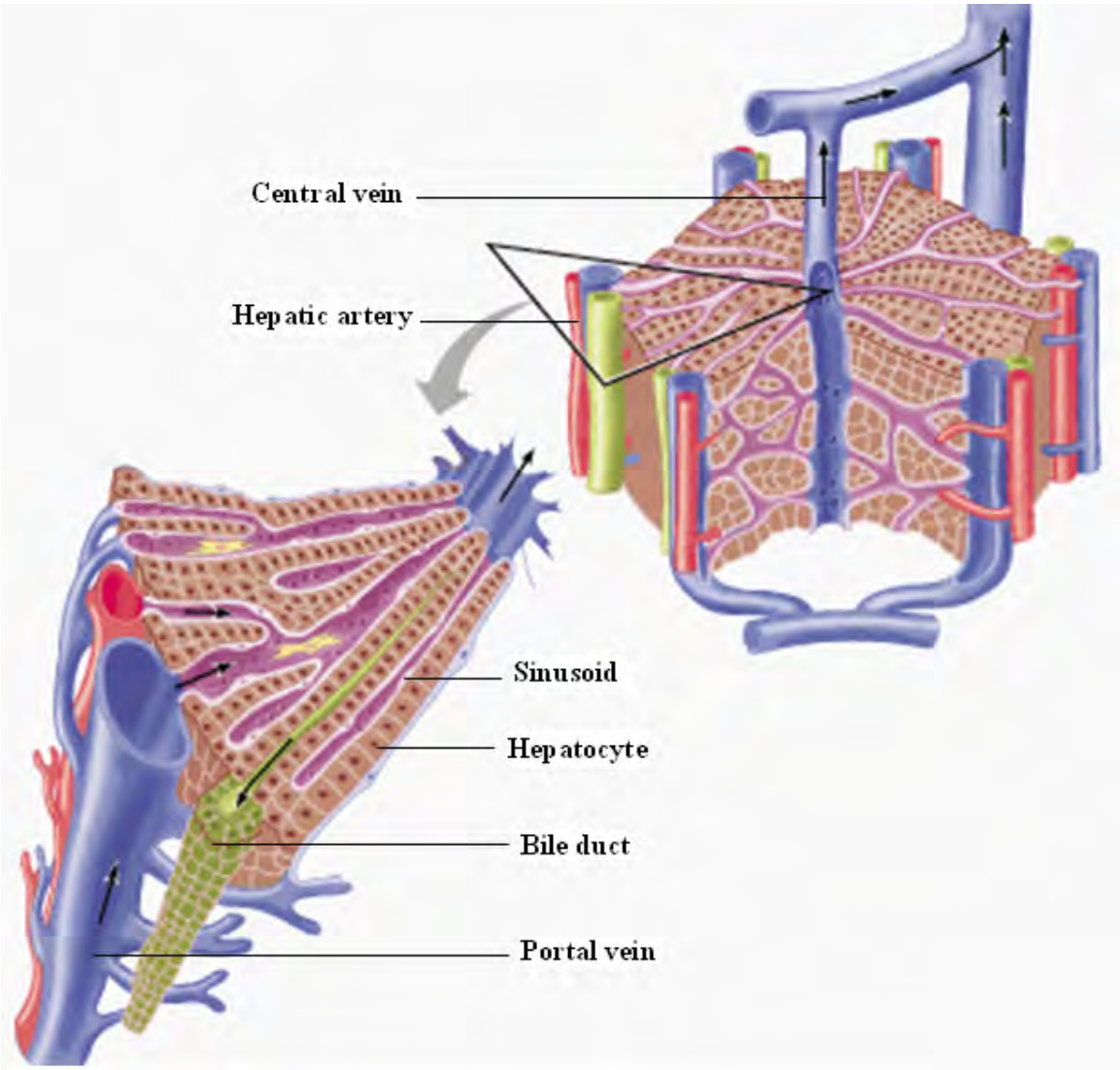

Fig. 1.2: The hepatic blood supply. Both the portal vein and the hepatic artery enter the liver at the hilus, the site where the bile duct leaves the liver (arrows). The blood flows through the hepatic sinusoids from the periportal to the pericentral region of the liver lobule. Then it drains into the central veins which collect into the liver vein. The liver veins finally drain into the caudal vena cava (Source: jw1.nwnu.edu.cn/jpkc/ jwc/2009jpkc/rtkx/jp.htm).

1.1.3 Cellular composition of the liver and heterogeneity along the porto-central axis of the liver lobule

The liver involves both parenchymal (hepatocytes) and non parenchymal cells. The integration of these cells allows the liver to fulfill a wide variety of functions (Saxena and Theise, 2004).

1.1.3.1 Hepatocytes

Hepatocytes (parenchymal cells) are polygonal epithelial cells. They are arranged in plate like cords separated by the adjacent sinusoids. They are the most predominant cell type of the liver, accounting for about 60-65% of the total cell number and about 80% of liver mass. The average diameter is 25-30µm. About 25% of hepatocytes are binucleated (Weibel et al., 1969; MacSween and Scothorne, 1994; Desmet, 2001). Hepatocytes are polarized epithelial cells having basal, apical and lateral surfaces. The basal surface faces the sinusoidal endothelium and has microvilli to increase the surface area for exchange of materials between hepatocytes and the blood. The apical surface faces the adjacent hepatocytes and forms the bile canaliculi. It has microvilli to increase the surface area for bile secretion (Cardell and Cardell, 1997). There is a small discrepancy between the periportal and pericentral hepatocytes regarding the cell volume. Drochmans et al. (1975) reported a difference ranging from 3800-4800µm^3 for periportal and perivenous hepatocytes, respectively.

1.1.3.2 Sinusoids

Hepatic sinusoids are unique micro-vascular structures. They are formed of fenestrated endothelial cells, macrophages (Kupffer cells), lymphocytes and stellate cells (table 1.1). Sinusoidal cells account for about 30-40% of the total cell number and approximately 6.3% of the liver mass (Bioulac-Sage et al., 1990).

1.1.3.2.1 Endothelial cells

Endothelial cells account for 15-20% of the total liver cells and 2.8% of liver volume (Kuntz and Kuntz, 2006). They are flat fenestrated cells lacking the basement membrane. They function as a filter that controls the exchange of materials between the blood and hepatocytes (Schuppan et al., 1998). The fenestrae of endothelial cells exhibit heterogeneity along the porto-central axis of the liver lobule. The fenestrae at the periportal area are larger in size, fewer in number and less porous in comparison to the pericentral area of the liver lobule (Wisse et al., 1985; Vidal-Vanaclocha and Barbera, 1985).

1.1.3.2.2 Kupffer cells

Kupffer cells constitute about 8-12% of the total liver cells and 2.1% of the liver volume. Although phagocytosis was reported to be higher in the pericentral area of the liver lobule, the number of Kupffer cells is higher in the periportal area (Bouwens et al., 1986; Lough et al., 1987; Te Koppele and Thurman, 1990).

1.1.3.2.3 Ito Cells

Ito cells are also known as fat-storing cells, hepatic stellate cells or lipocytes. They count about 3-8% of the total liver cells and 1.4% of the liver mass. They lie in the space of Disse with a higher frequency in the periportal area of the liver lobule. They function as storage for vitamin A. They are considered as a source of the hepatocyte growth factor (HGF) and the transforming growth factor beta (TGF-β) (Wake, 1974; Burt, 1999; Stockert and Wolkoff, 2001).

1.1.3.2.4 Liver-associated lymphocytes

Different types of liver associated lymphocytes have been described including granular lymphocytes (Pit cells). Pit cells are natural killer cells showing

a lower frequency compared to Kupffer cells. They play a role in defence against tumors and viruses (Nakatani et al., 2004).

Table 1.1: The cellular composition of the liver and the heterogeneity along the porto-central axis of the liver lobule (source: modified from Gebhardt, 1992b)

Cell type	Cell number (%)	Cell volume (%)	Lobular heterogeneity	
			Periportal	Pericentral
Hepatocytes	60-65	80	-	-
Endothelial cells	15-20	2.8	Larger in size	More porous, higher in number
Kupffer cells	8-12	2.1	Higher in number	More phagocytic activity
Ito cells	3-8	1.4	Higher in number	
Pit cells	<2	-	Not known	Not known

1.2 Metabolic zonation of the liver

1.2.1 Metabolic zones of the liver lobule

Metabolic zonation is a characteristic phenomenon for the site specific function of liver cells. Hepatocytes display different metabolic functions according to their position along the porto-central axis of the liver lobule. There are two well known metabolic zones in the liver lobule, the periportal and the pericentral zone (Fig. 1.3). The periportal zone (zone1) involves hepatocytes close to the hepatic blood inflow around the portal triad. The pericentral (perivenous zone, zone3) involves hepatocytes close to the central veins. In addition, there is a less-defined midlobular population of hepatocytes (zone2) (Jungermann and Kietzmann, 1996; Braeuning et al., 2006).

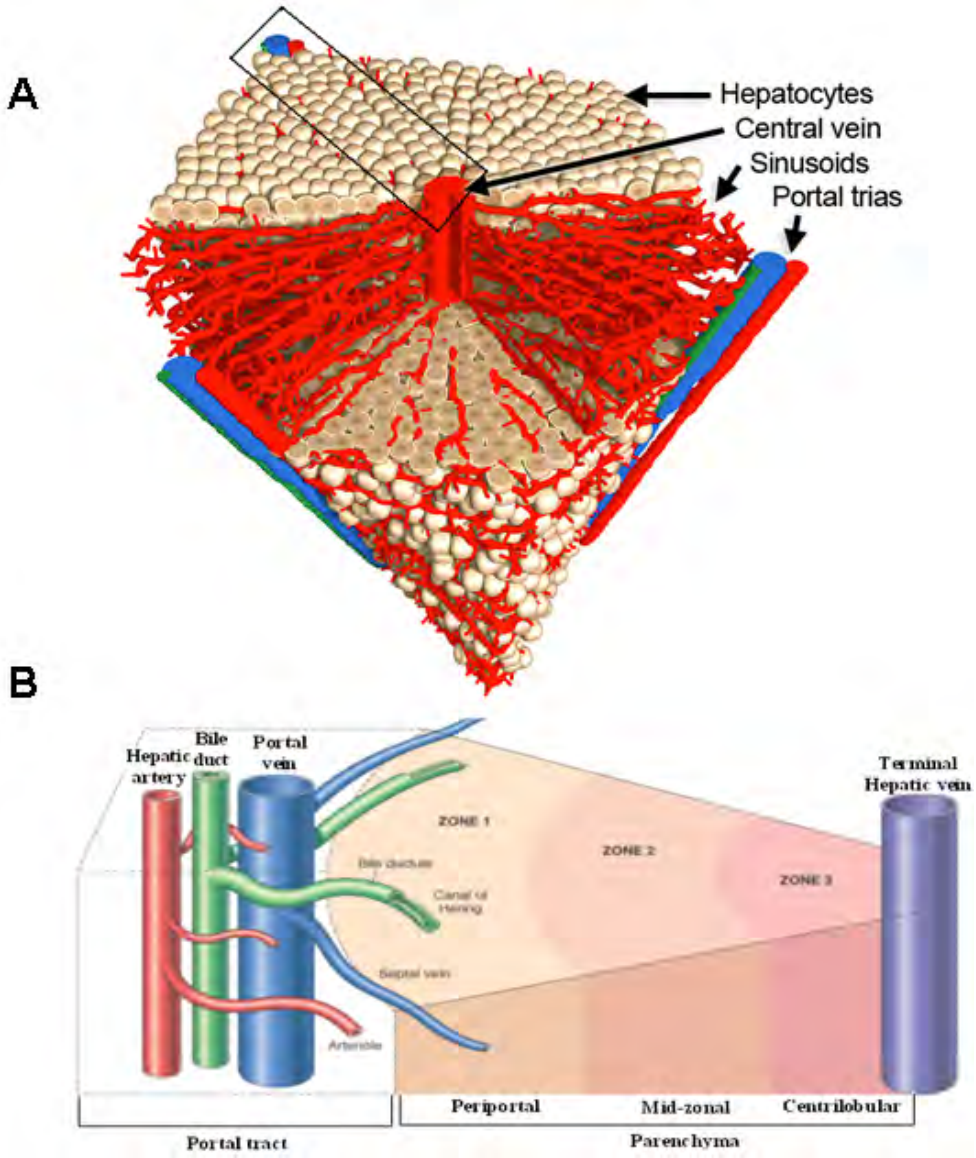

Fig.1.3: The structure and the metabolic zonation of the liver lobule. (A) Three dimensional structure of the liver lobule (source: Hoehme et al., 2010). The liver lobule is formed of a central vein surrounded by hepatocyte plates separated by sinusoids. At the portal area, a branch of the portal vein and the hepatic artery enter the liver lobule and a branch of the bile duct leaves. (B) Metabolic zonation of the liver lobule (source: www.Quizlet.com). Three metabolic zones can be defined in the liver lobule: (i) Zone 1, the periportal hepatocytes, involves hepatocytes surrounding the portal triad. (ii) Zone 3, the pericentral hepatocytes, involves hepatocytes surrounding the central vein. (iii) Zone 2, involves hepatocytes between zones 1 and 3.

1.2.2 Types of metabolic zonation of the liver

There are two types of metabolic zonation in the liver, the gradient and the compartment zonation. In the gradient type, there is a heterogeneous expression

of a certain metabolic process in all hepatocytes in a gradient manner. For example, the gluconeogenesis process shows a periportal to pericentral gradient of activity. In contrast, cholesterol7α-hydroxylase in lipid metabolism shows a pericentral to periportal gradient of activity. The most important feature of gradient zonation is the dynamic adaptation, i.e. if there is defect of the periportal hepatocytes the pericentral hepatocytes show a compensatory response and vise versa (Gebhardt and Gaunitz, 1997). In the compartment type of zonation a certain metabolic process is restricted to a certain region of the liver lobule without compensation even when the critical region is damaged (static). The best example for the compartment zonation is ammonia detoxification. Carbamoyl phosphate synthetase (CPS1), the rate limiting enzyme of the urea cycle, is only expressed in the periportal area of the liver lobule. In contrast, glutamine synthetase is restricted to 1-3 layers of the pericentral hepatocytes (Gebhardt, 1992b; Colnot and Perret, 2011).

1.2.3 Regulation of metabolic zonation of the liver

There are several hypotheses to explain the metabolic zonation in the liver:

1.2.3.1 The porto-central direction of the blood flow

The liver lobule receives its blood supply at the portal area through branches of the portal vein and the hepatic artery. The blood then flows through sinusoids and drains into the central vein. The concentration of substances, hormones and oxygen is usually highest at the periportal area of the liver lobule and decreases in a gradient manner towards the pericentral hepatocytes (Fig.1.4). Thus, according to the position of hepatocytes along the porto-central axis of the liver lobule, they are exposed to different microenvironments (Kietzmann and Jungermann, 1997). This model might explain the gradient type of zonation as in carbohydrate metabolism (Colnot and Perret, 2011).

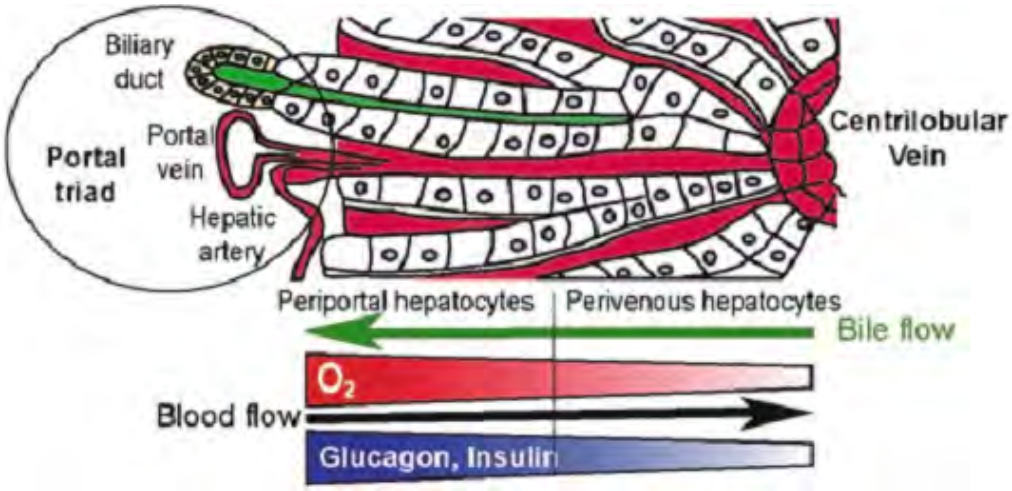

Fig. 1.4: The porto-central direction of the blood flow. The liver lobule receives its blood supply at the portal area through a branch of the portal vein and the hepatic artery. Then the blood flows through sinusoids (shown in red) and drains into the central vein. In contrast, the bile flows in the opposite direction (green) and leaves the liver lobule at the portal triad. The concentration of oxygen decreases in a gradient manner from the periportal to the pericentral hepatocytes (source: Colnot and Perret, 2011).

1.2.3.2 Cell-cell interaction

This phenomenon is very obvious in glutamine synthetase positive hepatocytes which are restricted to one to three layers of hepatocytes around the central vein. These hepatocytes need to be in contact with the central vein to express glutamine synthetase. This suggests that there is a cross talk between these hepatocytes and the endothelial cells lining the central vein (Kuo et al., 1991; Gebhardt, 1992a).

1.2.3.3 Transcriptional regulation

Wnt/β-catenin has been proven to be the master regulator of the genetic program and metabolic zonation of the liver. This comes after the discovery that glutamine synthetase is a direct target of β-catenin (Cadoret et al., 2002; Nicholes et al., 2002; Loeppen et al., 2002). Benhamouche et al. (2006) reported that there is complementary localization of the unphosphorylated β-catenin (the active form of β–catenin) in the perivenous hepatocytes and the adenomatous polyposis coli (APC) in periportal hepatocytes as a negative regulator. APC

knock out or over expression of β-catenin forces the perivenous genetic program throughout the whole liver. However, blocking the Wnt/ β-catenin pathway forces the periportal genetic program throughout the whole liver lobule (Fig.1.5)

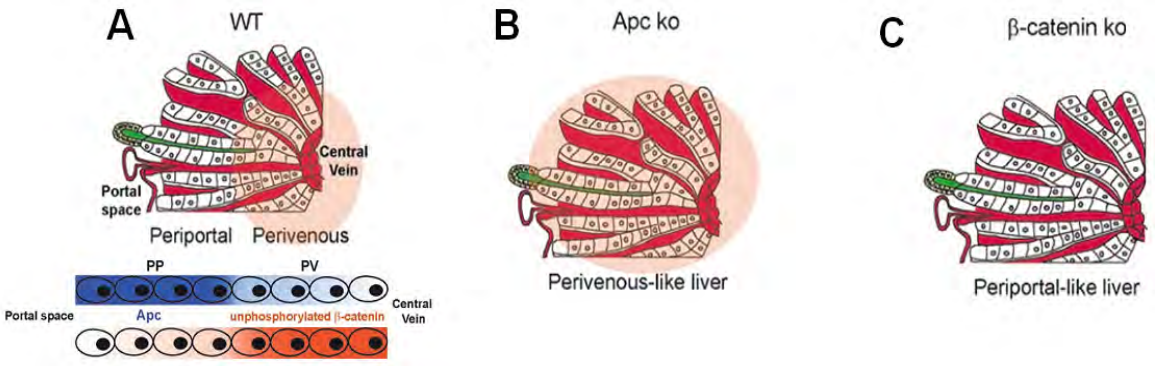

Fig. 1.5: Wnt/β-catenin is the master regulator of metabolic zonation of the liver. (A) there is a complementary distribution between the active β-catenin in the pericental hepatocytes (PC) and the adenomatous polyposis coli (APC) in periportal hepatocytes (PP). (B) Activation of β-catenin, mediated by APC knock out (APC ^{KO}) forces the pericentral genetic program throughout the whole liver lobule (perivenous like liver). (C) β-catenin knouck out (β-catenin ^{KO}) allows the expression of the periportal genetic program throughout the whole liver lobule (periportal like liver) (source: Benhamouche et al., 2006; Torre et al., 2011).

1.3 Metabolic function of the liver

The strategic position of the liver allows maintaining the metabolic homeostasis throughout the body. The liver receives absorbed substances from the intestinal tract via the portal vein and delivers metabolized harmless products to other body organs via the hepatic vein (Michalopoulos and De Frances, 1997; Michalopoulos, 2007).

1.3.1 Protein metabolism and ammonia detoxification

Ammonia metabolism is an obvious example for the compartment zonation of the liver. Ammonia is detoxified in the liver through the urea cycle and the glutamine synthetase reactions (Haussinger et al., 1992).

1.3.1.1 Sources of ammonia

About 40% of ammonia is generated by the intestine from nitrogenous substances by the action of bacterial ureases and amino acid oxidases. The remaining 60% is derived from the metabolism of glutamine and the transamination of the other amino acids (Lemberg and Fernandez, 2009). Within the liver, ammonia is generated through the glutaminase and trans-deamination reactions. Both occur in the periportal hepatocytes. Glutaminase degrades the circulating glutamine into ammonia and glutamate (Haussinger, 1983; Gebhardt et al., 1988). Transamination reactions help to collect the amino group from most of amino acids in the form of glutamate (Fig.1.7). Then the glutamate is deaminated by the action of the glutamate dehydrogenase to form ammonia and α-ketoglutarate (Christen and Metzler, 1985).

1.3.1.2 The role of the urea cycle in ammonia detoxification

The urea cycle is a high capacity low affinity system for ammonia detoxification. It is restricted to the periportal hepatocytes. It involves five enzymatic steps and ends with the production of urea (Fig.1.6). The urea cycle provides a permanent pathway for ammonia detoxification (Haussinger et al., 1992 and Rodés et al., 2007). Carbamoyl phosphate synthetase1 (CPS1), the enzyme which catalyzes the first step in the urea cycle, is considered to be the rate limiting enzyme for the urea cycle. CPS1 is expressed in approximately 93% of the liver parenchyma (Gaasbeek Janzen et al., 1984; Gebhardt, 1992b).

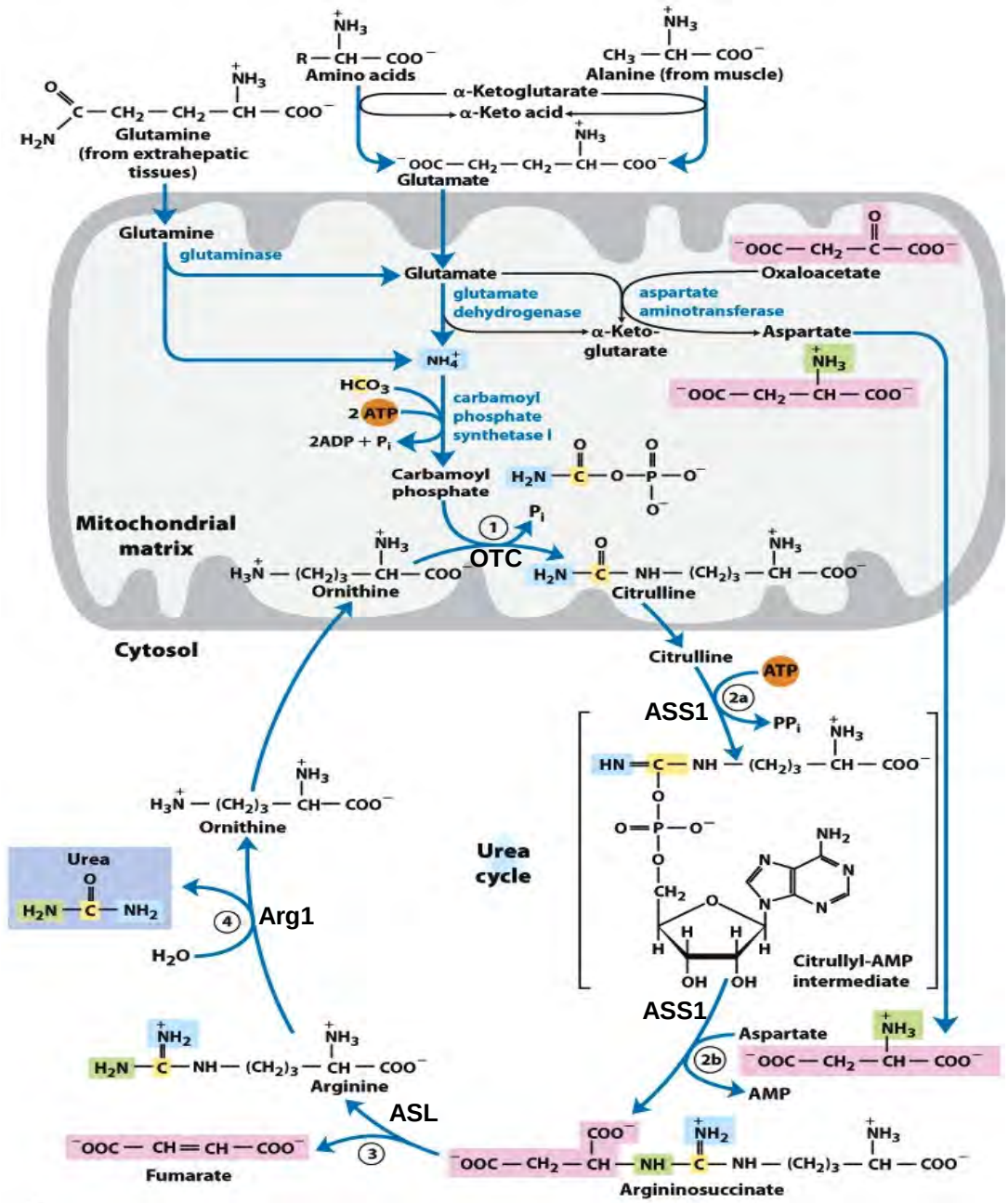

Fig. 1.6: Urea cycle and reactions that produce ammonia. There are two sources of ammonia in the periportal hepatocytes: (i) the glutaminase enzyme which degrades glutamine into ammonia and glutamate and (ii) the glutamate dehydrogenase enzyme which catalyzes the oxidative deamination of glutamate into ammonia and α-ketoglutarate. Ammonia is then passed to the urea cycle. The urea cycle involves five enzymatic steps: (i) carbamoyl phosphate synthetase 1 (CPS1) which catalyzes the formation of carbamoyl phosphate from ammonia and bicarbonate. (ii) Ornithine transcarbamoylase (OTC) catalyzes the formation of citrulline from ornithine and carbamoyl phosphate. Both CPS1 and OTC reaction occur in the mitochondria whereas, the subsequent three reactions occur in the cytoplasm. (iii) Argininosuccinate synthetase1 (ASS1) catalyzes the formation of agininosuccinate from citrulline and aspartate. (iv) Argininosuccinate lyase (ASL) degrades the agininosuccinate into arginine and fumarate. (v) Arginase1 (Arg1) forms urea and ornithine from arginine (Source: Lehninger Principles of Biochemistry, 2008).

1.3.1.3 The role of glutamine synthetase in ammonia detoxification

Glutamine synthetase (GS) is a low capacity high affinity system for ammonia detoxification. It temporarily detoxifies ammonia in the form of glutamine (Häussinger and Gerok, 1983). GS is restricted to the pericentral hepatocytes occupying approximately 7% of the liver parenchyma (Gebhardt et al., 2007). The anatomical localization of GS after the urea cycle allows it to act as a scavenger for ammonia that escapes the urea cycle (Häussinger, 1990).

1.3.2 Carbohydrate metabolism

The liver shows a zonated glucose metabolism. The gluconeogenesis process is mostly periportal, whereas the glycolysis process is mostly pericentral. Enzymes that are involved in gluconeogenic reactions, such as glucose-6-phosphatase, fructose-1,6-biphosphatase and phosphoenolpyruvate carboxykinase predominate in the periportal area. In contrast, enzymes that are involved in glycolysis reactions such as glucokinase and pyruvate kinase are higher expressed in the pericentral area of the liver lobule (Katz et al., 1977). In contrast to proteins, carbohydrate metabolism is a gradient type of zonation. To maintain the homeostasis of the blood glucose level, adaptation changes can happen according to the nutritional status. During starvation, the liver adapts by expansion of the gluconeogenetic region on the expense of the glycolytic area and vise versa (Jungermann, 1986; Gebhardt, 1992b).

1.3.3 Metabolism of drugs and xenobiotics

The liver is an effective barrier preventing toxicants from passing to the systemic circulation. Drugs and xenobiotics are converted in the liver to an easily excreted compound through two phases: (I) Phase I, in which a basic structural alteration happens in the drug molecule either by oxidation, reduction or hydrolysis. (II) Phase II, in which a water soluble moiety is attached to the drug molecule through a process termed conjugation (Williams et al., 2003). Phase I is catalyzed by cytochrome P450 enzymes. Whereas, the conjugation reactions

(phase II) are catalyzed either by glutathione S-transferases, sulphotransferases, N-acetyltransferases or UDP-glucuronoyl transferases (Park et al., 2005; Parkinson and Ogilvie, 2008). The metabolism of drugs and xenobiotics also shows a well-defined zonation, occurring mostly in the pericentral hepatocytes (Colnot and Perret, 2011). CYP2E1 and CYP1A2, which are important drug metabolizing enzymes, show a restricted pericentral zonation (Apte et al., 2009; Torre et al., 2011). In phase II, glucuronidation occurs in the pericentral hepatocytes. Incontrast, sulfation is predominant in the periportal hepatocytes (Jungermann and Kietzmann, 1996).

1.3.4 Lipid metabolism

The liver is also the center of lipid metabolism including lipogenesis, β-oxidation, ketogenesis, cholesterol biosynthesis and lipoprotein metabolism. The zonation of lipid metabolism is not clear in liver (Jungermann and Katz, 1989).

1.3.5 Bile formation and secretion

The metabolism of bile acids, bilirubin and glutathione displays a well defined zonation. Cholesterol 7α-hydroxylase, involved in bile acid synthesis, is highly expressed in the pericentral hepatocytes (Ugele et al, 1991). UDP-glucuronyl transferase, the enzyme responsible for the conjugation of bilirubin to glucuronic acid, shows predominantly a pericentral activity (Ullrich et al., 1984). Glutathione-S-transferases and glutathione peroxidases catalyze the antioxidant reactions of glutathione. Glutathione-S-transferases display predominantly a pericentral activity. In contrast, glutathione peroxidases display predominantly a periportal activity (Kera et al., 1987).

1.4 Liver damage and regeneration

1.4.1 Selective zonal necrosis of the liver lobule by CCl_4

Carbon tetrachloride (CCl_4) is one of the hepatotoxic agents which require metabolic activation in the liver. The major drug metabolizing enzyme of CCl_4 is

cytochrome P4502E1 (CYP2E1) (Gruebele et al., 1996). CCl_4 is metabolized by CYP2E1 to the trichloromethyl (CCl_3*) radical (Fig.1.7) (Slater, 1966). In presence of oxygen, the CCl_3* radical is further metabolized to trichloromethyl peroxy (CCl_3OO*) radical (Connor et al., 1986; Lutz et al., 2003). These free radicals can react with polyunsaturated fatty acids of the membrane of hepatocytes leading to lipid peroxidation and consequently cell necrosis (Recknagel and Glende, 1973; Recknagel et al., 1989). CCl_4 intoxication selectively kills the pericentral hepatocytes. This is due to the restricted zonation of CYP2E1 to the pericentral region of the liver lobule which corresponds for approximately 40% of the entire liver mass (Hoehme et al., 2007; 2010).

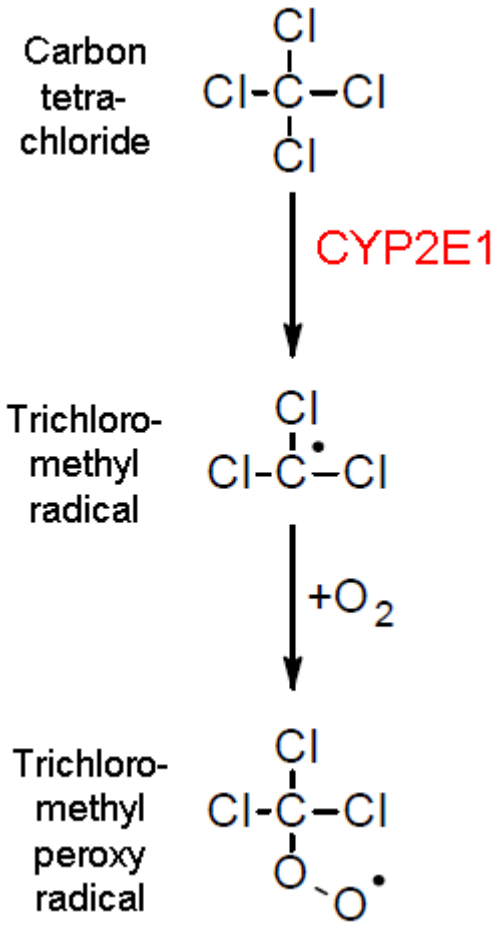

Fig. 1.7: Metabolic activation of carbon tetrachloride (CCl_4). CCl_4 is metabolized by cytochrome P450 2E1 (CYP2E1) to the trichloromethyl radical (CCl_3*). In the presence of oxygen, the CCl_3* radical is further metabolized to the trichloromethyl peroxy radical (CCl_3OO*).

1.4.2 Liver regeneration

Due to critical functions of the liver, particularly the metabolic homeostasis, a rapid well-orchestrated regeneration process is essential after liver injury (Taub, 2004; Michalopoulos and DeFrances, 2005). Normally the adult liver represents a non proliferating organ. The proliferation rate of hepatocytes is less than 1% in normal liver (Fausto and webber, 1994; Taub, 2004). In contrast, the liver has the capacity to fully regenerate after loss of its mass (Michalopoulos and DeFrances, 1997; Taub, 2004; Michalopoulos, 2007). The regenerative response of the liver differs according to the type of injury and the duration of exposure. A single injection of 1.6 g/kg CCl_4 leads to selective pericentral damage of the liver lobule. In this case, the periportal hepatocytes proliferate and the dead cell area is fully restored within six days in mice (Hoehme et al., 2007; 2010). However, after chronic exposure to CCl_4 the liver regenerates with scar formation leading to liver cirrhosis (Michalopoulos and DeFrances, 2005). In contrast to the selective zonal necrosis of the liver lobule induced by CCl_4, whole liver lobes are removed in case of partial hepatectomy. In this model of liver regeneration three lobes of the liver are surgically removed (70% of the liver mass). Under these conditions, the remaining liver lobes increase in size to restore the original liver mass within five to seven days (Higgins and Anderson, 1931; Michalopoulos and DeFrances, 2005). At the cellular level all hepatic cells cooperate after liver injury to restore the lost tissue (Fig.1.8). After liver injury some endotoxins like lipopolysaccharide (LPS) travel to the liver through the portal vein (Taub, 2004; Michalopoulos and DeFrances, 2005). This stimulates the production of cytokines, like tumor necrosis factor alpha (TNF-α) and interleukin 6 (IL6) from stellate and Kupffer cells. These cytokines activate downstream signals which guide hepatocytes to pass the restriction point at the G1-phase of the cell cycle. Various growth factors, especially HGF, EGF and TGF-α, then allow the progression of hepatocytes through the cell cycle (Michalopoulos and DeFrances, 1997; Taub, 2004; Fausto et al., 2006, Bohm et al., 2010). Liver regeneration is controlled by the liver size. Once the liver

reaches the appropriate liver body weight ratio, termination of liver regeneration occurs (Michalopoulos and De Frances, 1997). The transforming growth factor beta (TGF-β) is the main terminator of liver regeneration (Campbell et al., 2001; Taub, 2004).

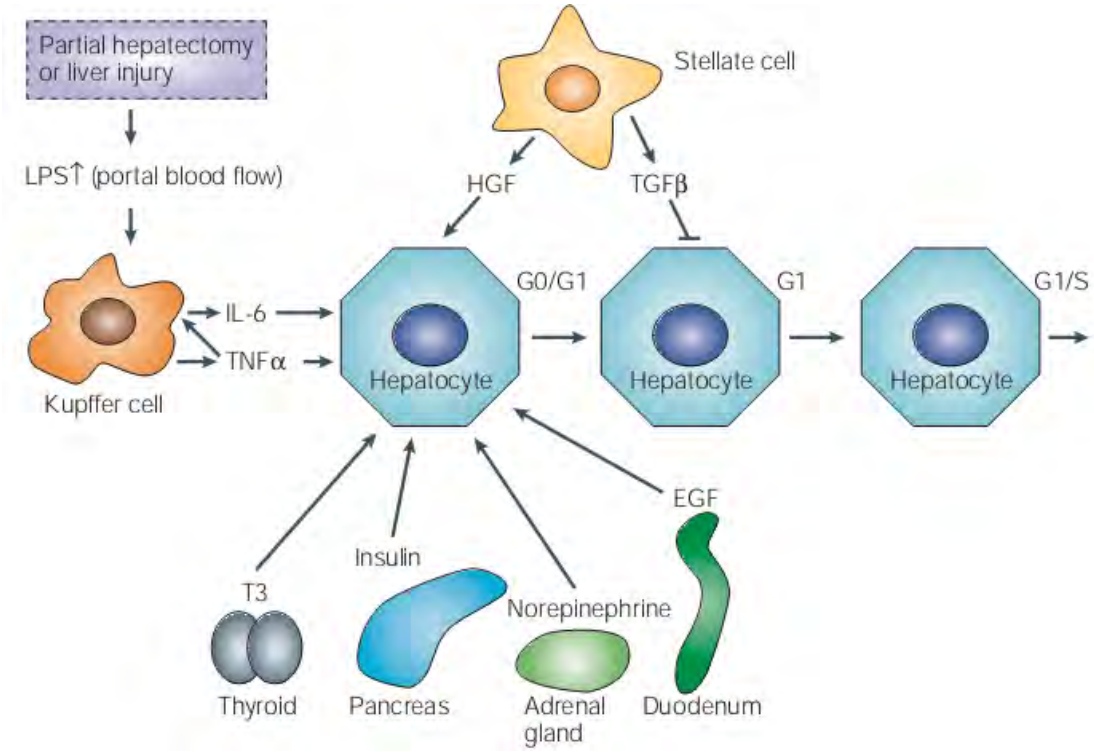

Fig. 1.8: Control of liver regeneration after injury. Liver regeneration is controlled by various cytokines and growth factors. (i) The role of cytokines: after liver injury, the gut derived lipopolysaccharides (LPS) are up regulated and reach the liver through the portal vein. This stimulates the production of the tumor necrosis factor alpha (TNF-α) and interleukin 6 (IL6) from stellate and Kupffer cells. These cytokines stimulate hepatocytes to pass the restriction point at the G1-phase of the cell cycle. (ii) The role of growth factors: after passing the restriction point, cooperative signals from intra hepatic and extra hepatic tissues allow the progression of hepatocytes through the cell cycle. These include insulin from the pancreas, epidermal growth factor (EGF) from the duodenum or salivary glands, nor epinephrine from the adrenal gland, triodothronine (T3) from the thyroid gland and the hepatocyte growth factor (HGF) from stellate cells. The transforming growth factor beta (TGF-β) terminates the regeneration process when the liver reaches the normal size (source: Taub, 2004).

1.5 Aim of the work

The most vital function of the liver is the maintenance of the metabolic homeostasis throughout the body. Although extensive studies on the field of liver regeneration are available, little is known about how the complex metabolic function of the liver is restored after liver injury. The aim of this study is to model the metabolic alterations during liver damage and regeneration after CCl_4 intoxication. The main goals are to

- study the alteration of the metabolic function of the liver after CCl_4 intoxication
- model ammonia detoxification during liver damage and regeneration
- study the alteration of metabolic zonation during liver damage and regeneration
- identify the possible compensatory mechanisms for ammonia detoxification during liver damage and regeneration

2 Materials and methods

2.1 Materials

2.1.1 Chemicals

Acetic acid	Carl Roth, Karlsruhe, Germany
Adenosine diphosphate	Sigma-Aldrich Corp., St. Louis, MO, USA
Adenosine 5-triphosphate disodium salt solution	Sigma-Aldrich Corp., St. Louis, MO, USA
Albumin	Carl Roth, Karlsruhe, Germany
Alpha-ketoglutaric acid	Sigma-Aldrich Corp., St. Louis, MO, USA
3,3′-Amino-9-ethylcarbazole	Sigma-Aldrich Corp., St. Louis, MO, USA
Aminotriazole	Sigma-Aldrich Corp., St. Louis, MO, USA
Ammonium chloride	Carl Roth, Karlsruhe, Germany
2, 3-Butanedione monoxime	Sigma-Aldrich Corp., St. Louis, MO, USA
Calcium chloride	Sigma-Aldrich Corp., St. Louis, MO, USA
Carbon tetrachloride	Carl Roth, Karlsruhe, Germany
Citric acid monohydrate	Carl Roth, Karlsruhe, Germany
L-Citrulline	Sigma-Aldrich Corp., St. Louis, MO, USA
Collagenase	Sigma-Aldrich Corp., St. Louis, MO, USA
Collagen (rat tail)	Roche diagnostics GmbH, Manheim, Germany
Dexamethason	Sigma-Aldrich Corp., St. Louis, MO, USA
Diaminobenzidine	Sigma-Aldrich Corp., St. Louis, MO, USA
Disodium hydrogen phosphate	Applichem GmbH, Darmstadt, Germany

Dulbecco´s Modified Eagle Medium (DMEM)	PAN Biotech GmbH, Aidenbach, Germany
N,N-Dimethylformamide	Sigma-Aldrich Corp., St. Louis, MO, USA
Eosin Y disodium salt	Sigma-Aldrich Corp., St. Louis, MO, USA
Entellan	Merk, Darmstadt, Germany
Ethanol, absolute	Carl Roth, Karlsruhe, Germany
Ethyline diamine tetra acetic acid disodium salt	Sigma-Aldrich Corp., St. Louis, MO, USA
EGTA	Sigma-Aldrich Corp., St. Louis, MO, USA
Fetal calf serum	Biochrom AG, Berlin, Germany
Gentamycin	Invitrogen GmbH, Karlsruhe, Germany
D-(+)- Glucose monohydrate	Sigma-Aldrich Corp., St. Louis, MO, USA
L- Glutamine	Sigma-Aldrich Corp., St. Louis, MO, USA
L- Glutamate	Sigma-Aldrich Corp., St. Louis, MO, USA
L- Glycine	Carl Roth, Karlsruhe, Germany
Goat Serum	Sigma-Aldrich Corp., St. Louis, MO, USA
Guanosine 5′-triphosphate sodium salt hydrate	Sigma-Aldrich Corp., St. Louis, MO, USA
HEPES	Carl Roth, Karlsruhe, Germany
Hydrochloric acid 4mol/L	Carl Roth, Karlsruhe, Germany
Hydrogen peroxide 30%	Carl Roth, Karlsruhe, Germany
Hydroxylamine-Hydrochloride	Sigma-Aldrich Corp., St. Louis, MO, USA
Iron (III)chloride	Sigma-Aldrich Corp., St. Louis, MO, USA
Imidazol	Sigma-Aldrich Corp., St. Louis, MO, USA

Ketamin	Ratio pharm, Ulm, Germany
L-Leucine	Sigma-Aldrich Corp., St. Louis, MO, USA
L-Lysine	Sigma-Aldrich Corp., St. Louis, MO, USA
Magnesium sulfate	Sigma-Aldrich Corp., St. Louis, MO, USA
Manganese(II) chloride	Sigma-Aldrich Corp., St. Louis, MO, USA
Mayer's hemalum solution	Merk, Darmstadt, Germany
N,N-Dimethylformamide	Sigma-Aldrich Corp., St. Louis, MO, USA
N-Acetyl-L-glutamic acid	Sigma-Aldrich Corp., St. Louis, MO, USA
Nonidet P40 (NP-40)	Sigma-Aldrich Corp., St. Louis, MO, USA
O-(Carboxymethyl) hydroxylamine hemihydrochloride	Sigma-Aldrich Corp., St. Louis, MO, USA
L-Ornithine monohydrochloride	Sigma-Aldrich Corp., St. Louis, MO, USA
Penicillin/ streptomycin	PAN Biotech GmbH
Phenyl methyl sulfonyl fluoride	Sigma-Aldrich Corp., St. Louis, MO, USA
Potassium chloride	Sigma-Aldrich Corp., St. Louis, MO, USA
Potassium dihydrogen phosphate	Sigma-Aldrich Corp., St. Louis, MO, USA
Phosphatase inhibitor Cocktail I and II	Sigma-Aldrich Corp., St. Louis, MO, USA
Protease inhibitor Cocktail	Roche, Mannheim, Germany
2-Propanol	Carl Roth, Karlsruhe, Germany
2,6-Pyridinedicarboxylic acid	Sigma-Aldrich Corp., St. Louis, MO, USA
Rompun 2%	Bayer health care, Leverkusen, Germany
Roti®-Histo-fix 4 %	Carl Roth, Karlsruhe, Germany

L-Serine	Sigma-Aldrich Corp., St. Louis, MO, USA
Sodium chloride	Sigma-Aldrich Corp., St. Louis, MO, USA
Sodium dodecyl sulfate (SDS), ultra grade	Carl Roth, Karlsruhe, Germany
Sodium deoxycholate	Sigma-Aldrich Corp., St. Louis, MO, USA
Swine serum	DakoCytomation, Glostrop, Denmark
Thiosemicarbazide	Sigma-Aldrich Corp., St. Louis, MO, USA
Tris	Carl Roth, Karlsruhe, Germany
Trizma Hydrochloride	Sigma-Aldrich Corp., St. Louis, MO, USA
Tween20	Sigma-Aldrich Corp., St. Louis, MO, USA
William's Medium E	PAN Biotech GmbH
Xylene	Merk, Darmstadt, Germany

2.1.2 Consumables

BD Microlance™ 3- 26G 5/8 0.45x16mm	Becton Dickinson (BD) GmbH, Heidelberg, Germany
Cell culture plates (6-well)	Sarstedt, Numbrecht, Germany
Cell scrapers	Sarstedt, Numbrecht, Germany
Cover slips	Menzel, Braunschweig, Germany
Glass spectrophotometer cuvettes	Sigma-Aldrich Corp., St. Louis, MO, USA
Inject – f	B\Braun, Wertheim, Germany
MicroAMP optical 96-well plate	Applied Biosystems, California, USA
Microscopic slides	Thermo Scientific, Braunschweig, Germany

Pestle/micro tube (1.5ml)	VWR international, Darmstadt, Germany
Pipette tip	Sarstedt, Numbrecht, Germany
Plastibrand disposable cuvettes	Brand, Wertheim, Germany
QIAshredder spin column	Qiagen, Hilden, Germany
Safe Seal tubes	Sarstedt, Numbrecht, Germany
Serological pipettes	Sarstedt, Numbrecht, Germany
Sterican - 0,3 x 12 – 30g x ½	B\Braun, Wertheim, Germany
96-Well Assay Plate	Corning Incorporated, USA

2.1.3 Equipment

ABI 7500 Fast Real-Time PCR System	Applied Biosystems
Micro Centrifuge	Kendo, Hanau, Germany
Fluorescence Microscope BX41	Olympus, Hamburg, Germany
Incubator	Binder GmbH, Tuttlingen, Germany
Microwave	Sharp Electronics (Europe) GmbH, Hamburg, Germany
Nanodrop ND-1000	Thermo Scientific, Braunschweig, Germany
Perfusions pump Type D0132	Fresenius Medical Care AG & Co. KGaA, Bad Homburg, Germany
Phase contrast Microscope Nicon eclipse TS100	Nikon GmbH, Dűsseldorf, Germany
pH-Meter (Seven Easy)	Mettler-Toledo GmbH, Gießen,, Germany
Sonopuls Ultrasonic homogenizer	Bandelin Electronic · GmbH & Co. KG, Berlin, Germany

Spectrophotometer V-530	Jasco, USA
Water bath	GFL, Burgwedel, Germany
Vortex	Beyer GmbH, Dűsseldorf, Germany
Micro Plate reader, infinite M200 PRO	Tecan, Switzerland
Balance BL150S	Sartorius AG, Göttingen, Germany
HM 450 Sliding Microtome	Microm, Walldorf, Germany
Spin Tissue Processor STP 120	Microm, Walldorf, Germany
EC 350 – Modular tissue embedding center	Microm, Walldorf, Germany
Thermocycler T3000	Biometra, Göttingen, Germany

2.1.4 Buffers and solutions

2.1.4.1 Prepared buffers and solution

0.01 M Citrate buffer, pH 6.0

Citric acid monohydrate (2.1 g/L), set to pH 6 with NaOH

Collagen gel (10 mg vial)

- Reconstitution with 12ml of sterile acetic acid (0.2%)
- Further dilution with 1.2ml of 10x DMEM
- pH neutralization with 1M NaOH

EDTA (anticoagulant)

Na_2EDTA 32mg in 1 ml distilled H_2O

Eosine 1%

1 g Eosin Y disodium salt in 100 µl distilled H_2O, 1 drop glacial acetic acid

GS activity assay buffers (Amount for 100ml distilled H_2O)

- Imidazol buffer (250mM)

Imidazol 1.7g, set to pH 6.8 with HCl

- L-Glutamine (250mM) — L-Glutamine 3.655 g, set to pH 6.8 with 1M NaOH
- Hydroxylamine-Hydrochloride (250mM) — NH_2OH HCl 1.735 g
- Adenosindiphosphat (1.6mM) — ADP 75.4 g
- Di-Sodium-Hydrogen arsenate (250mM) — $Na_2HAsO_4x\ 7H_2O$ 7.8 g
- Manganese chloride (10mM) — $MnCl_2$ 99 mg
- Stop-Mix — $FeCl_3$ x $6H_2O$ 2.42 g, TCA 1.45 g, HCl 14.5 ml

Perfusion buffers

- Calcium chloride solution — 19 g/L $CaCl_2$*2 H_2O
- Collagenase buffer
  - 55 ml glucose (9 g/L)
  - 25 ml KH Buffer pH 7.4
  - 25 ml HEPES, pH 8.5
  - 30 ml amino acids solution
  - 10 ml $CaCl_2$ (19 g/L)
  - 2.5 ml glutamine (7 g/L)

  → Add 90 mg collagenase freshly before use
- EGTA buffer
  - 124 ml glucose (9 g/L)
  - 20 ml KH buffer pH 7.4
  - 20 ml HEPES pH 8.5
  - 30 ml amino acids solution
  - 2 ml Glutamine (7 g/L)
  - 0.8 ml EGTA pH 7.6
- EGTA, pH 7.6 — 47.5 g/L in d.H_2O dissolve with a bit of NaOH, set to pH 7.6 with HCl
- HEPES buffer, pH 7.6 — 60 g/L set to pH 8.5 with NaOH
- HEPES buffer, pH 8.5 — 60 g/L set to pH 8.5 with NaOH

• Krebs-Henseleit buffer (KH buffer)	60 g/L NaCl, 1.75 g/L KCl, 1.6 g/L KH_2PO_4 Set to pH 7.4 using NaOH
• Suspensions buffer	- 124 ml glucose (9 g/L) - 20 ml KH Buffer pH 7.4 - 20 ml HEPES pH 7.6 - 30 ml amino acids solution - 2 ml glutamine (7 g/L) - 1.6 ml $CaCl_2$ (19 g/L) - 0.8 ml $MgSO_4$ (24.6 g/L $MgSO_4$*7 H_2O) → Add 400 mg BSA freshly before use
Staining solution	5 mg 3,3′-Diaminobenzidine , 20 mg aminotriazole and 3.3 µl H_2O_2 in 10 ml 0.1 M Tris/HCL (pH 7.6)
10x TBS, pH 7.4	265 g NaCl, 60 g Tris, add 5 L distilled H_2O
1x TBS-T	250mL 10x TBS, 2.5mL Tween 20, add 2.5 L distilled H_2O
1x TE buffer – 1liter	10ml 1M Tris (pH 8), 2ml 0.5M Na_2EDTA (pH 8), in 1L distilled H_2O
0.1M Tris/ HCl, pH 7.6	15.76 g/L Trizma® hydrochloride, set to pH 7.6 with NaOH

2.1.4.2 Commercial buffers and solutions

Amino acids solution	PAN Biotech GmbH, Aidenbach, Germany
Diethylpyrocarbonate (DEPC) treated water	Sigma-Aldrich Corp., St. Louis, MO, USA
QuantiTech Primer assays	Qiagen, Hilden, Germany

2.1.5 Hepatocyte cultivation media

Full media	William's E Medium, 10% FCS, Pen/Strep (100 U/ml Penicillin , 0.1 mg/ml Streptomycin), 10 µg/ml Gentamycin, 100nM Dexamethason, 2mM Glutamine
Normal cultivation media	William's E Medium, Pen/Strep (100 U/ml Penicillin , 0.1 mg/ml Streptomycin), 10 µg/ml Gentamycin, 100nM Dexamethason, 2mM Glutamine

2.1.6 Commercial kits

L-Alanine Assay Kit	Abcam, Cambridge, UK
Alpha Ketoglutarate Assay Kit	Abcam, Cambridge, UK
Ammonia Assay Kit	Sigma-Aldrich Corp., St. Louis, MO, USA
Avidin and Biotin blocking	Vector laboratories, Burlingame, USA
Deproteinizing Sample Preparation Kit	Abcam, Cambridge, UK
Glucose (HK) Assay Kit	Sigma-Aldrich Corp., St. Louis, MO, USA
Glutamate Dehydrogenase Detection Kit	Abcam, Cambridge, UK
High-capacity cDNA Reverse Transcription kit	Applied Biosystems, California, USA
Lactate Colorimetric Assay Kit	Abcam, Cambridge, UK
Pyruvate Assay Kit	Abcam, Cambridge, UK
QuntiTect SYBR Green RT-PCR Kit	Qiagen, Hilden, Germany

RNeasy Mini Kit	Qiagen, Hilden, Germany
Urea Assay Kit	BioAssay Systems, Hayward, USA

2.1.7 Antibodies

2.1.7.1 Primary antibodies

Rabbit Anti-CPS1 antibody - Liver mitochondrial marker	Abcam, Cambridge, UK
Rabbit Anti-CYP2E1	Sigma-Aldrich Corp., St. Louis, MO, USA
Mouse Anti-glutamine synthetase monoclonal antibody	BD Bioscience, San Jose, USA
Purified Mouse Anti-Arginase I	BD Bioscience, San Jose, USA

2.1.7.2 Secondary antibodies

Anti-mouse IgG-POD	Sigma-Aldrich Corp., St. Louis, MO, USA
Polyclonal swine anti-rabbit immunoglobulins/HRP	DakoCytomation, Glostrop, Denmark

2.2 Methods

2.2.1 Induction of liver damage by CCl_4

2.2.1.1 Experimental animals

10-12 weeks old male C57BL/6N mice were used (Charles River, Sulzfeld, Germany). Animals were housed under specific pathogen-free conditions and fed ad libitum with Ssniff R/M-H, 10 mm standard diet (Ssniff, Soest, Germany). All experiments were approved by the German authorities.

2.2.1.2 CCl_4 administration

2.2.1.2.1 Induction of maximum pericentral liver damage

For induction of maximum liver damage a single dose of 1.6 g/kg body weight CCl_4 was administered intraperitoneally (i.p.) in olive oil (Hoehme et al., 2007; 2010). A control group received only olive oil as a vehicle control. The application volume was 4 ml/kg (0.4 g/ml). Three mice were used for each of the time periods given in the results section.

2.2.1.2.2 Administration of various doses of CCl_4

For induction of various degrees of liver damage various doses of CCl_4 were injected intraperitoneally in olive oil (table 2.1). A control group received only olive oil as a vehicle control. The application volume was 4 ml/kg. Three mice were used for each dose given in the results section.

Table 2.1 Dosing schedule of CCl_4

Dose (mg/kg)	CCl_4 (µl)	Olive oil (µl)
0	0	0
10.9	6.81	3993.19
38.1	23.81	3976.19
132.4	82.75	3917.25
460	287.5	3712.5
1600	1000	3000
Oil	0	4000

2.2.2 Blood and liver tissue samples collection

At the specified period of time mice were anaesthetized by an i.p. injection of a mixture of rompun 2% (20 mg/kg) and ketamin (120 mg/kg) intraperitoneally (Flecknell, 1996). After loss of all reflexes, the abdominal wall of the mouse was carefully opened.

2.2.2.1 Blood sampling and plasma separation

For later metabolic analysis blood samples were collected from three different positions of the vascular system of mouse: (i) from the portal vein representing the “liver inflow”, (ii) from the hepatic vein representing the “liver outflow” and (iii) from the right heart chamber representing the “systemic circulation” (Fig. 2.1). For collection of the blood from the hepatic and portal veins a 30 gauge needle was used. In order to visualize the hepatic vein the median liver lobe was carefully reflected cranially and the left liver lobe was gently pulled caudally. The tip of the needle was inserted in the hepatic vein and the blood was collected slowly. In order to expose the portal vein the median and left liver lobes were carefully reflected cranially. The abdominal viscera were gently pulled outside the abdominal cavity. The needle tip was inserted in the portal vein against the direction of the blood flow. For collection

of the blood from the heart, all liver lobes were returned to their normal anatomical position. A 25 gauge needle passed the diaphragm and was inserted into the right heart chamber. All blood samples were collected on EDTA as anticoagulant (50 µl/ml of blood). About 170 µl of blood were collected from each site. For plasma separation the blood was directly centrifuged for 10 min at 13000 rpm at 4°C. 60 µl of clear plasma was carefully transferred into a pre-cooled eppendorf tube. The plasma was stored at -80 °C until analysis except for ammonia which was measured directly before freezing.

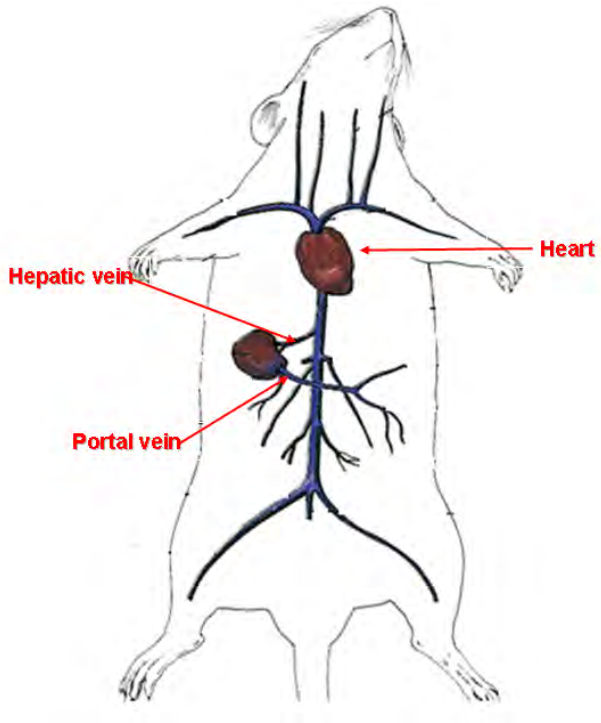

Fig. 2.1: Sites of blood collection. The blood was collected under anesthesia from three different positions of the vascular system of mouse: (i) from the portal vein representing the "liver inflow", (ii) from the hepatic vein representing the "liver outflow" and (iii) from the right heart chamber representing the "systemic circulation". About 170 µl of blood was collected from each position using EDTA as anticoagulant.

2.2.2.2 Collection of liver tissue samples

After the blood collection the whole liver was carefully excised without damaging the liver capsule. Three pieces about 20 mg in weight were collected from the median liver lobe and snap frozen in liquid nitrogen. Subsequently, the snap frozen liver tissue samples were stored at -80°C for later RNA isolation and enzyme activity assay. For the immunohistochemical analysis a piece of 1.5-2.5 cm^2 size was collected from the left liver lobe and fixed in 4% paraformaldehyde (PFA) for 48h at 4°C (Fig. 2.2).

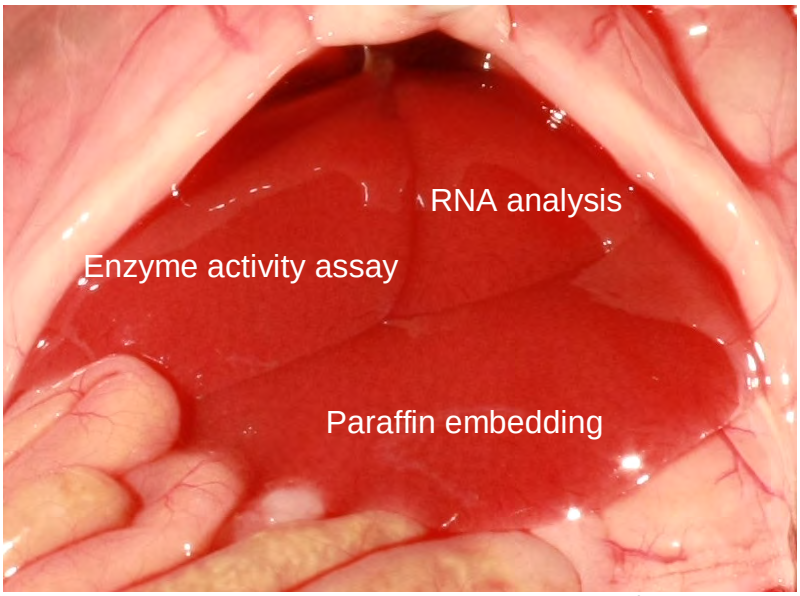

Fig. 2.2: Collection of liver tissue samples. A piece of 1.5-2.5 cm^2 size was collected from the left lobe of the liver and fixed in 4% paraformaldehyde for the immunohistochemical analysis. Two pieces about 20 mg in weight were collected from the right segment of the median liver lobe and snap frozen in liquid nitrogen then stored at -80°C for enzymes activities assay. One piece about 20 mg in weight was collected from the left segment of the median liver lobe and snap frozen in liquid nitrogen then stored at -80°C for the RNA analysis.

2.2.2.3 Paraffin embedding of the mouse liver

After fixation, samples were washed in PBS for 48h at 4°C to remove the PFA. Subsequently, the tissue was embedded in paraffin with the use of Microm STP120 embedding automate (Microm, Walldorf, Germany). The embedding

program is summarized in table (2.2). After embedding solid paraffin blocks suitable for cutting were made using the EC 350 – modular tissue embedding center (Microm, Walldorf, Germany).

Table 2.2: Embedding program of the mouse liver tissue

Step	Treatment	Time (minute)
1	70% Ethanol	30
2	70% Ethanol	60
3	90% Ethanol	30
4	90% Ethanol	30
5	99% Ethanol	30
6	99% Ethanol	35
7	99% Ethanol	60
8	Xylol	30
9	Xylol	35
10	Xylol	60
11	Paraffin Histowax	80
12	Paraffin Histowax	105

2.2.3 Visualization and quantification of necrotic lesions

2.2.3.1 Hematoxylin and eosin staining

Using a microtome (Microm, Walldorf, Germany) 5 µM tissue sections were prepared and mounted on microscopic slides. For dewaxing, sections were warmed at 56-60°C for 30min and then briefly at 65-70°C until the paraffin started melting. Sections were then incubated three times for 5min in xylene. After deparaffinization, sections were then rehydrated through an isopropanol gradient (98%, 96%, 90%, 80% and 70% respectively for 5min each). After washing in distilled H_2O for 5min, sections were incubated in hematoxylin for 5min for nuclear staining. Subsequently, sections were rinsed for 15min in a running tap water to remove the excess of hematoxylin. For staining of the cytoplasm sections were incubated for 3min in 1% eosin followed by a brief rinsing in distilled H_2O for 10s. Sections were then

dehydrated through an isopropanol gradient (70%, 80%, and 90%, for 5s each and two times for 5min in absolute isopropanol). Finally, sections were incubated for 3 min in xylene and preserved by mounting with enellan.

2.2.3.2 Quantification of necrotic lesions

2.2.3.2.1 Quantification of the area of necrotic lesions

In order to quantify the area of necrotic lesions, images were acquired from the hematoxylin and eosin stained liver using the Cell ^ M software (Olympus, Hamburg, Germany). The dead cell area was defined as the area where no nuclei of hepatocytes were visible (Hoehme et al., 2010). In order to precisely quantify the necrotic lesion three areas were measured using the NIS element software (Nicon, Dusseldorf, Germany): (i) The total image area "A_1" (ii) the area of the necrotic lesion including the central vein "A_2" and (iii) the area of the central vein "A_3" (Fig. 2.3). The percentage of necrotic lesion was calculated according to the following formula:

$$\text{Dead cell area (\%)} = \frac{A_2 - A_3}{A_1} \times 100$$

Three mice were used for each of the time periods and CCl_4 doses given in the results section. Ten representative images were analyzed from each mouse.

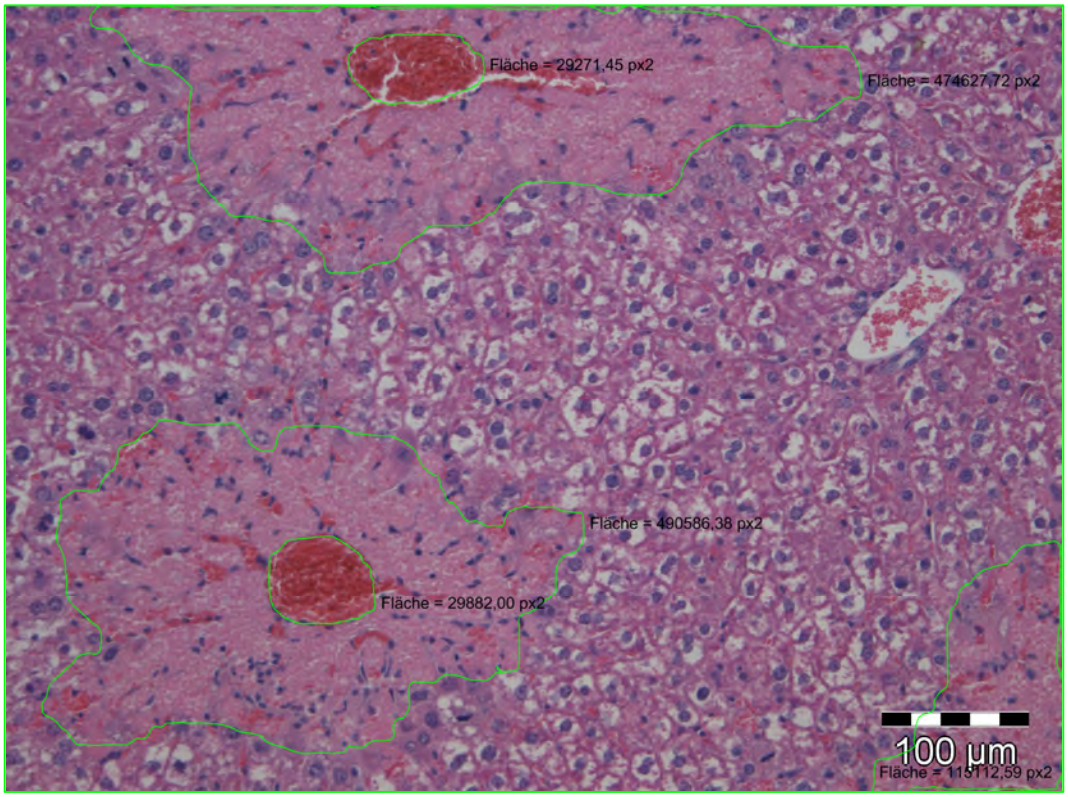

Fig. 2. 3: Quantification of the necrotic lesion using the NIS element software. The dead cell area defined as the area where no nuclei of hepatocytes were visible. Lines defining the total image area, the dead cell area (including the area of the central vein "CV") and the area of the central vein were drawn. The percentage of the necrotic lesion was calculated as: {dead cell area (including the area of the CV) - area of the CV} / the total image area. Hematoxylin and eosin staining, scale bar: 100 µM.

2.2.3.2.2 Counting of necrotic lesions

In order to calculate the number of necrotic lesions, whole slide scans were prepared. Images were acquired from the whole slide using the Cell ^M software (Olympus, Hamburg, Germany). These images were organized to reconstruct the whole slide (Fig. 2.4). All necrotic lesions on the slide, controlled by central veins, were counted manually and normalized to the total slide area. Three mice were used for each of the CCl_4 doses given in the results section.

Fig. 2.4: A whole slide scan of mouse liver at day one after injection of 1.6 g/kg CCl_4. images were captured using the Cell ^M software (Olympus) and organized to reconstruct the whole slide. All pericentral necrotic lesions were counted manually and normalized to the total slide area. Hematoxylin and eosin staining, scale bar: 200 µM.

2.2.3.2.3 Measurement of hepatic damage markers

Alanine aminotransferase (ALT) and aspartate aminotransferase (AST) levels were measured in plasma separated from the heart blood. The measurement was done in cooperation with our cooperation partner (LADR Medizinisches Versorgungszentrum, Dortmund, Germany).

2.2.4 Metabolic analysis

2.2.4.1 Ammonia assay

Ammonia was measured enzymatically in the plasma using a commercially available kit according to the manufacturer's instructions (Sigma, St. Louis, MO, USA). Ammonia reacts with α-ketoglutaric acid (KGA) and reduces nicotinamide adenine dinucleotide phosphate (NADPH) in the presence of L-glutamate dehydrogenase (GDH) to form L-glutamate and oxidized nicotinamide adenine dinucleotide phosphate ($NADP^+$). The decrease in absorbance at 340nm wavelength due to the oxidation of NADPH is proportional to the concentration of ammonia in the sample (Bergmeyer and Beutler, 1985).

2.2.4.2 Amino acids assay

Glutamine, glutamate, alanine and arginine were measured in plasma by HPLC in cooperation with our cooperation partner (LADR Medizinisches Versorgungszentrum, Dortmund, Germany).

2.2.4.3 Urea assay

Urea was measured colorimetrically in plasma using a commercially available kit (BioAssay Systems, Hayward, USA). The test is based on the use of a chromogenic reagent which specifically forms a colored complex with urea. The intensity of the color, measured at 520nm wavelength, is proportional to the concentration of urea. With the aid of the urea standard the concentration of urea in the sample was calculated.

2.2.4.4 Glucose assay

Glucose was measured enzymatically in plasma using a commercially available kit (Sigma, St. Louis, MO, USA). The principle was that glucose can be phosphorylated by adenosine triphosphate (ATP) in a reaction catalyzed by hexokinase to generate glucose-6-phosphate (G6P). In the presence of nicotinamide adenine dinucleotide (NAD), G6P can be oxidized by the action of glucose-6-phosphate dehydrogenase (G6PDH) into 6-phospho gluconate plus reduced NAD (NADH). The consequent increase in absorbance at 340nm wavelength is directly proportional to the concentration of glucose (Bondar and Mead, 1974).

$$\text{Glucose} + \text{ATP} \xrightarrow{\text{Hexokinase}} \text{G6P} + \text{ADP}$$

$$\text{G6P} + \text{NAD} \xrightarrow{\text{G6PDH}} \text{6-Phosphogluconate} + \text{NADH}$$

2.2.4.5 Lactate assay

The plasma lactate was measured colorimetrically using a commercially available kit according to the manufacturer's instructions (Abcam, Cambridge, UK). The test based on the oxidation of lactate by the lactate dehydrogenase enzyme. The product then reacts with a probe to generate a color (λmax = 450nm). The intensity of the color was detected using a micro plate reader at an optical density of 450nm. With the aid of the lactate standard curve the lactate content in the sample was calculated (Fig. 2.5).

.

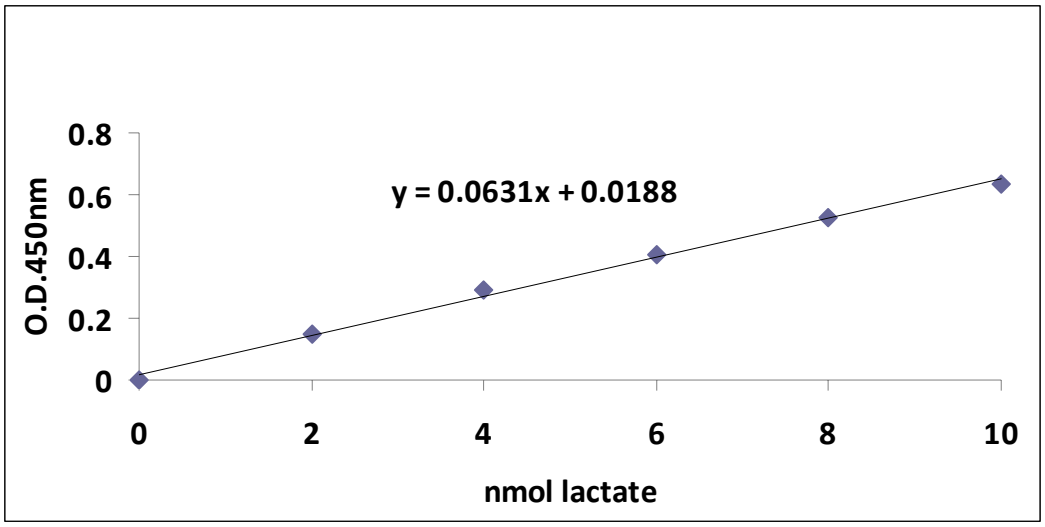

Fig. 2.5: Lactate standard curve. Concentrations of 0, 2, 4, 6, 8 and 10 nM lactate /well were incubated with the reaction mix for 30min in a 96 well plate. The intensity of the developed color was measured by a micro plate reader at an optical density of 450nm. The background was corrected by subtracting the value derived from zero from all readings

2.2.4.6 Pyruvate assay

The level of pyruvate in plasma was measured colorimetrically using a commercially available kit according to the manufacturer's instructions (Abcam, Cambridge, UK). The test principle was that pyruvate can be oxidized by pyruvate dehydrogenase to generate a colored product (λmax = 570nm). The color intensity was detected using a micro plate reader at an optical density of 570nm. After performing a pyruvate standard curve (Fig. 2.6) the concentration of pyruvate in the sample was calculated.

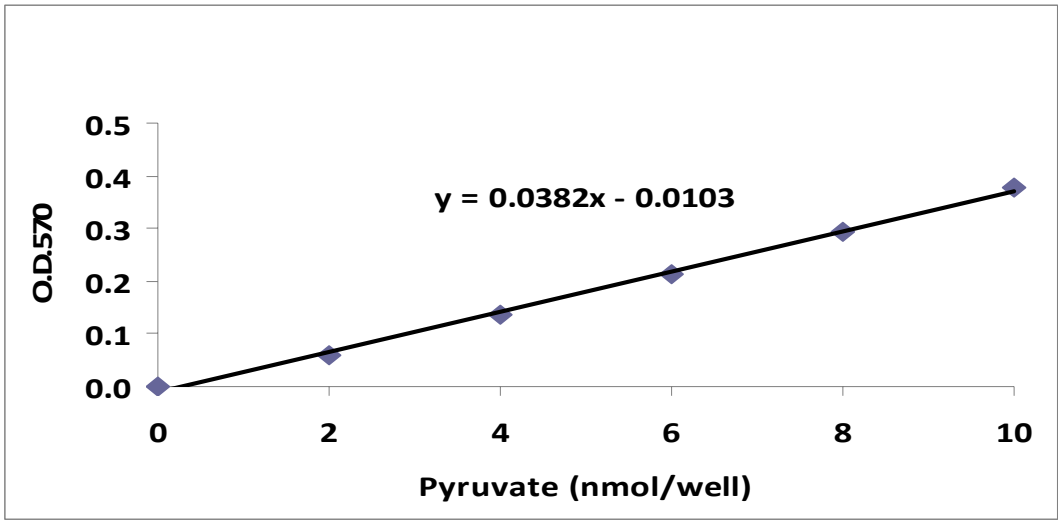

Fig. 2.6: Pyruvate standard curve. Concentrations of 0, 2, 4, 6, 8 and 10 nM pyruvate/well were incubated with the reaction mix for 30min in a 96 well plate. The intensity of the developed color was measured using a micro plate reader at an optical density of 570nm. The background was corrected by subtracting the value derived from zero from all readings.

2.2.4.7 Alpha-ketoglutarate assay

The concentration of alpha-ketoglutarate (α-KG) in plasma was measured colorimetrically using a commercially available kit according to the manufacturer's instructions (Abcam, Cambridge, UK). The test was based on the transamination of α-KG into pyruvate by an enzyme mixture. Pyruvate then reacts with a probe leading to color development (λmax = 570nm). The color intensity was measured using a micro plate reader at an optical density of 570nm. To avoid false positive results from pyruvate a blank sample in which the converting enzymes mixture was omitted was run in parallel with the test samples. Subsequently, the background was controlled by subtracting the blank value from the test value. After performing a standard curve from the α-KG standard the concentration of α-KG in the sample was calculated (Fig. 2.7).

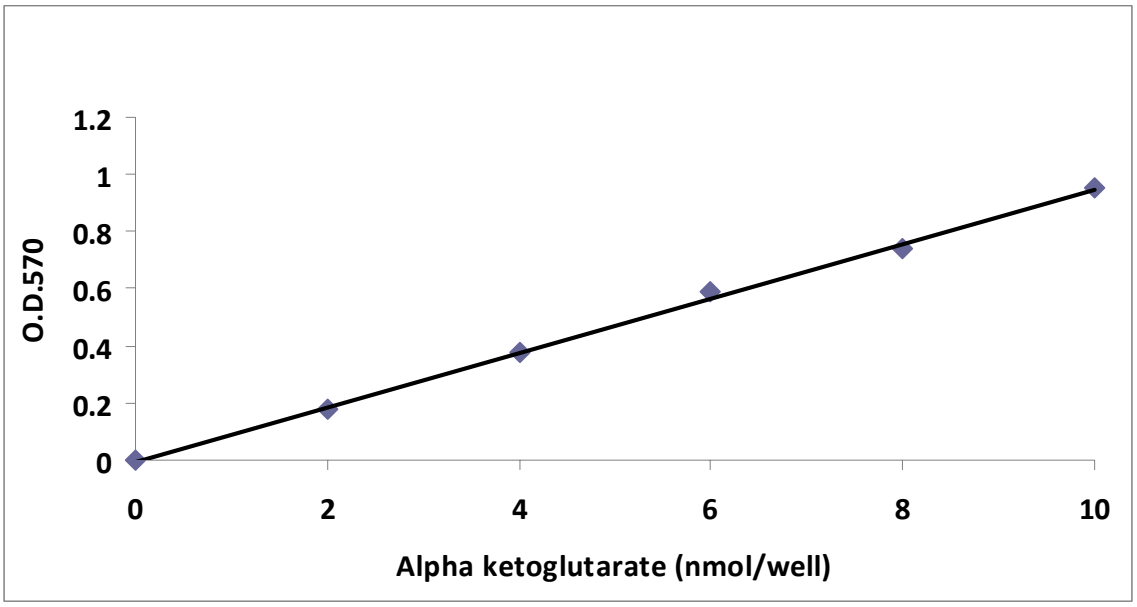

Fig. 2.7: Alpha-ketoglutarate (α-KG) standard curve. Concentrations of 0, 2, 4, 6, 8 and 10 nM α-KG /well were incubated with the reaction mixture for 30min in a 96 well plate. The intensity of the developed color was measured using a micro plate reader at an optical density of 570nm. The background was corrected by subtracting the value derived from zero from all readings.

2.2.5 Immunohistochemical staining

The Immunohistochemical staining was done using paraffin slices. Sections of 5 µM thickness were prepared using a microtome (Microm, Walldorf, Germany) and mounted on microscopic slides. Sections were then warmed at 56-60°C for 30min and then briefly at 65-70°C until the paraffin started melting. For deparaffinization sections were incubated in xylene two times for 5min each. Rehydration of the tissue sections was done by incubation in a descending ethanol gradient: absolute ethanol (two times for 3min each), 96% and 70% (one time for 3min). Before proceeding to the next step sections were washed in distilled H_2O for 3min and in TBS for 5min. For antigen retrieval sections were boiled in 0.01M citrate buffer (pH 6.0) three times for 5min each (Shi et al., 1998). Subsequently, sections were allowed to cool down for 30 min at room temperature followed by washing for 5min in distilled H_2O. After antigen retrieval blocking of the endogenous peroxidase activity was done by incubation in 0.3% H_2O_2 in TBS for 15min at room temperature (Ramos-Vara, 2005). Sections were

then washed briefly in distilled H_2O and in TBS two times for 10 min each. Non specific binding sites were blocked by incubation with 5% goat serum (for the GS and Arginase1 staining) or with 5% swine serum (for the CPS1 and CYP2E1 staining) in TBST. Moreover, endogenous avidin and biotin were blocked using the commercially available kit according to the manufacturer's instructions (Vector laboratories, Burlingame, USA) (Rodriguez-Soto et al., 1997). Leaving out the washing step, sections were then incubated overnight with the primary antibody in a humid chamber at 4°C (Table 2.1). Before proceeding to the next step sections were washed in TBST three times for 5min each. To identify primary antibody bindings sections were incubated with the secondary antibody in a humid chamber for 2h at room temperature (Table 2.3). Subsequently, sections were washed three times in TBST for 5min each and one time in 0.1M Tris HCl for 5min. Sections were then incubated with the DAB staining solution for 4-7min according to the intensity of the color development. The reaction was stopped by washing in TBS for 5min. In order to stain the nucleus sections were counter stained with Mayer's hemalum (Merk, Darmstadt, Germany) for 90 sec. Sections were then rinsed in a running tap water for 10min. Subsequently, sections were dehydrated using a graded ethanol series (70%, 90%, 95%, and 100% for 30sec each) and then incubated in roti-histol four times for 1min each. The slides were mounted with entellan and stored at room temperature.

Table 2.3: Concentrations of primary and secondary antibodies

Antigen	Primary antibodies		Secondary antibodies	
	Antibody	**Concentration**	**Antibody**	**Concentration**
CPS1	Rabbit anti-CPS1	1:1000	Swine anti-rabbit	1:25
GS	Mouse monoclonal anti-GS	1:1000	anti-mouse IgG-POD	1:500
CYP2E1	Rabbit anti-CYP2E1	1:20	Swine anti-rabbit	1:25
Arginase1	Mouse Anti-Arginase I	1:400	anti-mouse IgG-POD	1:500

2.2.6 Enzyme activity assay

2.2.6.1 Glutamine synthetase activity assay

The activity of the glutamine synthetase (GS) enzyme was measured in liver tissue homogenate according to the method of Gebhardt and Williams (1986). The principle of the test was that GS exerts a glutamyl-transferase activity. It catalyzes the formation of γ-Glutamylhydroxymate from glutamine and hydroxyl amine in the presence of ADP and either phosphate or arsenate (Levintow, 1954).

$$\text{L-Gln} + NH_2OH \xrightarrow[PO_4 \text{ or } AsO_4]{\text{ADP}} \gamma\text{-Glutamylhydroxymate} + NH_3$$

γ-Glutamylhydroxymate can react with ferric tri-chloride generating a colored complex. The intensity of the color was proportional to the activity of the GS enzyme. The color development was measured in a photometer at 540nm wavelength. Results were normalized to the protein content of the sample.

2.2.6.2 Glutamate dehydrogenase activity assay

The activity of the GDH enzyme was measured colorimetrically using a commercially available kit according to the manufacturer's instructions (Abcam, Cambridge, UK). GDH catalyzes the deamination of glutamate into ammonia and alpha ketoglutarate. During this reaction NADP is converted to $NADPH^+$ leading to color development. The intensity of the color was measured using a micro plate reader at 450nm wavelength. Plasma samples were measured directly. However, liver tissue samples (20 mg) were firstly homogenized in the GDH assay buffer centrifuged at 13000 rpm for 10min at 4 °C and the clear supernatant was used for the assay. To avoid the false positive results a blank sample in which glutamate was omitted was used. Both the sample and the blank

were measured at 3min and 30min after incubation with the reaction mixture. The 3min reading was subtracted from the 30min reading. Subsequently, blank values were subtracted from test values. The NADPH standard curve was used to calculate the GDH enzyme activity in plasma and liver samples (Fig. 2.8). The GDH activity in the liver tissue was normalized to the protein content.

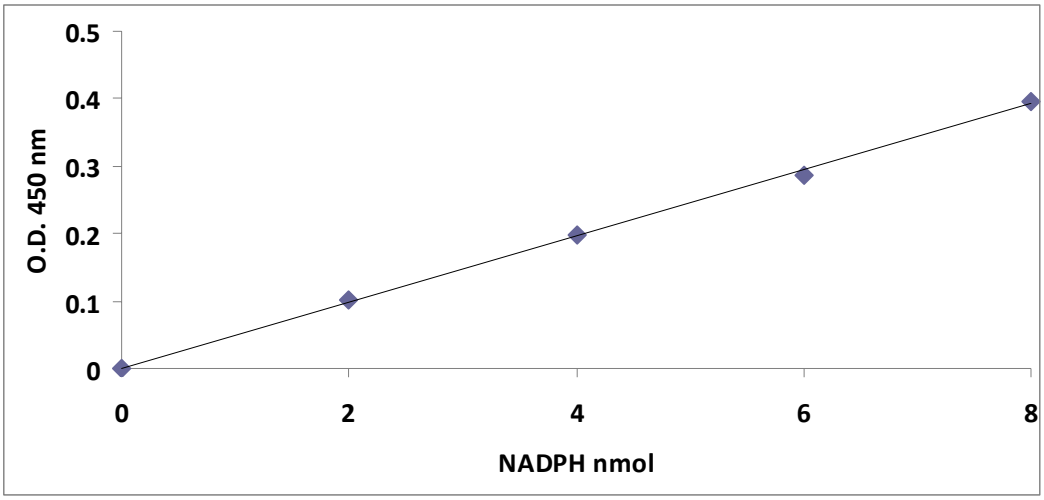

Fig. 2.8: NADPH standard curve. Concentrations of 0, 2, 4, 6 and 8 nM NADPH /well were incubated with the reaction mixture for 3 min in a 96 well plate. The intensity of the color was measured using a micro plate reader at an optical density of 450 nm.

2.2.7 Protein assay

Protein was measured colorimetrically using the Thermo Scientific Pierce BCA Protein Assay kit (Kessler and Fanestil, 1986). The sample was diluted 1:320 by adding 2.5 µl sample to 797.5 µl distilled H_2O. 200 µl working reagent were prepared from reagent A and B (50:1) and added to the diluted sample. After mixing, the sample was incubated at 60°C for 30min with shaking. Subsequently, the sample was allowed to cool down for 10min. The protein concentration was measured at 562nm wavelength using the UV/VIS spectrophotometer (Jasco, USA). With the aid of a standard curve prepared with bovine serum albumen, the protein concentration of the sample was calculated.

2.2.8 Total RNA analysis

2.2.8.1 RNA extraction

Extraction of the total RNA was done using the RNeasy Mini kit according to the manufacturer's instructions (Qiagen, Hilden, Germany). A piece of 20 mg weight of the frozen liver tissue was homogenized in a buffer containing guanidium thiocyanate using a pestle. Guanidium thiocyanate helped in lysis of the cells and in maintaining the RNA integrity by denaturation of RNases (Chomczynski and Sacchi, 1987). The lysate was then transferred into a QIAshredder spin column placed in a collection tube (Qiagen, Hilden, Germany) and centrifuged for 2min at 13000 rpm. A further centrifugation step of the lysate was done at 13000 rpm for 3min. The supernatant was then transferred into a new micro-centrifuge tube and one volume of 50% ethanol was added. Subsequently, the sample was transferred into an RNeasy spin column and centrifuged at 11000 rpm for 15sec. For washing of the RNA, one volume of a buffer contains ethanol was added to the spin column. Subsequently, centrifugation at 11000 rpm for 15sec was done. The washing step was repeated and the centrifugation was done at 11000 rpm for 15sec and for 2min. To elute the RNA, the spin column was transferred into a new collection tube and 30 µl of RNase-free water were added. The spin column was then centrifuged at 11000 rpm for 1 min. The extracted RNA was stored at -20 °C.

2.2.8.2 RNA quantification

RNA was quantified by measuring the absorption at 260nm using nanodeop ND-1000 (Thermo Scientific, Braunschweig, Germany). The RNase-free water was used as a blank. The purity of RNA was insured by the ratio of the absorbance at 260 and 280nm. The 260/280 ratio close to 2.0 indicated pure RNA. Whereas, lower 260/280 ratio indicated contamination particularly from protein (Glasel, 1995).

2.2.8.3 Reverse transcription polymerase chain reaction (RT-PCR)

cDNA synthesis was done using the High-Capacity cDNA Reverse Transcription Kit (Applied Biosystems, California, USA). 2 µg of the RNA in a final volume of 10 µl in DEPC-treated water were added into a 0.2 ml strip tube. Subsequently, 10 µl of the master mix were added to the RNA. The master mix contains 2 µl of the10x reverse transcription buffer, 0.8 µl of 25x dNTPs (100 mM), 2 µl of 10x reverse transcription random primers, 1 µl of the Multiscripe Reverse Transcriptase (50 U/ µl) and 4.2 µl of the DEPC-treated water. The reverse transcription was done in a thermo-cycler (Biometra, Göttingen, Germany) using the conditions illustrated in table (2.4). Following the reverse transcription the sample was diluted with DEPC-treated water to a final concentration of 10 ng/ µl and stored at -20°C.

Table 2.4: The thermo-cycling profile of the reverse transcription polymerase chain reaction

Stage	Duration (min)	Temperature (°C)
1	10	25
2	120	37
3	5	85
4	∞	4

2.2.8.4 Quantitative real-time polymerase chain reaction (qRT-PCR)

The qRT-PCR was done using custom-designed Quantitect assay primers and SYBR Green reagents (Qiagen, Hilden, Germany). qRT-PCR allows the detection and quantification of a target gene at each cycle of amplification (VanGuilder et al., 2008). The SYBR Green dye binds to all double stranded DNA leading to the emission of fluorescence. The fluorescence increased at each amplification cycle reflecting the quantity of the target gene (Schneeberger

et al., 1995). The measurement was done in a MicroAMP optical 96-well plate (Applied Biosystems, California, USA) in a 25 µl reaction. The Quantitect assay primer was reconstituted with 1.1 ml TE buffer, pH 8. In each reaction, 12.5 µl SYBR Green reagents, 2.5 µl assay primer and 5 µl of DEPC-treated water were added to 50 ng cDNA (5 µl). All samples were measured in triplicate. DEPC-treated water was used as a negative control whereas GAPDH was used as a house keeping gene. The plate was briefly centrifuged. The qRT-PCR was done using the Applied Biosystems 7500 real time PCR system (Applied Biosystems, California, USA). The running conditions were summarized in table (2.5).

Table 2.5: Running conditions of the quantitative real-time polymerase chain reaction

Stage	Repetitions	Duration (min)	Temperature (°C)	Function
1	1	02.00	50	Initiate the DNA polymerase
2	1	15.00	95	
3	40	00.15 00.30 00.35	94 55 72	DNA denaturation Primer annealing Extension
4	1	00.15 00.20 00.15 00.15	95 60 95 60	Create a melt curve

2.2.8.5 Data analysis

The relative total RNA expression was calculated using the ΔΔCt method (Livak and Schmittgen, 2001). The Ct value is the cycle number at which the fluorescence signal crosses the threshold. Firstly, the expression of the target gene was compared to the expression of the house keeping gene (ΔCt). Secondly, the expression of the target gene was normalized to controls (0h) (ΔΔCt). The fold change was calculated as $2^{-\Delta\Delta Ct}$.

2.2.9 Isolation and cultivation of mouse hepatocytes

2.2.9.1 Mouse hepatocytes isolation

Male C57BL/6N mice (8-12 weeks old) were used for hepatocytes isolation. The experiment was approved by the experimental animals committee. Animals were handled and housed according to specific pathogen-free conditions. Hepatocyte isolation was done according to Seglen (1972) and Klingmüller et al. (2006). The mouse was anaesthetized with an i.p. injection of a mixture of 2% Rompun (20 mg/kg) and ketamin (120 mg/kg). The liver was perfused through the caudal vena cava with the EGTA buffer for 15min at 37 °C. Subsequently, the perfusion was continued with the collagenase buffer for 5-7min at 37 °C. After perfusion, the liver was excised out from the animal and dissociated in a suspension buffer. The liver cell suspension was filtered through gauze and centrifuged for 5min at 50g. Subsequently, cells were washed twice with the suspension buffer and re-centrifuged. Cells were re-suspended in 10 ml suspension buffer. Before counting cells, the suspension was diluted 1:5 with the suspension buffer and thereafter a 1:1 dilution in trypan blue solution was done.

2.2.9.2 Sandwich cultures of mouse hepatocytes

Hepatocytes were cultivated on 6-well plates. Before plating of cells, the plate was prepared by adding 250 µl of rat tail collagen (1^{st} collagen layer). The gel was allowed to polymerize for 30min and then 2 ml of full media were added. 800000 cells per well were seeded (confluent culture). Subsequently, cells were allowed to attach for 3h at 37 °C, 5 % CO_2. After attachment, cells were washed 3 times with William's E medium to remove the floating cells. Subsequently, the second layer of collagen was added (250 µl of rat tail collagen) and allowed to dry for 30min at 37 °C, 5 % CO_2. Cells were further cultivated overnight in normal cultivation media (2 ml/well) before starting the experiment.

2.2.10 Mathematical modelling

The mathematical simulation model was established in cooperation with our cooperation partners Dr. Stefan Höhme and Dr. Dirk Drasdo (IZBI, Leipzig, Germany); Dr. Dominik Driesch and Dr. Sebastian Henkel (BioControl Jena GmbH, Jena, Germany). The technique of the spatial-temporal model has been described in Hoehme et al. (2010).

2.2.11 Statistical analysis

Statistical analysis was done using the SPSS software (Dunnett-t- test). At least three mice were used for each set of experiments. Data were expressed as means ± standard error. Differences were considered significant at $P < 0.05$ (Levesque, 2007).

3 Results

3.1 Alteration of ammonia and carbohydrate metabolism in relation to CCl_4-induced liver damage

3.1.1 Induction of liver damage by a high dose of CCl_4

In order to provide a data base that could be used for later mathematical modelling a mouse system was used where the hepatotoxic compound CCl_4 was injected. The aim of these experiments was to study the degree to which ammonia and carbohydrate metabolism is altered in response to liver damage. For this purpose, a single dose of 1.6 g/kg body weight CCl_4 was injected intraperitoneally into mice and sampling was done using the time dependent experimental schedule outlined in Fig. 3.1.

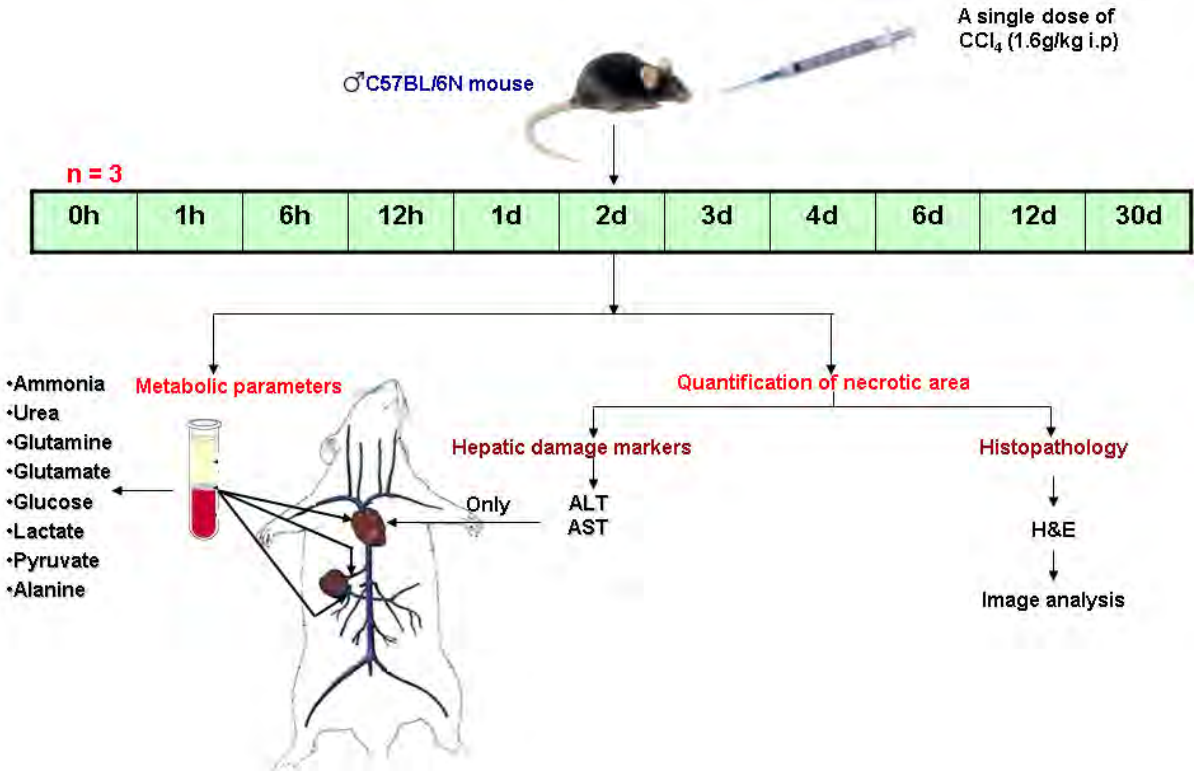

Fig. 3.1: Induction of liver damage and metabolic analysis. Mice received 1.6 g/kg CCl_4 and blood samples were collected at different time intervals from the portal vein, hepatic vein and the right heart chamber. Liver tissue was also collected and stained with hematoxylin and eosin (H&E). Three mice were analyzed per time point.

CCl_4 intoxication caused obvious hepatic macroscopical alterations in the form of white spots, especially evident from days one to three after injection (Fig. 3.2). By day six after CCl_4 administration the liver looked similar to the control.

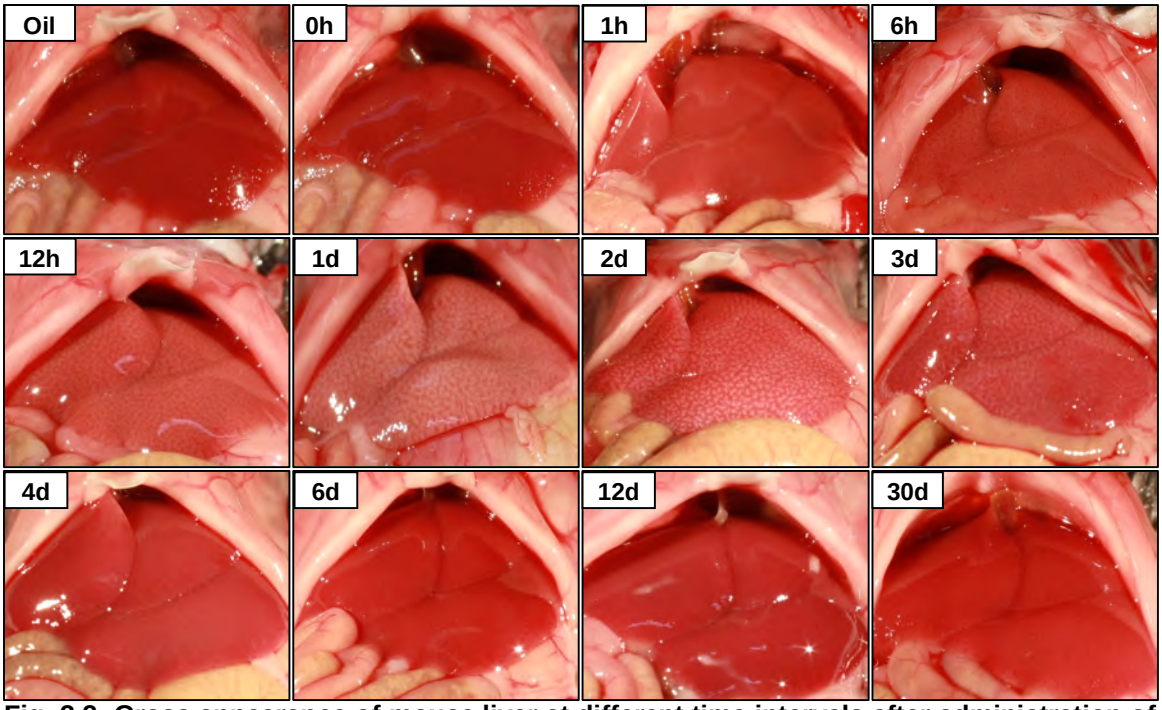

Fig. 3.2: Gross appearance of mouse liver at different time intervals after administration of 1.6 g/kg CCl_4. The Liver showed a characteristic spotted pattern from day one up to day three after CCl_4 injection. After six days the liver looked similar to the control.

In order to visualize the hepatic lesion induced by CCl_4 formalin fixed paraffin embedded liver sections were stained with hematoxylin and eosin. Microscopically, the liver of CCl_4-treated mice showed a pericentral necrosis which became obvious approximately one day after injection (Fig. 3.3). Between days two and four, the dead cell area became smaller, and after six days the damaged area was almost fully regenerated.

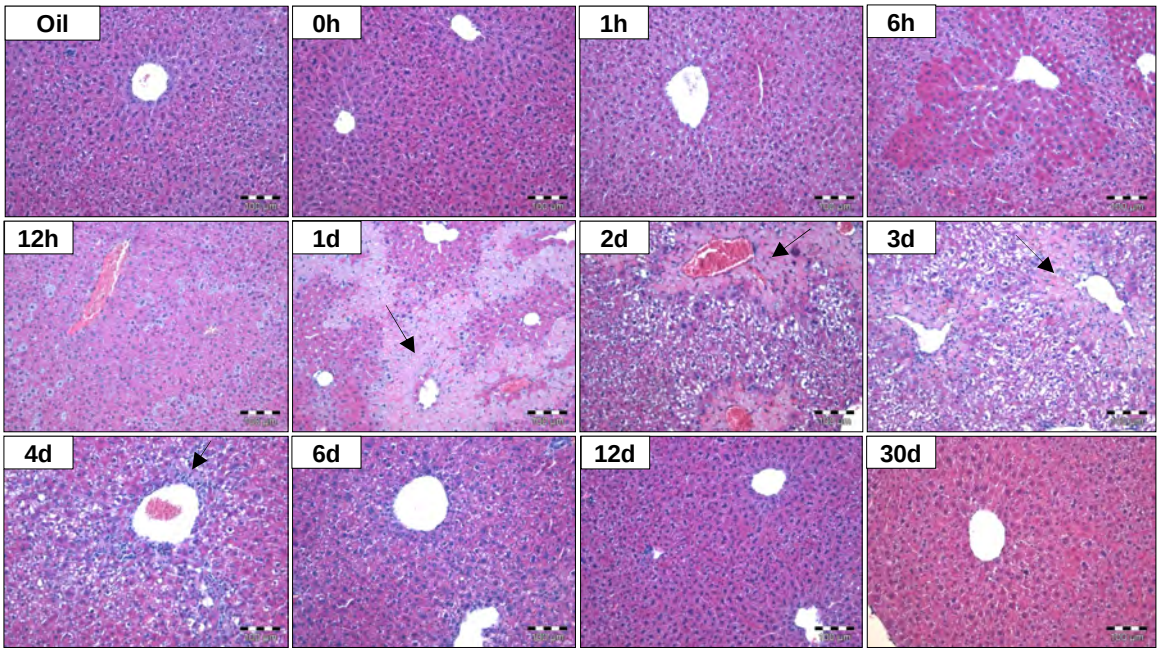

Fig. 3.3: Microscopic appearance of mouse liver at different time intervals after administration of 1.6 g/kg CCl_4. Between 6 and 12h after CCl_4 injection the liver shows deep eosinophilic staining in the cytoplasm of pericentral hepatocytes. From day one up to day four; the liver shows pericentral necrosis (arrows), whereas six days after injection; the liver appeared similar to the control. Hematoxylin and eosin staining, scale bars: 100µm

In order to obtain quantitative measures for the CCl_4-induced liver damage the dead cell area was quantified using image analysis software. This analysis showed that the peak of pericentral necrotic lesion was obtained on day one after CCl_4 injection, with approximately 40% of the entire liver affected. This value decreased during the following three days to approximately 9% on day four (Fig. 3.4). Six days after the CCl_4 injection the liver was back to the control level.

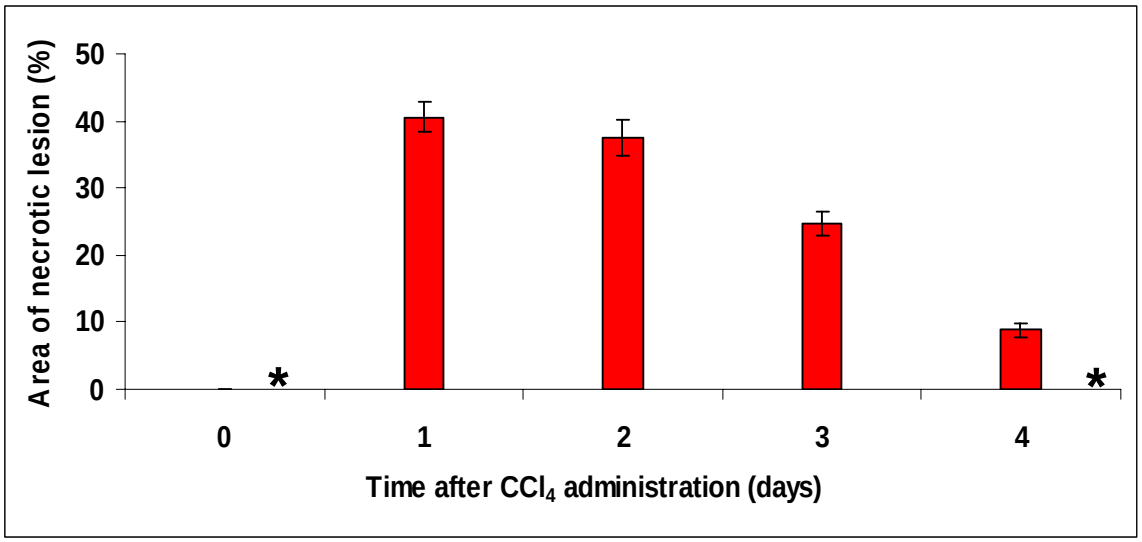

Fig. 3.4: Quantification of the area of the necrotic lesion at different time intervals after injection of 1.6 g/kg CCl_4. The liver damage was most evident one day after CCl_4 injection with recovery by day six. The data are mean ± S.E. and obtained from three mice per time point. * No necrotic area detectable.

Moreover, the degree of liver damage was further quantified by measuring the plasma concentrations of hepatic damage markers alanine transaminase (ALT) and aspartate transaminase (AST). Both liver enzymes were elevated with a maximum concentration measured on day one after CCl_4 injection. Enzyme concentrations returned back to the basal level six days after CCl_4 injection (Fig. 3.5 and 3.6).

In conclusion, the morphological alterations of the liver tissue and the elevation of liver enzymes are similar to those reported in previous studies (Hoehme et al., 2010). Therefore, the present experimental set up sufficiently allow for the quantification of alterations of ammonia and carbohydrate metabolism in response to liver damage.

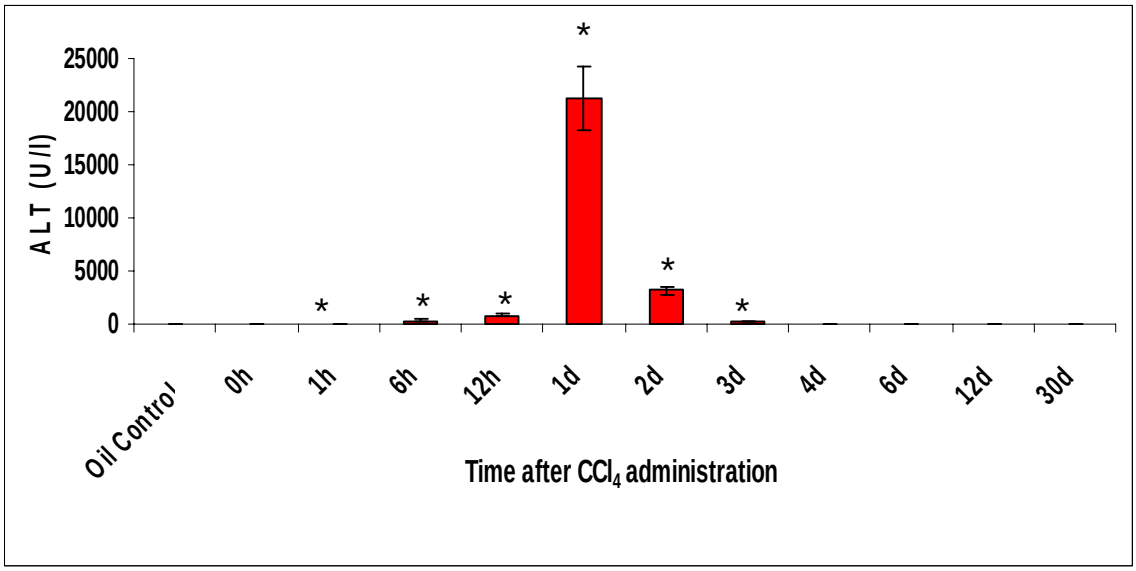

Fig. 3.5: Injection of 1.6 g/kg CCl_4 resulted in elevation of plasma level of alanine transaminase (ALT). The peak concentration was reached one day after injection and returned to the basal level by day four. Data obtained from six mice per time point and expressed as mean ± S.E. * P< 0.05 compared to the control (0h).

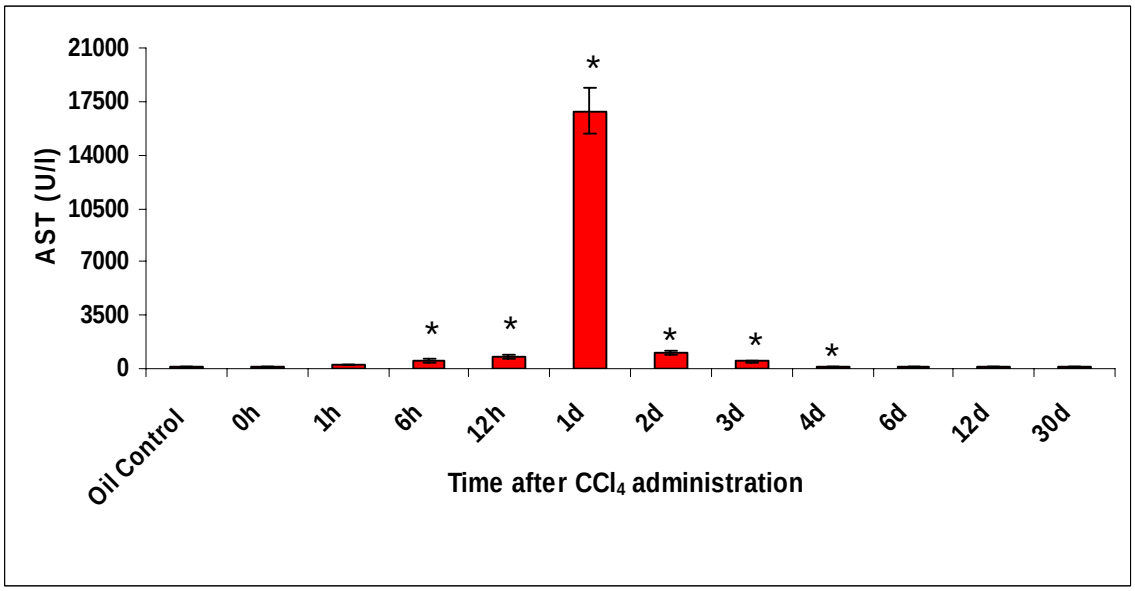

Fig. 3.6: Changes of plasma aspartate transaminase (AST) level (U/l) at different time intervals after administration of 1.6 g/kg CCl_4, showing the time curve of AST elevation which is maximal one day after injection and returns to the basal level by day four. Data obtained from six mice per time point and expressed as mean ± S.E. * P< 0.05 compared to the control (0h).

3.1.2 Quantification of metabolic alterations during liver damage and regeneration

In order to quantify the alterations in ammonia and carbohydrate metabolism during the destruction and regeneration process after CCl_4 intoxication blood samples were collected from 3 positions in each mouse: (i) from the portal vein (representing “liver inflow”), (ii) from hepatic vein (representing “liver outflow”) and (iii) from the right heart chamber (to determine the extra hepatic contribution particularly for ammonia detoxification). From these blood samples, plasma was separated and different metabolic parameters relevant for ammonia and carbohydrate metabolism were measured, including ammonia, glutamate, glutamine, urea, glucose, alanine, lactate and pyruvate.

In control mice, the highest ammonia concentration was measured in the portal vein (approximately 250µM), while in plasma obtained from the hepatic vein, ammonia concentration was very low (approximately 40µM), and was slightly higher in the systemic circulation (approximately 55 µM). After CCl_4 intoxication there was a time-dependent increase in ammonia that peaked on days one and two after injection. Although it was increased at all positions where the blood was collected, ammonia was low in the heart blood compared to the hepatic and portal vein (Fig. 3.7). By day four after CCl_4 injection, ammonia concentrations returned to the basal level in the portal vein and systemic circulation. In contrast, in hepatic vein blood it remained approximately two fold higher compared to the control, which took almost one month for recovery.

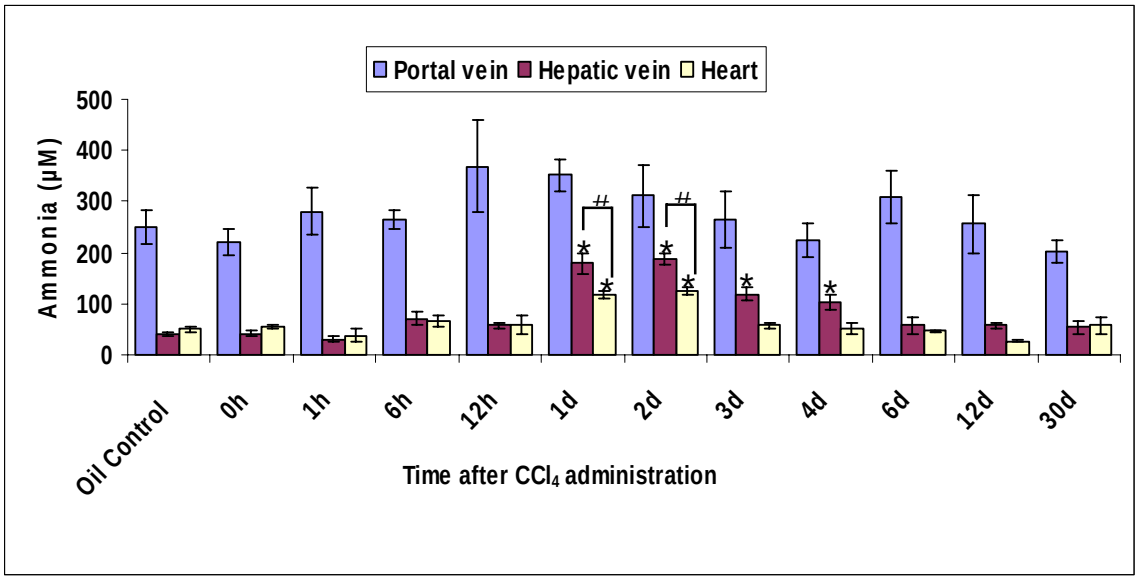

Fig. 3.7: Concentrations of ammonia (µM) in plasma obtained from the portal vein, the hepatic vein and the heart of mice at different time intervals after injection of 1.6 g/kg CCl_4. The control mice had high ammonia concentration in the portal vein and lower levels in the hepatic vein and heart blood. After CCl_4 injection, ammonia increased at all positions of the mice with peak concentrations measured on days one and two after injection. By day four, ammonia recovered in the portal vein and heart blood while it took one month for recovery in hepatic vein. Data are mean ± S.E. of three mice per time point. * $P< 0.05$ compared to the corresponding control (0h). # $P< 0.05$ compared to the corresponding hepatic vein results.

Similar to the results of ammonia, glutamate concentration in the control mice was high in the portal vein (approximately 80µM) and very low in the hepatic vein (approximately 20µM), with a small increase in heart blood (approximately 36µM). After CCl_4 intoxication glutamate concentration was increased at the three measured positions of the vascular system especially at the time of pericentral necrosis (day one up to day four). The concentration of glutamate was lower in the heart blood compared to the hepatic and portal vein values. Six days after CCl_4 injection, glutamate levels recovered in the portal vein and heart blood, while it took almost one month for glutamate levels to reach the basal level in the hepatic vein blood (Fig. 3.8).

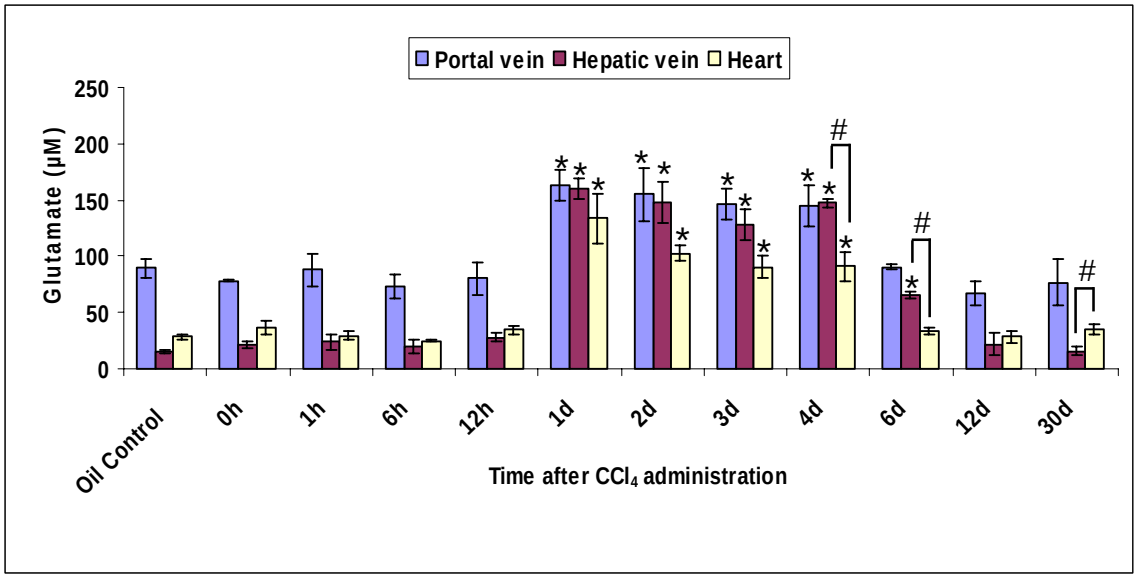

Fig. 3.8: Concentrations of glutamate (µM) in plasma obtained from the portal vein, the hepatic vein and the heart of mice at different time intervals after injection of 1.6 g/kg CCl_4. Glutamate in the control mice is very high in the portal vein and minimal in hepatic vein and heart. After CCl_4 injection; glutamate increased at all positions of the mice especially from day one up to day four. By day six, glutamate levels recovered in the portal vein and heart blood, while in hepatic vein it took one month for recovery. Data are mean ± S.E. of three mice per time point. * P< 0.05 compared to the corresponding control (0h). # P< 0.05 compared to the corresponding hepatic vein results.

In contrast to ammonia and glutamate, glutamine levels were not significantly different between the portal and hepatic vein values, and only slightly increased in heart blood. After CCl_4 intoxication, glutamine was markedly elevated in the systemic circulation and also in the portal vein in a time dependent manner, peaking on day one after injection and returning to the basal level one month after injection. In hepatic vein blood, glutamine concentration was lower than the control at most of the tested time points except on days one, two and three where it was slightly elevated. Twelve days after CCl_4 injection, the glutamine concentration became similar to the control (Fig. 3.9). In the case of urea there was no observable difference between the three measured positions for both control and CCl_4-treated mice. A transient decrease in urea was recorded only at day one after CCl_4 injection at all positions in mice, while at all other time points, urea measurement was comparable to the control values (Fig. 3.10).

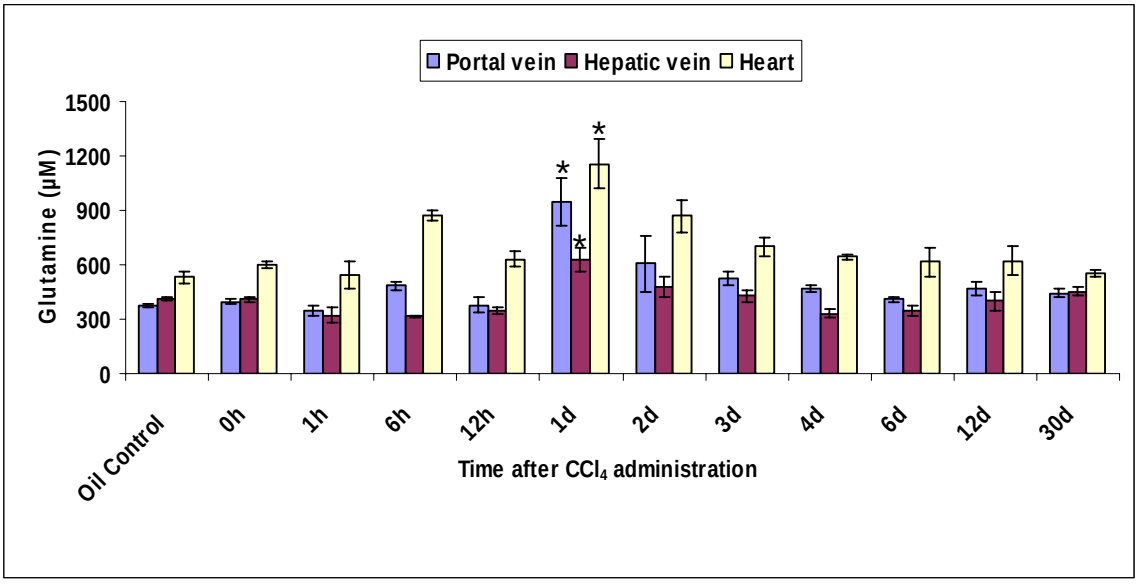

Fig. 3.9: Concentrations of glutamine (µM) in plasma obtained from the portal vein, the hepatic vein and the heart of mice at different time intervals after injection of 1.6 g/kg CCl_4, showing marked elevation of glutamine in heart and portal vein plasma with peak at day one and recovered 30days post injection. In hepatic vein; glutamine is lower than the control at most of the tested time points except days one,two& three, and become similar to control after 12days after injection. Data are mean ± S.E. of three mice per time point. * P< 0.05 compared to the corresponding control (0h).

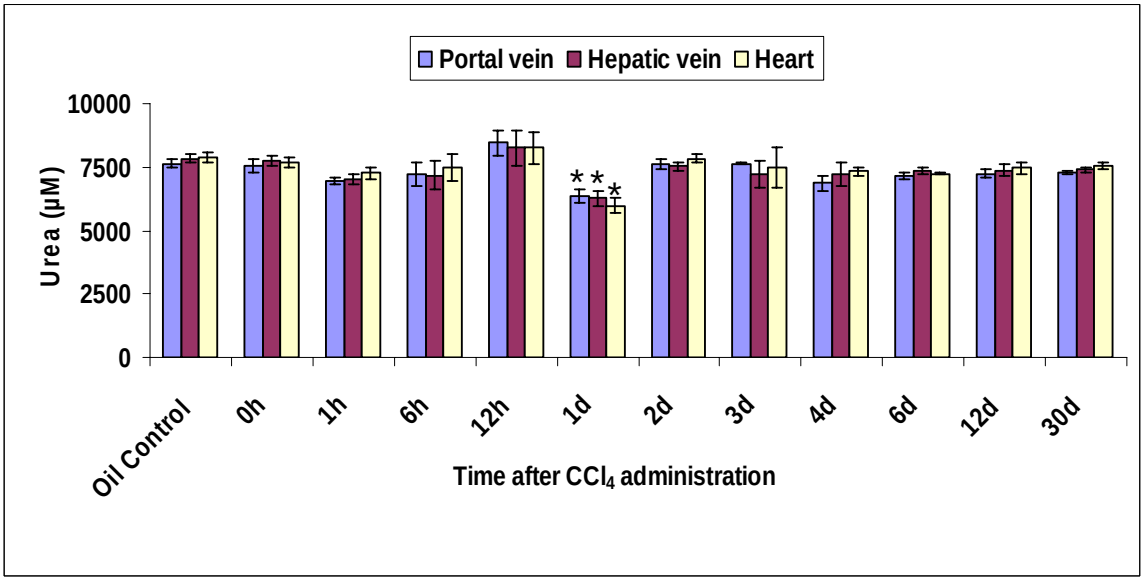

Fig. 3.10: Concentrations of urea (µM) in plasma obtained from the portal vein, the hepatic vein and the heart of mice at different time intervals after injection of 1.6 g/kg CCl_4, showing decreased blood urea concentration one day after CCl4 injection. Data are mean ± S.E. of three mice per time point. * P< 0.05 compared to the corresponding control (0h).

The glucose level was not changed between the plasma obtained from the portal vein, hepatic vein or heart of control mice. After CCl_4 injection, there was a transient hypoglycemia at all measured positions, which was lowest on day one following injection. By day six after CCl_4 injection, glucose values had returned to the normal levels at all positions (Fig. 3.11). In contrast to glucose there was a clear discrepancy in alanine concentration between portal vein, hepatic vein and heart of control mice. The highest value was in the portal vein (approximately 800µM), whereas it was minimal in hepatic vein (approximately 250µM) and increased again in the heart blood (approximately 450µM). Induction of liver damage by CCl_4 leads to the elevation of alanine at all positions of the mice with maximum concentration measured on day one after injection. Alanine levels returned to the basal level in portal vein and in the heart blood after six days, and after twelve days in hepatic vein blood (Fig. 3.12).

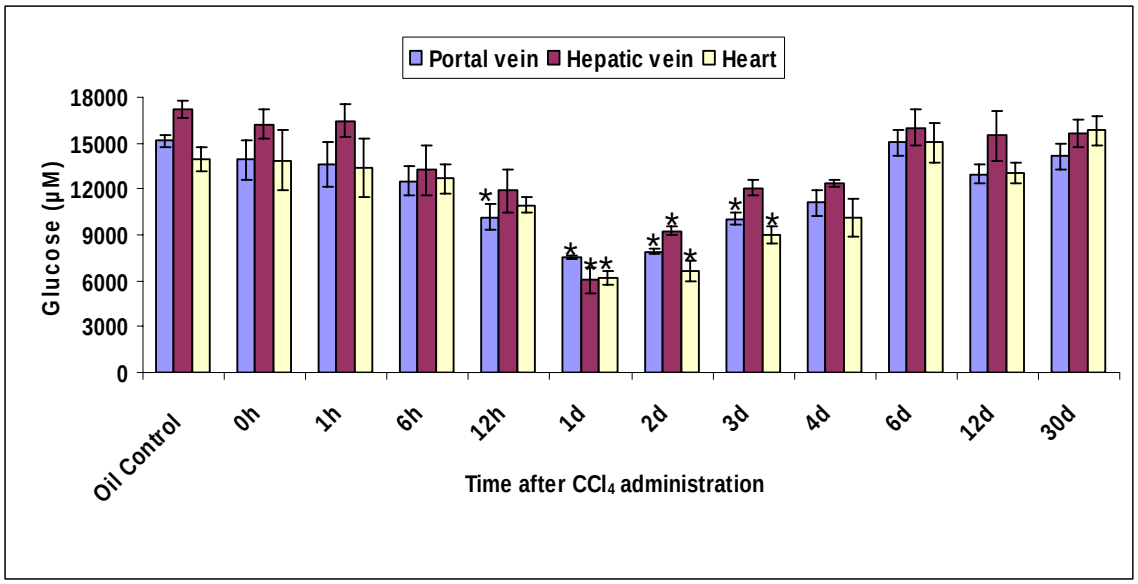

Fig. 3.11: Concentrations of glucose (µM) in plasma obtained from the portal vein, the hepatic vein and the heart of mice at different time intervals after injection of 1.6 g/kg CCl_4, showing marked hypoglycemia after CCl_4 injection especially on day one, and returned to the basal level by day six after injection. Data are mean ± S.E. of three mice per time point. * P< 0.05 compared to the corresponding control (0h).

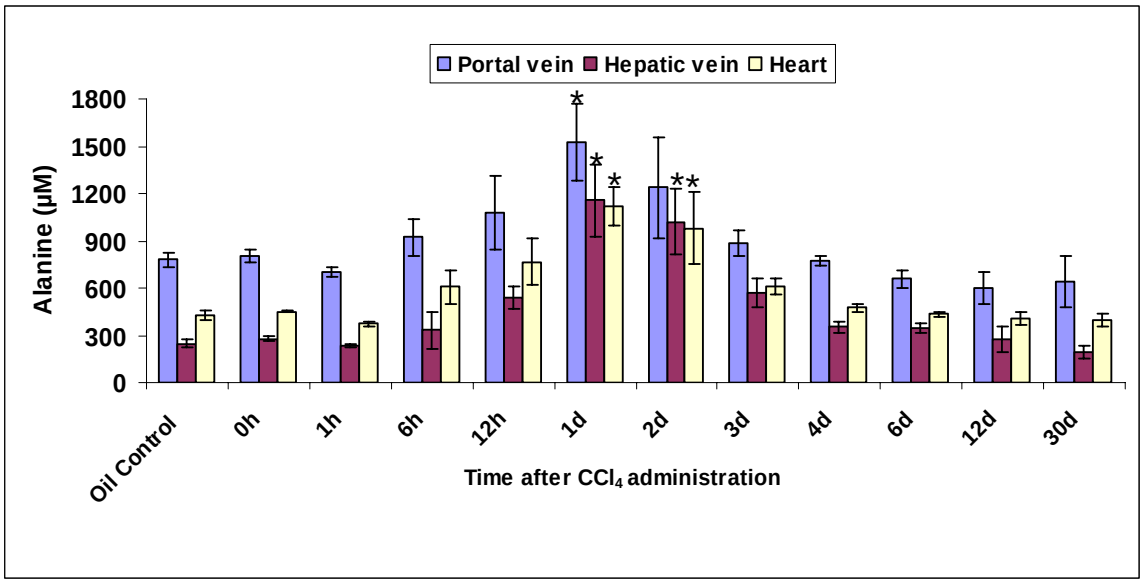

Fig. 3.12: Concentration of alanine (µM) in plasma obtained from the portal vein, the hepatic vein and the heart of mice at different time intervals after injection of 1.6 g/kg CCl_4. Alanine showed a marked elevation after CCl_4 injection especially on day one, and returned to the basal level by day six in portal vein and heart, and by day twelve in hepatic vein. Data are mean ± S.E. of three mice per time point. * P< 0.05 compared to the corresponding control (0h).

There was no clear discrepancy in either lactate and pyruvate levels between portal vein, hepatic vein or heart. Both metabolites were elevated time dependently after CCl_4 intoxication and reached the peak concentration one day after injection. The plasma concentrations of both metabolites returned to the basal level on day four post injection (Fig. 3.13 and 3.14).

In conclusion, CCl_4 induced liver damage leads to obvious alterations in ammonia and carbohydrate metabolism. The time period approximately one day after CCl_4 intoxication seems to be the most critical period showing the largest alterations of metabolic parameters.

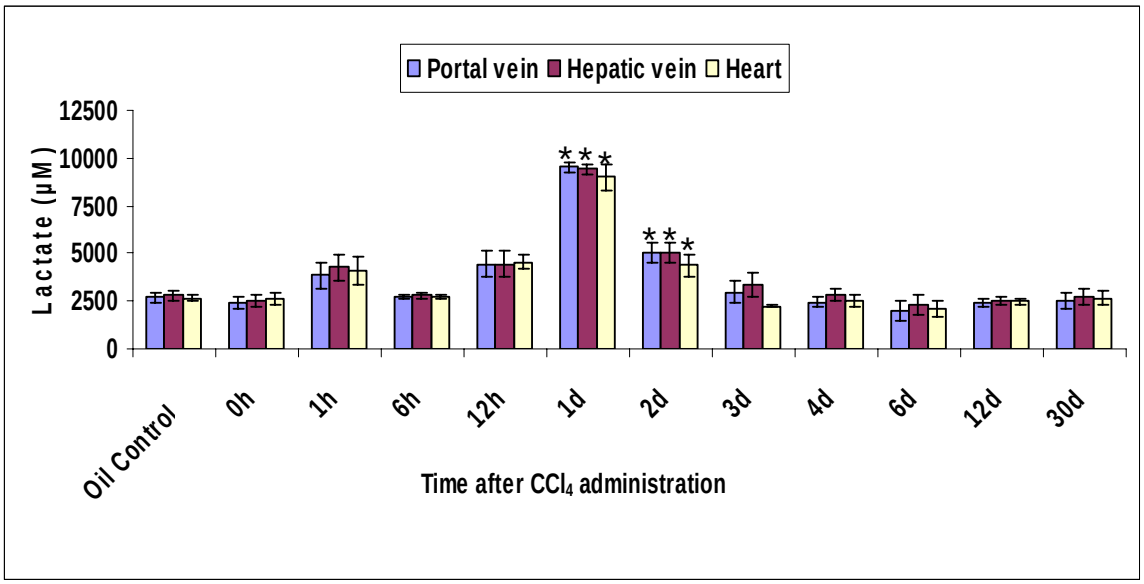

Fig. 3.13: Concentration of lactate (µM) in plasma obtained from the portal vein, the hepatic vein and the heart of mice at different time intervals after injection of 1.6 g/kg CCl_4. Lactate showed a marked elevation on day one after CCl_4 injection and returned to the basal level by day four. Data are mean ± S.E. of three mice per time point. * P< 0.05 compared to the corresponding control (0h).

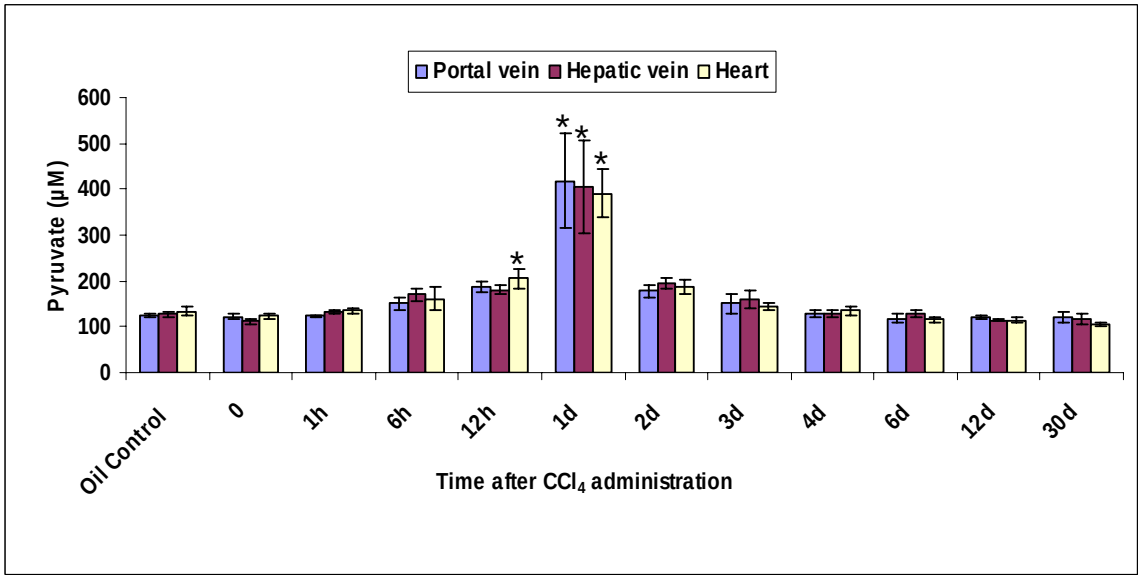

Fig. 3.14: Concentration of pyruvate (µM) in plasma obtained from three positions in mice at different time intervals after injection of 1.6 g/kg CCl_4. Pyruvate showed a marked elevation on day one after CCl_4 injection and returned to the basal level by day four. Data are mean ± S.E. of three mice per time point. * P< 0.05 compared to the corresponding control (0h).

3.1.3 Dose dependent induction of liver damage by CCl_4

As the metabolic alteration was most obvious at day one after CCl_4 intoxication, it became important to investigate the alteration of ammonia and carbohydrate metabolism after administration of different doses of CCl_4. For this purpose, mice received various doses of CCl_4 intraperitoneally (Fig. 3.15). Blood and liver samples were collected 24h after injection.

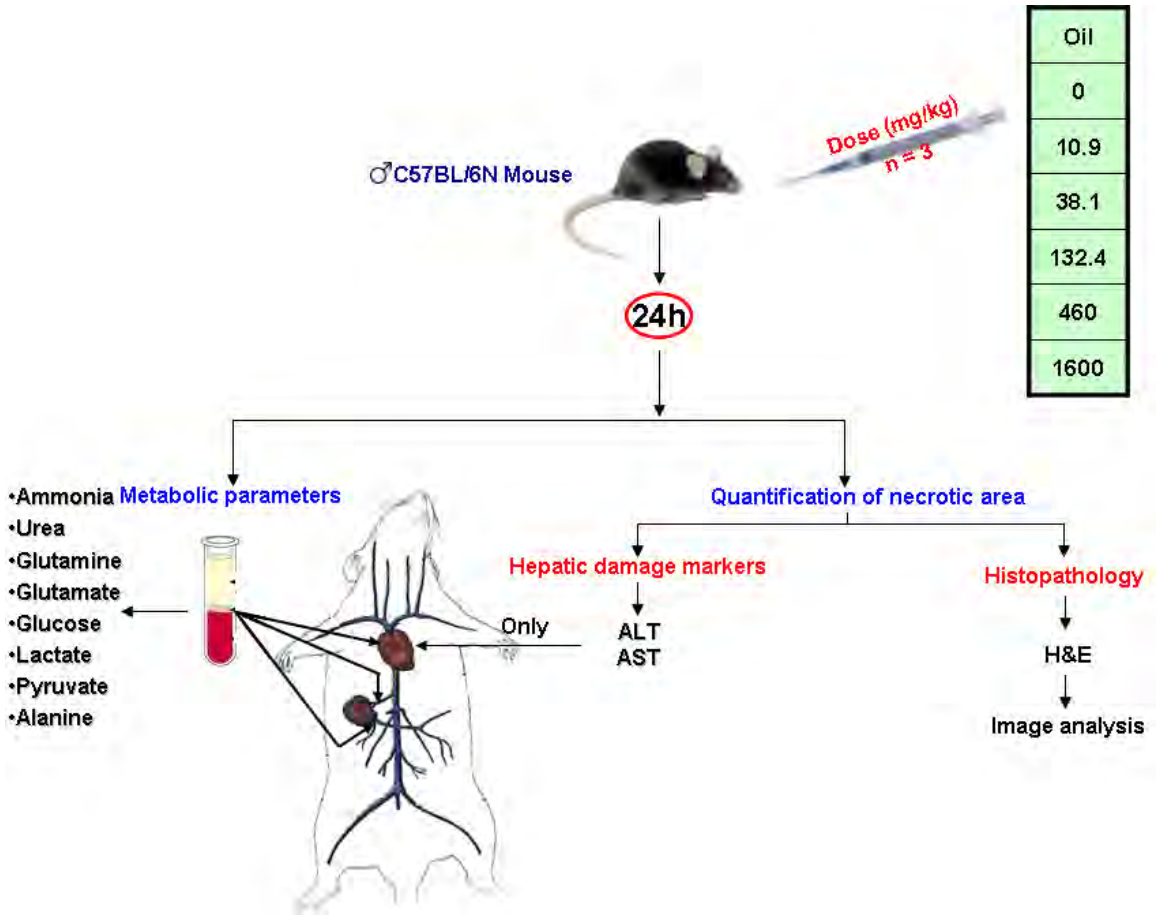

Fig. 3.15: Induction of liver damage by different doses of CCl_4. Mice received various i.p. injections of CCl_4 and 24h later, blood samples were collected from the portal vein, hepatic vein and the right heart chamber. Liver tissue was collected and stained with hematoxylin and eosin (H&E). Three mice were analyzed for each dose of CCl_4.

Grossly, the characteristic white spotted liver was observed only after injection of 132.4mg/kg CCl_4 and higher doses. Lower doses (38.1 and 10.9 mg/kg) failed to causes any macroscopic lesions (Fig. 3.16).

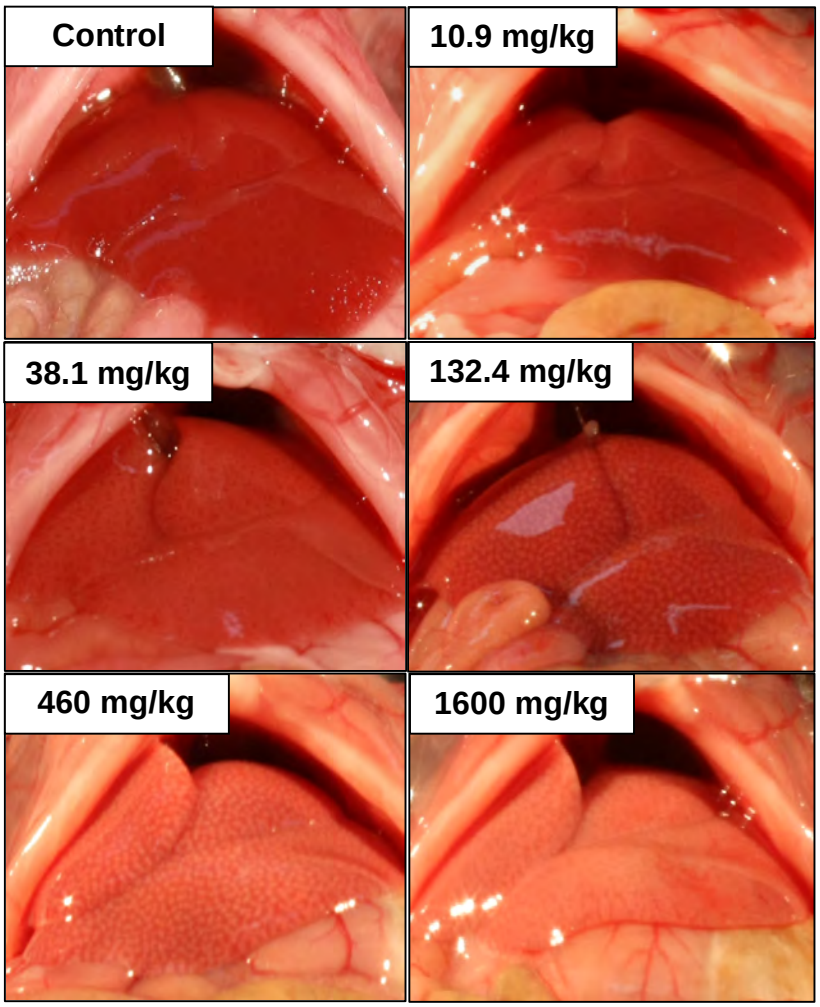

Fig. 3.16: Macroscopic appearance of mouse liver at day one after administration of different doses of CCl_4, showing a characteristic spotted pattern. The white spots are evident after injection of 132.4 mg/kg CCl_4 or higher doses, while the liver looks similar to the control after exposure to lower doses.

It was not known whether lowering the dose of CCl_4 decreased the diameter of necrotic lesions or caused a mosaic pattern, where the dead cell area still contains some living hepatocytes. To study this, formalin fixed paraffin embedded sections of liver tissue were stained with H&E and examined microscopically. The pericentral necrotic lesion was detectable only after injection of 132.4 mg/kg CCl_4 and higher doses, while the lower doses failed to induce any necrotic lesion. Interestingly, the dead cell area was completely free of any viable hepatocytes (Fig. 3.17).

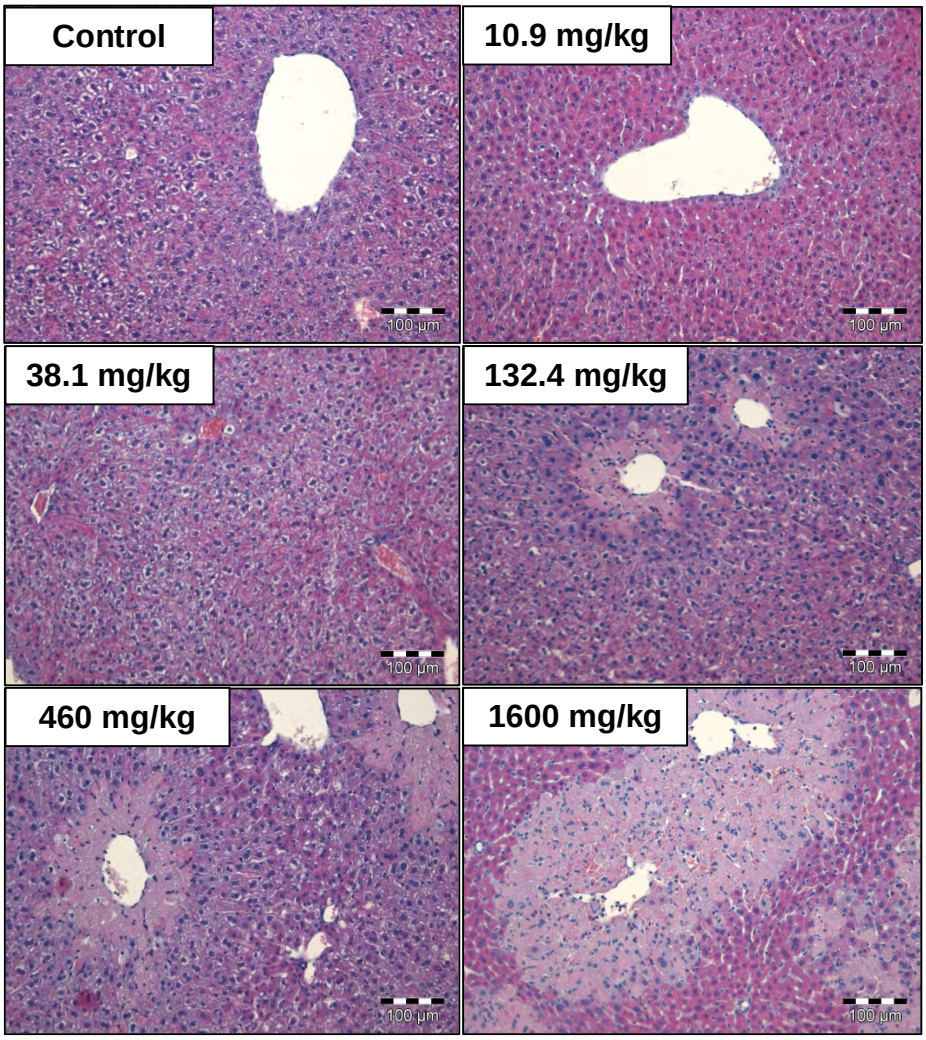

Fig. 3.17: Microscopic appearance of mouse liver at day one after administration of different doses of CCl_4. The liver shows dose related centrilobular necrosis. The necrotic area is free from any living hepatocytes. Hematoxylin and eosin staining, scale bars: 100µm

In order to quantify the lesion induced by each dose of CCl_4, the dead cell area was quantified using image analysis software. The highest diameter of the necrotic lesion was recorded after injection of the highest studied dose of 1.6 g/kg (approximately 38% of the total area). The diameter of this lesion decreased in a dose dependent manner to 14% after injection of 132.4 mg/kg (Fig. 3.18). With even lower doses the necrotic lesion was no longer detectable.

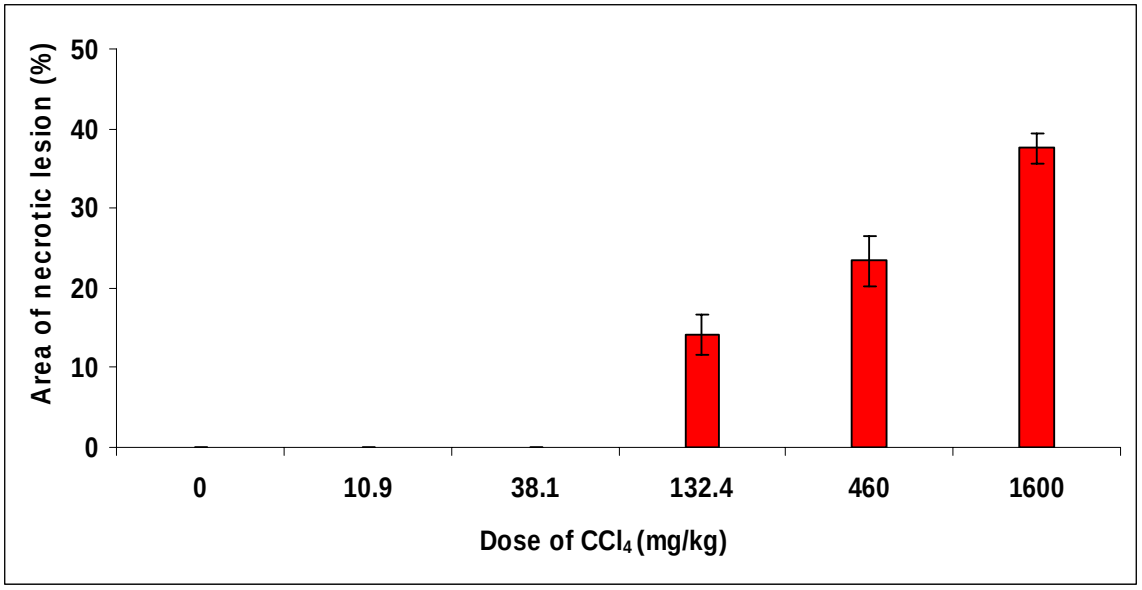

Fig. 3.18: The area of necrotic lesion (%) at day one after administration of different doses of CCl_4. The area of necrotic lesion is detectable after injection of 132.4 mg/kg CCl_4 and increased in a dose dependent manner by increasing the dose of CCl_4. The data are mean ± S.E. of three mice per time point.

Also, it was not clear whether the dead cell area only decreased in diameter due to the lower doses of CCl_4 or whether there were also a reduced number of necrotic lesions. To investigate this whole slide scans were done and all necrotic lesions were quantified manually. The result revealed that all doses of CCl_4 which induced necrotic lesions resulted in similar numbers of necrotic lesions (Fig. 3.19). Therefore, it seems that lowering the dose of CCl_4 reduces only the diameter of the necrotic area but not the total number of necrotic lesions.

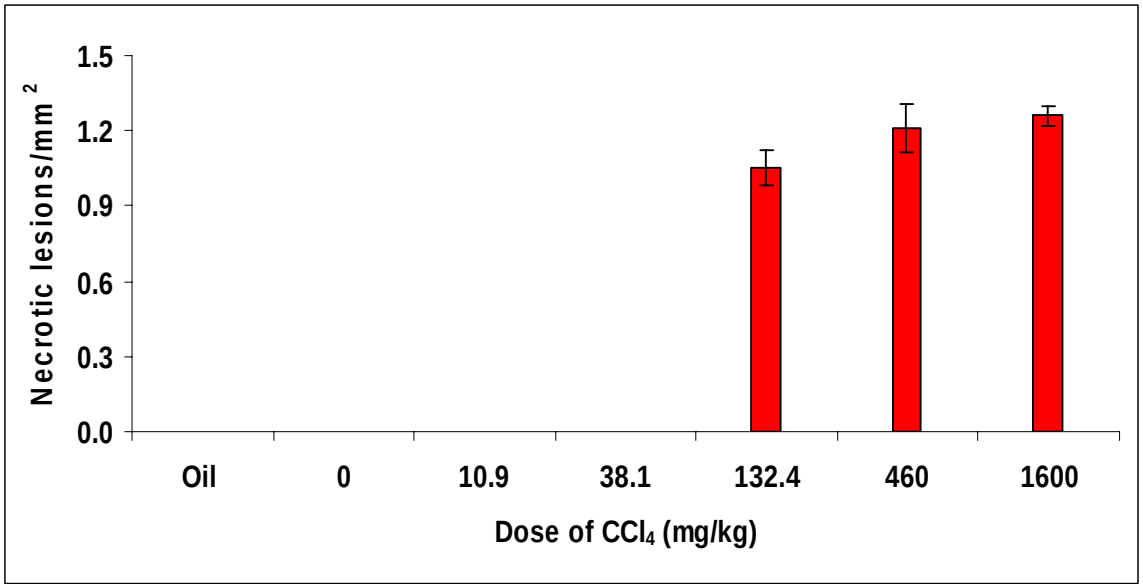

Fig. 3.19: Quantification of necrotic lesions/mm^2 in liver at day one after administration of different doses of CCl_4. For doses which induce necrotic lesion (132.4 mg/kg and higher) the liver showed a similar number of necrotic lesions. The data are mean ± S.E. of three mice per time point.

In addition, the dose dependent liver damage seen after CCl_4 injection was also controlled by the analysis of the liver enzymes ALT and AST. Both enzymes were elevated in a dose-dependent manner after CCl_4 administration (Fig. 3.20 and 3.21). In conclusion, administration of different doses of CCl_4 leads to dose-dependent alterations of liver tissue morphology.

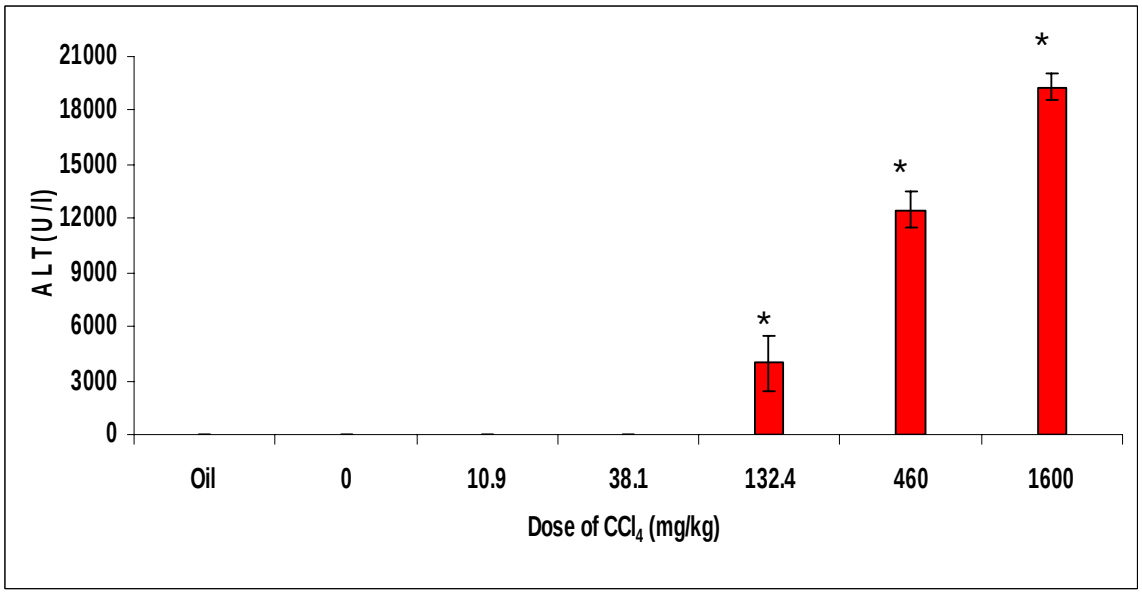

Fig. 3.20: Plasma alanine transminase (ALT) levels (U/l) at day one after administration of different doses of CCl_4. ALT increased in a dose-dependent manner after CCl_4 intoxication. Data were obtained from six mice per time point and were expressed as mean ± S.E. * P< 0.05 compared to controls (0).

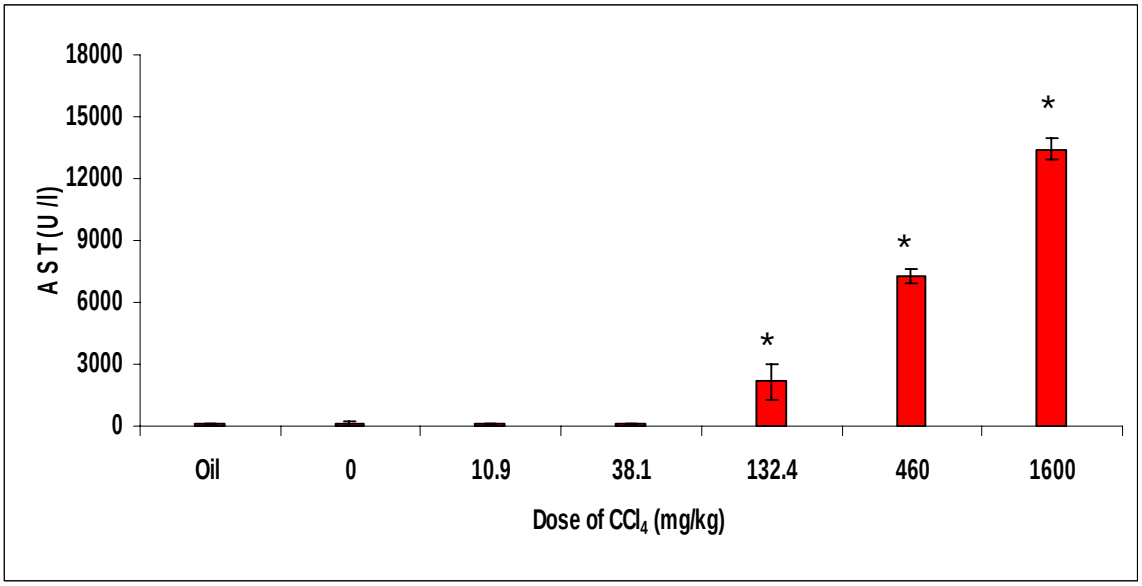

Fig. 3.21: Plasma aspartate transaminase (AST) levels (U/l) at day one after administration of different doses of CCl_4. AST increased in a dose dependent manner after CCl_4 intoxication. Data were obtained from six mice per time point and were expressed as mean ± S.E. * P< 0.05 compared to controls (0).

3.1.4 Relation between CYP2E1 expression and CCl_4 induced liver damage

After injection of 1.6 g/kg CCl_4, the diameter of the necrotic lesion reached the highest level, i.e. by increasing the dose of CCl_4 in contrast, the diameter of dead cell area did not increase. To investigate whether this was associated with the expression pattern of CYP2E1, the enzyme responsible for metabolic activation of CCl_4, formalin fixed paraffin embedded sections of liver tissue were immunostained using antibodies against CYP2E1. The control liver showed the typical pericentral zonation of CYP2E1. Injection of 132.4 mg/kg CCl_4 led to small central spots of dead cells surrounded by surviving CYP2E1 positive hepatocytes. By increasing the dose of CCl_4 (460 mg/kg), the diameter of the dead cell area increased and only a small rim of surrounding CYP2E1 positive hepatocytes remained visible. After injection of 1.6 g/kg CCl_4, all CYP2E1 positive hepatocytes were killed. Even with such a high dose (1.6 g/kg), the periportal region, which is negative for CYP2E1, did not show any morphological alterations (Fig. 3.22).

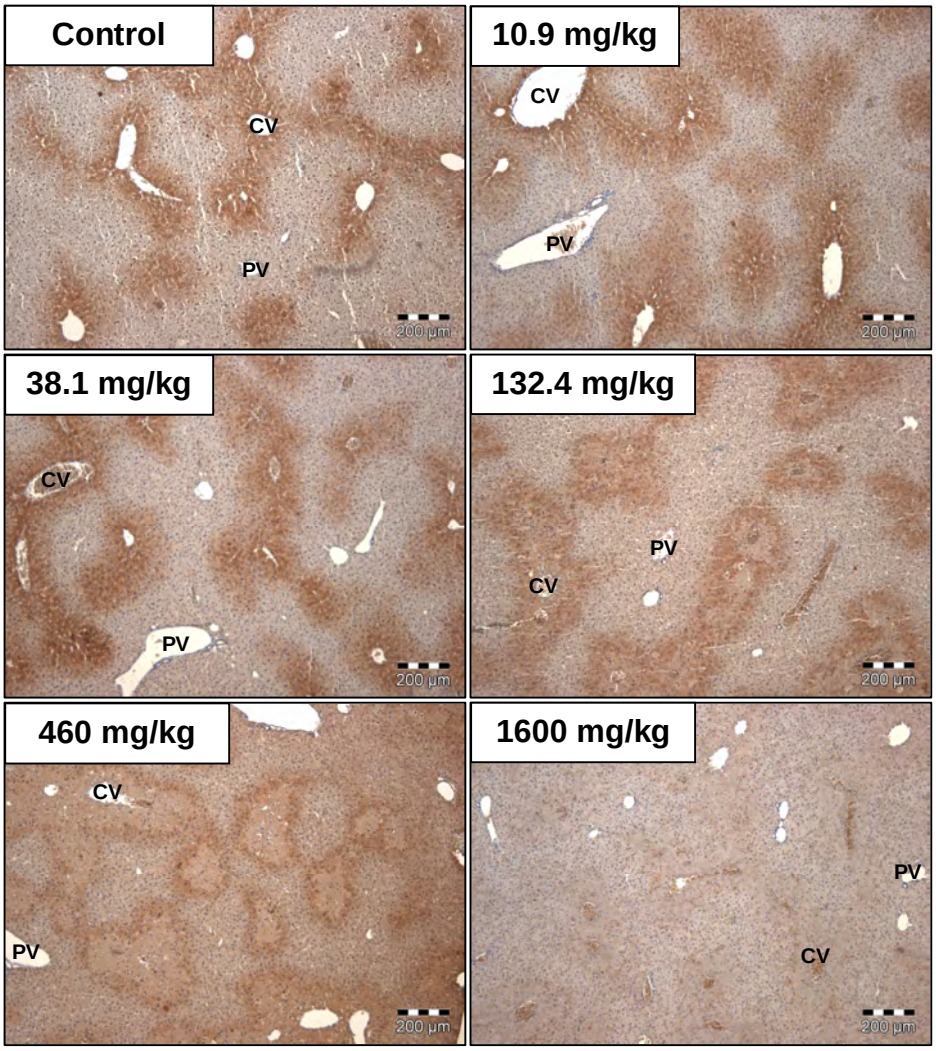

Fig. 3.22: Relationship of CYP2E1 expression and CCl_4 induced hepatotoxicity in mouse livers at day one after administration of different doses of CCl_4. The control liver shows the pericentral zonation of CYP2E1. Low doses of CCl_4 kill only the central fraction of CYP2E1 positive hepatocytes whereas after injection of 1.6 g/kg CCl_4 the entire area of CYP2E1 positive hepatocytes was killed. The periportal region, which is negative for CYP2E1, did not show any morphological alterations after CCl_4 intoxication. CV= central vein, PV= portal vein. Scale bars: 200µm.

3.1.5 Quantification of metabolic changes at various degrees of liver damage induced by CCl_4

The aim of this experiment was to quantify the changes of the metabolic function of the liver, specifically ammonia and carbohydrate metabolism, at various degrees of liver damage induced by injection of different doses of CCl_4. For this purpose, blood samples were collected from the three aforementioned positions (portal vein, hepatic vein and heart) in each mouse on day one after CCl_4 injection. Then plasma was separated and various metabolic parameters relevant for ammonia and carbohydrate metabolism were analyzed.

Ammonia and glutamate analysis showed the previously mentioned discrepancies between portal vein, hepatic vein and heart in the control group. CCl_4 intoxication caused a dose dependent elevation of ammonia and glutamate concentrations at all three analyzed positions of vascular system (Fig. 3.23 and 3.24). Even with the highest dose (1.6 g/kg), ammonia and glutamate were lower in the heart blood compared to the hepatic and portal vein. In contrast, a dose dependent elevation of glutamine concentration was measured in the heart blood after CCl_4 injection (Fig. 3.25). The urea assay did not show any changes in CCl_4 treated groups compared to controls, except for the highest tested dose (1.6 g/kg), where urea concentrations were slightly lower compared to controls (Fig. 3.26).

The glucose assay after induction of liver damage by different doses of CCl_4 revealed a dose-dependent hypoglycemia (Fig. 3.27). In contrast, alanine, lactate and pyruvate analyses showed dose-dependent elevations at all analyzed positions of the vascular system (portal vein, hepatic vein and heart) after CCl_4 intoxication (Fig. 3.28; 3.29 and 3.30). In conclusion, the degree of alterations in metabolic function of the liver was associated with the degree of liver damage.

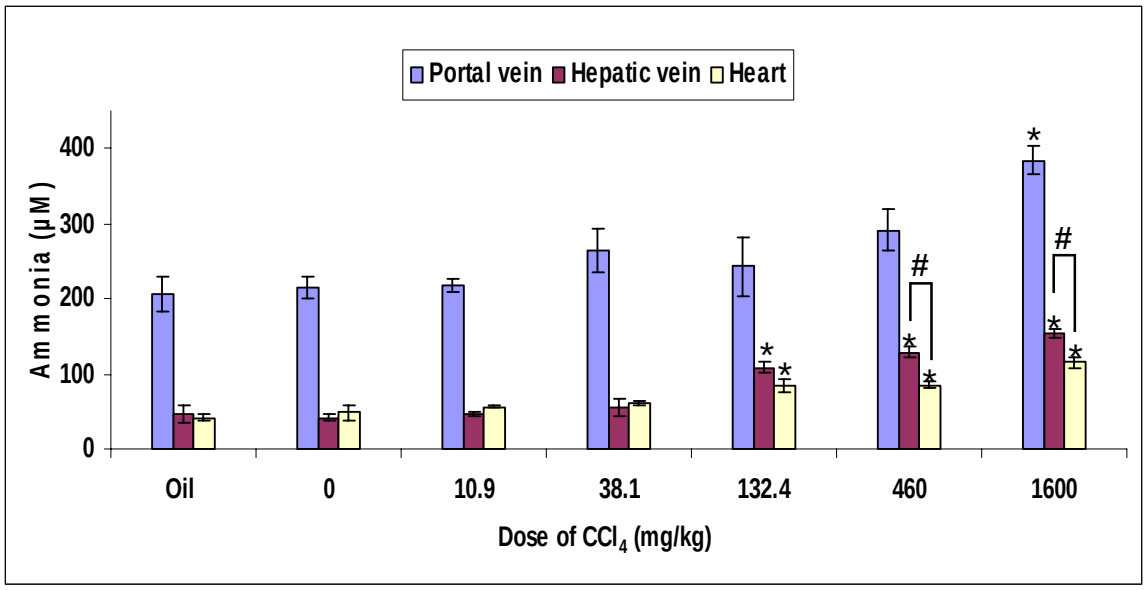

Fig. 3.23: Concentration of ammonia (µM) in plasma obtained from three positions in mice at day one after administration of different doses of CCl_4. The control mice show high ammonia concentrations in the portal vein and low ammonia concentrations in the hepatic vein and heart blood. After CCl_4 injection, ammonia increased at all positions of the mice in a dose-dependent manner. Data are mean ± S.E. of three mice per time point. * P< 0.05 compared to controls (0). # P< 0.05 compared to the corresponding hepatic vein results.

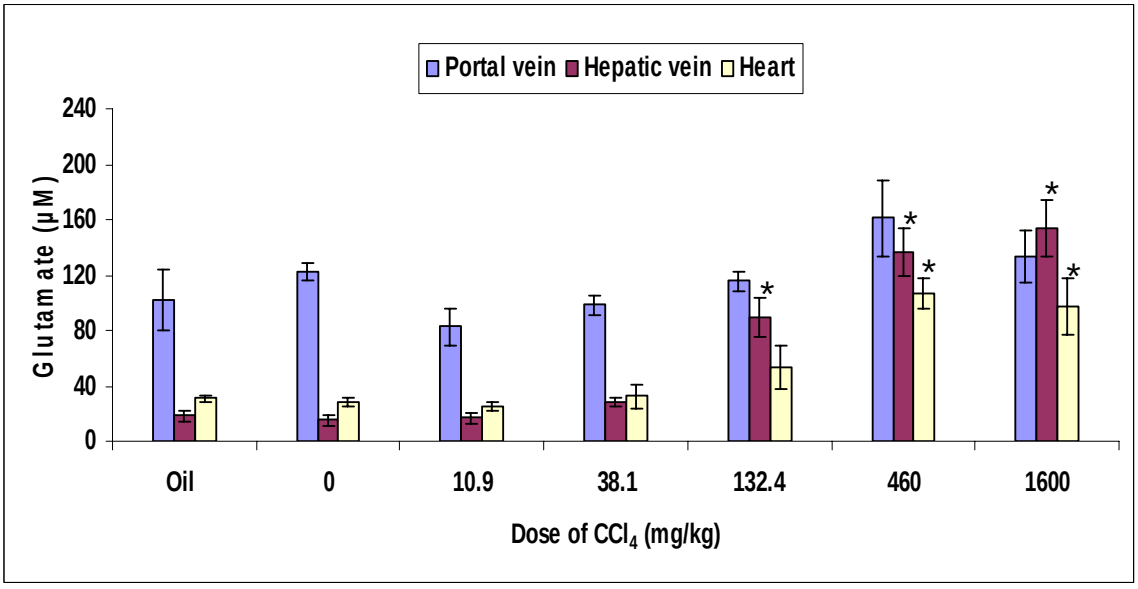

Fig. 3.24: Concentration of glutamate (µM) in plasma obtained from three positions in mice at day one after administration of different doses of CCl_4. In control mice glutamate concentrations were high in the portal vein and were low in the hepatic vein and heart blood. After CCl_4 injection, glutamate increased at all positions of the mice in a dose-dependent manner. Data are mean ± S.E. of three mice per time point. * P< 0.05 compared to controls (0).

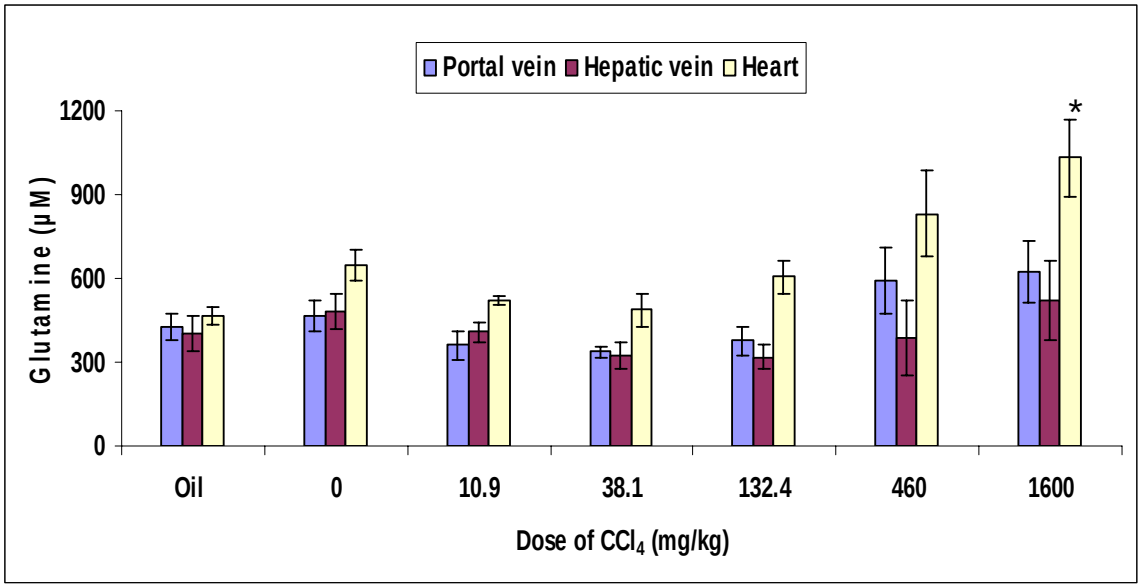

Fig. 3.25: Concentration of glutamine (µM) in plasma obtained from three positions in mice at day one after administration of different doses of CCl_4. There is a dose-dependent elevation of glutamine in heart blood after CCl_4 intoxication. Data are mean ± S.E. of three mice per time point. * P< 0.05 compared to controls (0).

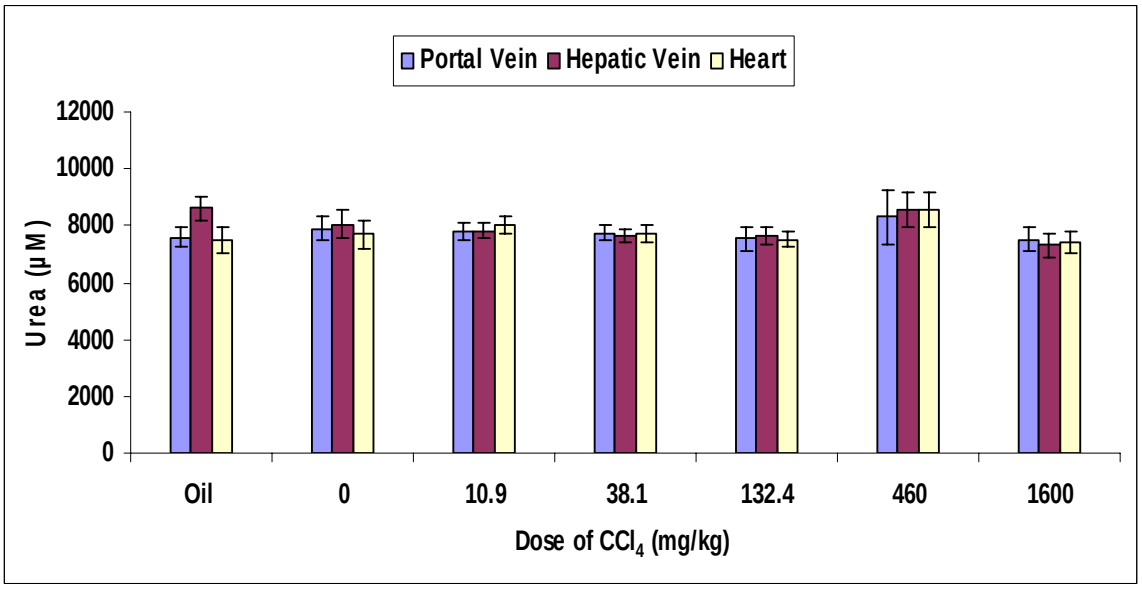

Fig. 3.26: Concentration of urea (µM) in plasma obtained from three positions in mice at day one after administration of different doses of CCl_4. Only after injection of the highest dose of CCl_4 (1.6 g/kg), a slight reduction of blood urea concentrations was observed. Data are mean ± S.E. of three mice per time point.

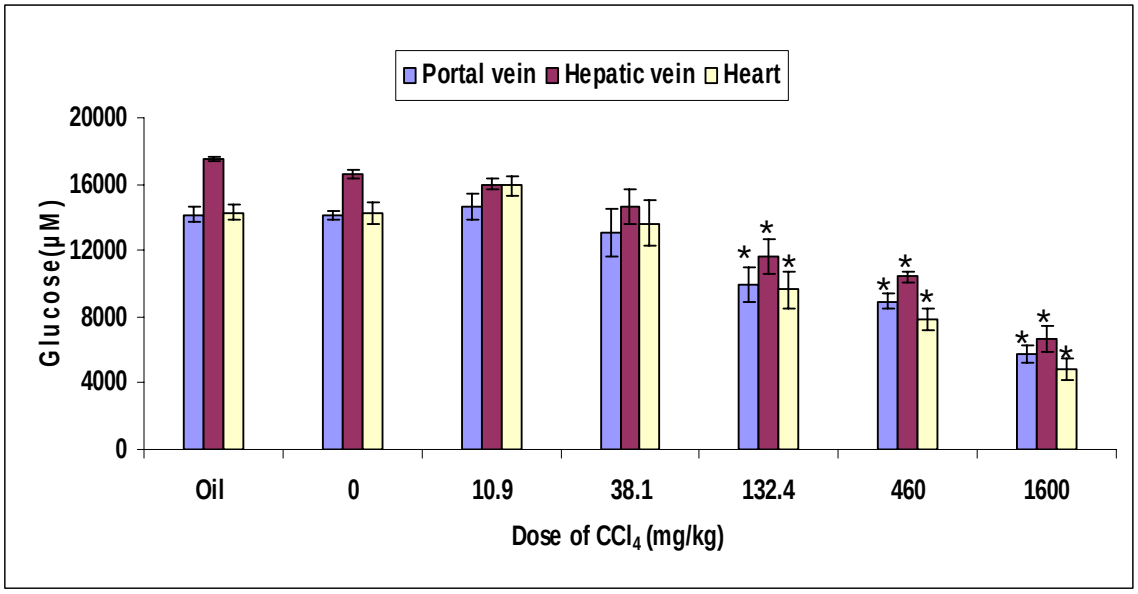

Fig. 3.27: Concentration of glucose (µM) in plasma obtained from three positions in mice at day one after administration of different doses of CCl_4, showing dose-dependent hypoglycemia at all positions of the mice. Data are the mean ± S.E. of three mice per time point. *P< 0.05 compared to controls (0).

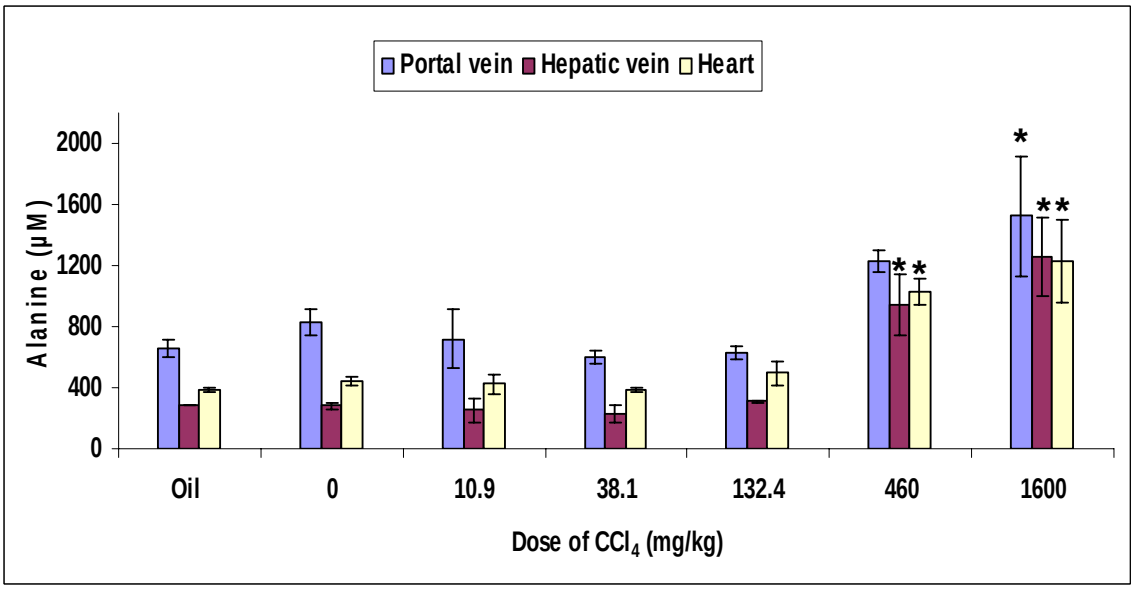

Fig. 3.28: Concentration of alanine (µM) in plasma obtained from three positions in mice at day one after administration of different doses of CCl_4, showing dose-dependent elevation at all positions of the mice. Data are mean ± S.E. of three mice per time point. * P< 0.05 compared to controls (0).

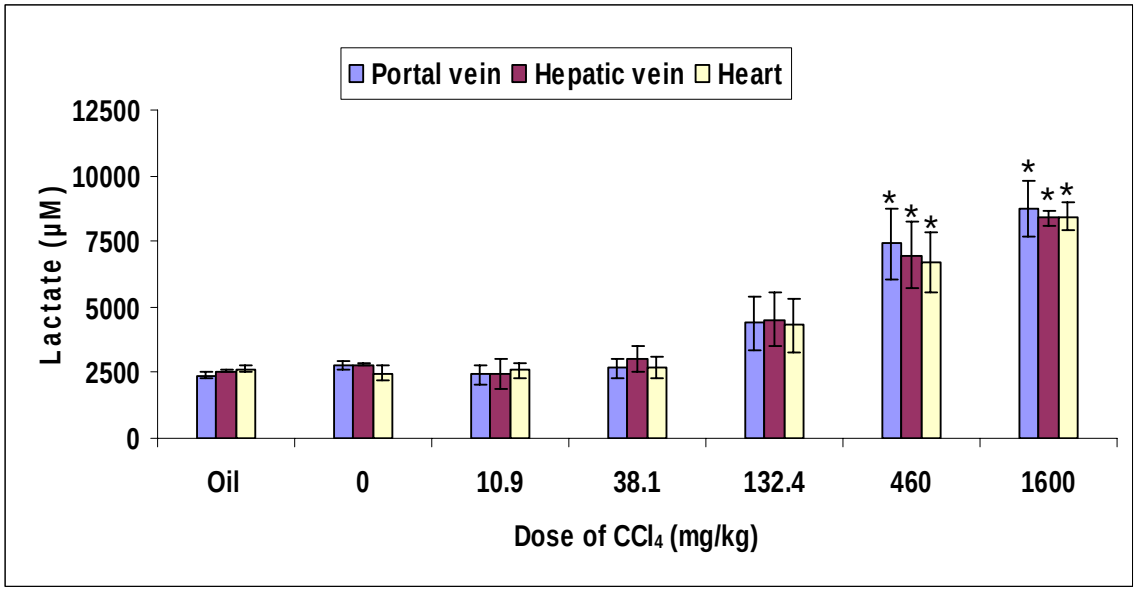

Fig. 3.29: Concentration of lactate (µM) in plasma obtained from three positions in mice at day one after administration of different doses of CCl_4, showing dose-dependent elevation at all positions of the mice. Data are mean ± S.E. of three mice per time point. * P< 0.05 compared to controls (0).

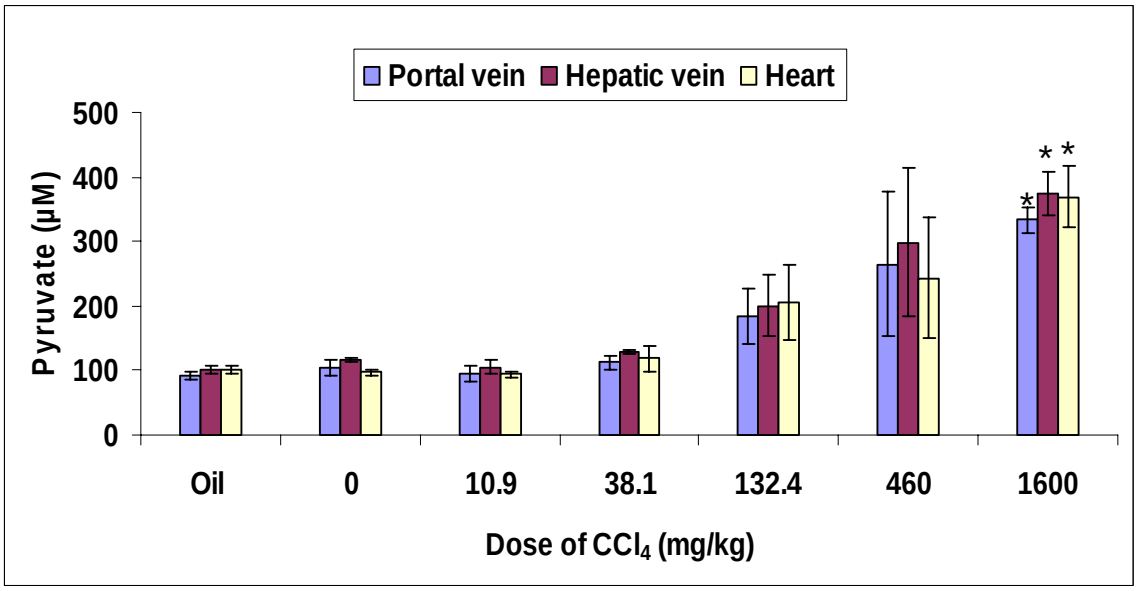

Fig. 3.30: Concentration of pyruvate (µM) in plasma obtained from three positions in mice at day one after administration of different doses of CCl_4, showing dose-dependent elevation at all positions of the mice. Data are means ± S.E. of three mice per time point. * P< 0.05 compared to controls (0).

3.2 Modelling of ammonia detoxification during liver damage and regeneration

3.2.1 Establishment of a metabolic model

In the previous section I have shown how liver damage influences the levels of metabolites involved in ammonia metabolism. A next question of interest is whether these changes in metabolites can be explained by a mathematical metabolic model that includes all known pathways of ammonia detoxification. Therefore a metabolic model was established (Fig. 3.31).

Ammonia detoxification occurs in both the periportal and the pericentral compartment of the liver lobule. The periportal compartment involves the glutaminase reaction and the urea cycle. The pericentral compartment involves the glutamine synthetase reaction. Glutaminase enzyme catalyzes the degradation of glutamine into ammonia and glutamate. Ammonia is then metabolized through the urea cycle into urea. Urea cycle is a high capacity low affinity system for ammonia detoxification. Ammonia that escapes the urea cycle in the periportal compartment can be metabolized by glutamine synthetase in the pericentral compartment into glutamine. Thus, glutamine degraded by glutaminase in the periportal compartment of the liver lobule is re-synthesized by glutamine synthetase in the pericentral compartment. Urea formation is the permanent pathway for the detoxification of ammonia. In contrast, glutamine formation is a temporary pathway for ammonia detoxification acting as a scavenger for ammonia that escapes the urea cycle.

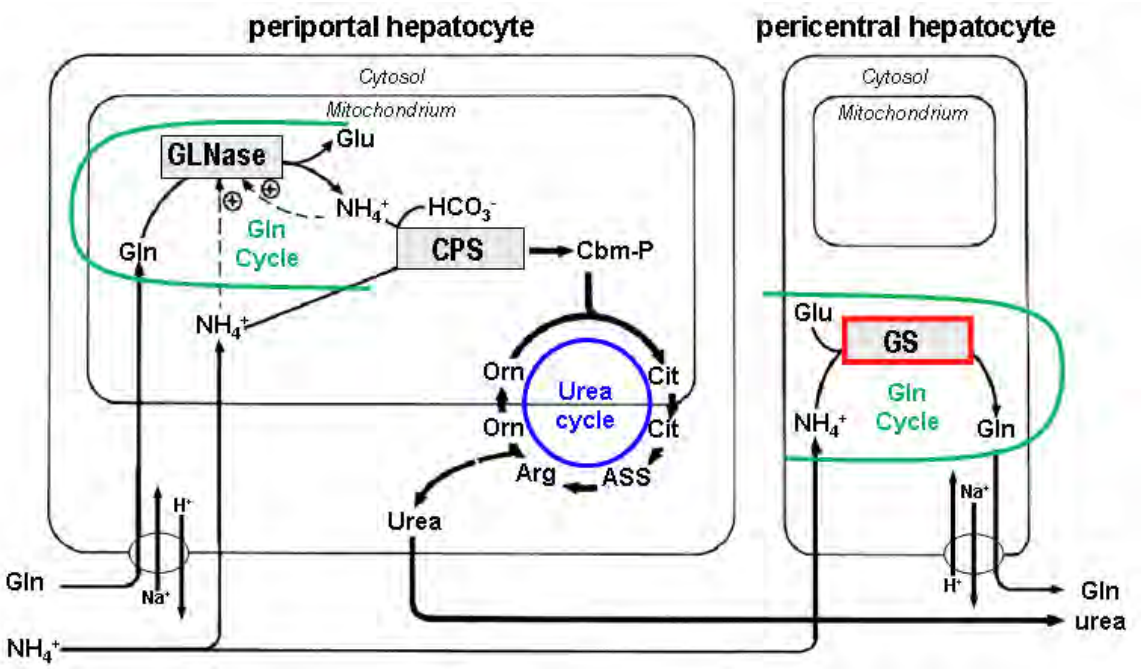

Fig. 3.31: Ammonia detoxification along the periportal (pp) and the pericentral (pc) compartment of the liver lobule: Ammonia passes to the liver through portal vein in the form of free ammonia and glutamine. Glutamine is then metabolized in the pp by glutaminase to form ammonia and glutamate. Ammonia is firstly metabolized permanantly through the urea cycle into urea, and any ammonia that escapes the urea cycle in the pp can be temporarly scavenged by glutamine synthetase in the PC to form glutamine. Thus glutamine breackdown by the glutaminase in the periportal compartment is re-synthesized by glutamine synthetase in the pericentral compartment.

The model is a two compartment model consisting of differential equations for the main metabolites, glutamine, ammonia and urea. In the periportal (pp) compartment, the glutaminase and the carbamoyl-phosphate synthetase (representing the urea cycle) reactions take place, whereas in the pericentral compartment (PC) the glutamine synthetase reaction occurs. Therefore, three main reactions were involved:

a) Glutaminase (G, periportal):

L-glutamine + H_2O → L-glutamate + NH_4^+

b) Carbamoyl-Phosphate Synthetase (CPS, periportal):

2ATP + NH_4^+ + CO_2 + H_2O → 2 ADP + phosphate + carbamoyl phosphate

Simplified sum reaction of CPS and urea cycle enzymes: NH_4^+ → 1/2Urea.

c) Glutamate-Ammonia Ligase (Glutamine Synthetase = GS, pericentral):

ATP + L-glutamate + NH_4^+ → ADP + phosphate + L-glutamine

Based on these three reactions, three state variables (entities or species that are supposed to change over time) were defined: glutamine, urea and ammonia. The change of these state variables described by inflows (portal vein values) and outflows (hepatic vein values) was modeled by ordinary differential equations (Fig. 3.32). For every measured time point, a steady-state was assumed.

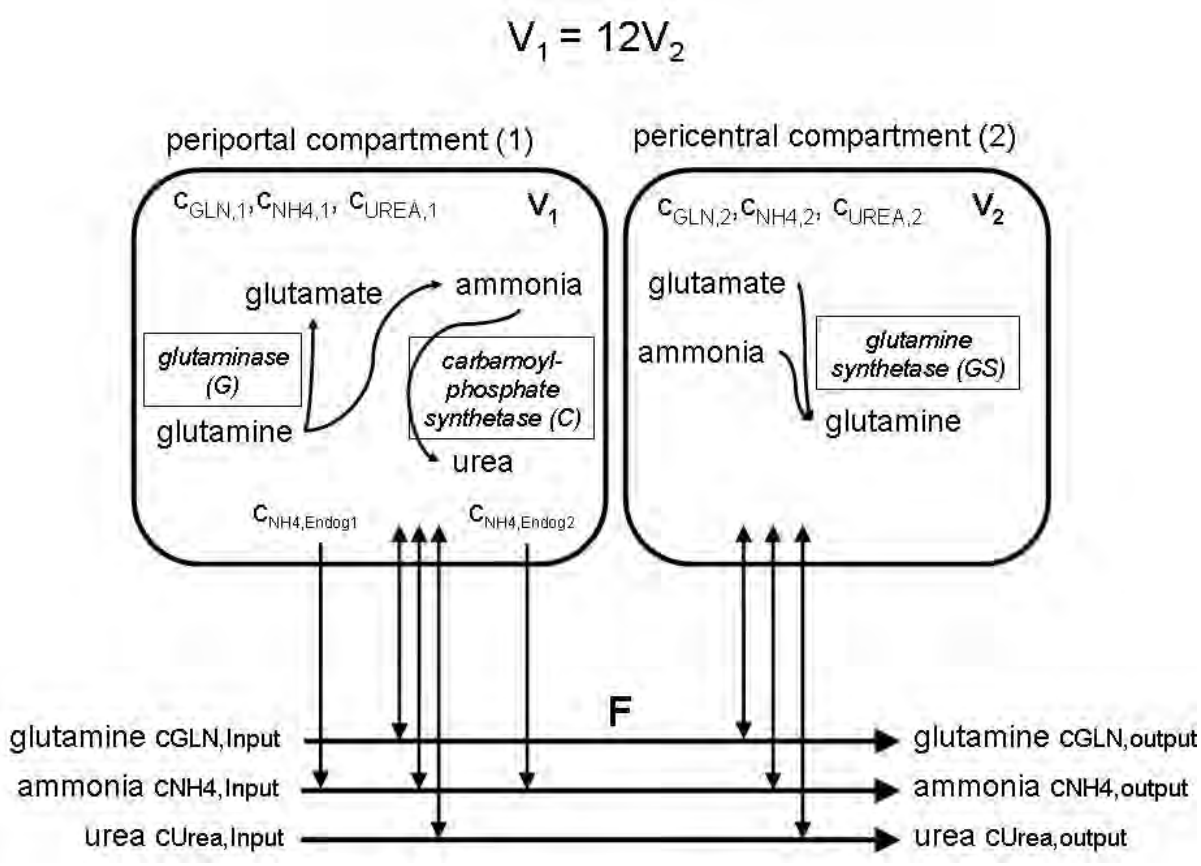

Fig. 3.32: Ammonia detoxification model. Glutamine, ammonia and urea enter ($c_{GLN,Input}$, $c_{NH4,Input}$, $c_{Urea,Input}$) and leave ($c_{GLN,output}$, $c_{NH4,output}$, $c_{Urea,output}$) the model structure at defined concentrations and a defined flow (F). The molecules can be taken up or released by both the periportal PP (1) and the pericentral compartment PC (2) as indicated by arrows. In the PP glutamine is degraded by *glutaminase (G)* to glutamate and ammonia. Ammonia is then converted to urea {*carbamoyl phosphate synthetase* (*C*)}. The concentrations of glutamine, ammonia and urea within the PP (1) are indicated by $c_{GLN,1}$, $c_{NH4,1}$ and $c_{UREA,1}$. In the PC glutamine is generated from ammonia and glutamate {*glutamine synthetase* (*GS*)}. Here the concentrations are given by $c_{GLN,2}$, $c_{NH4,2}$ and $c_{UREA,2}$. The volumes of the PP and the PC compartment are defined as V_1 and V_2, respectively. Ammonia is released from the PP ($C_{NH4, endog1}$) and close to the PC ($C_{NH4, endog 2}$).

3.2.2 Model simulation of experimental data

In order to model the changes of ammonia detoxification during liver damage and regeneration, a single dose of 1.6 g/kg CCl_4 was injected i.p. into mice (as described in section one). The changes in ammonia, urea and glutamine between the portal vein and hepatic vein were simulated using the described model. Interestingly, a transient discrepancy between the experimental and the simulated data was identified. The experimental data for ammonia and glutamine were less than the model prediction, especially for glutamine on days four and six after intoxication (Fig. 3.33 and 3.34).

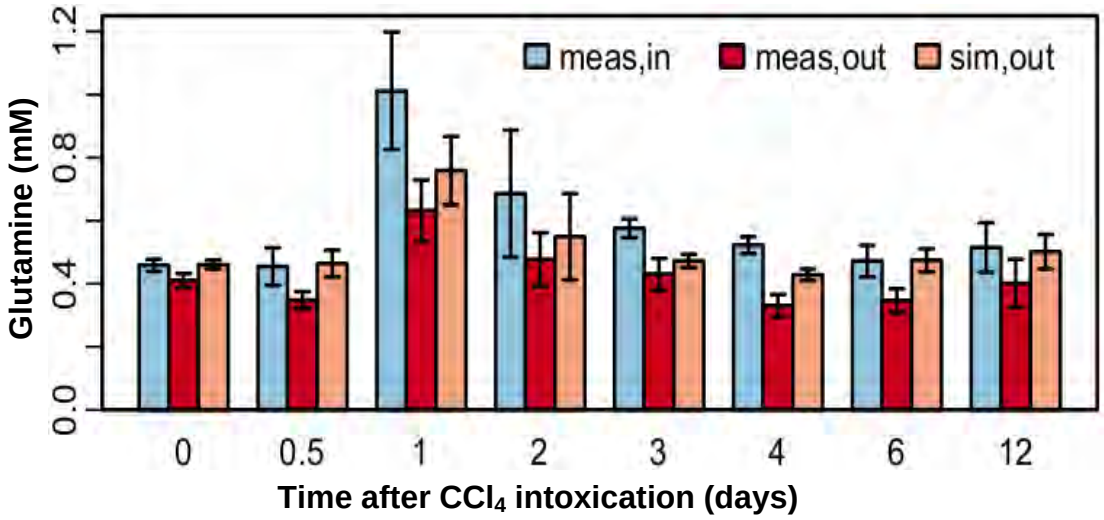

Fig. 3.33: Discrepancy between the measured (red) and simulated (orange) glutamine output (in hepatic vein) after CCl_4 intoxication. The measured glutamine is less than the model prediction at all tested time points especially on days four and six after CCl_4 injection. Data are mean ± S.D. of three mice per time point.

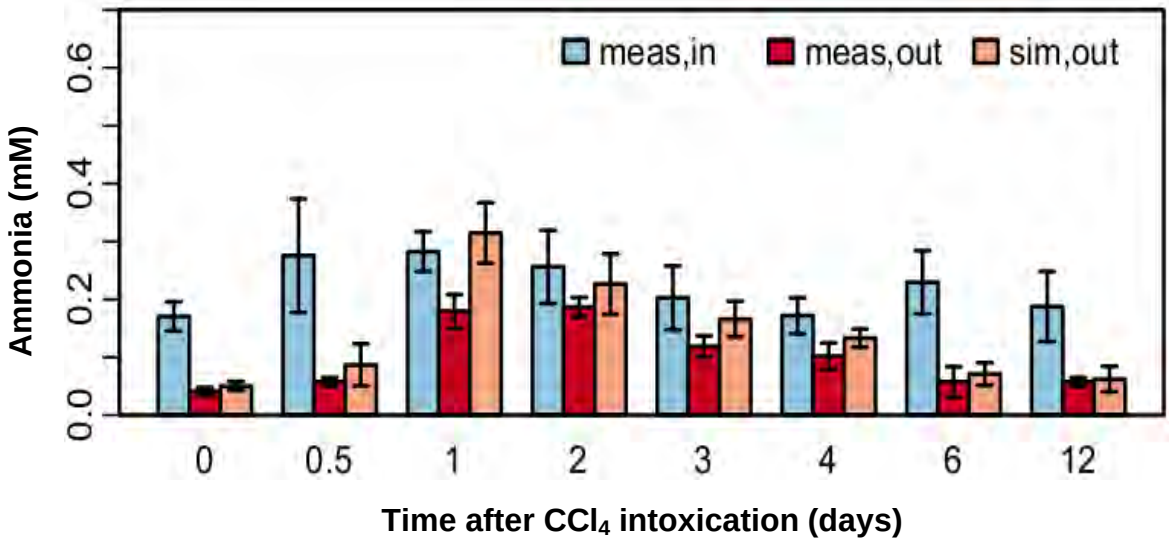

Fig. 3.34: Discrepancy between the measured (red) and simulated (orange) ammonia output (in hepatic vein) after CCl_4 intoxication. The measured ammonia is less than the model prediction at most of the tested time points, particularly on day one after CCl_4 injection. Data are mean ± S.D. of three mice per time point.

3.2.3 Delayed recovery of glutamine synthetase after CCl_4 intoxication

In order to find the reason for the deviations between the measured and simulated glutamine, the recovery of the glutamine synthetase (GS) was traced after CCl_4 intoxication. For this purpose, RNA was isolated from frozen liver tissue to quantify the relative RNA expression of GS by qPCR. Moreover, at the protein level the activity of GS was measured from frozen liver tissue. In addition, formalin fixed paraffin embedded liver sections were immunostained using antibodies against glutamine synthetase. qPCR analysis of GS after CCl_4 intoxication revealed lower levels of GS as early as six hours post injection. GS expression returned to controls levels one month after CCl_4 injection (Fig. 3.35).

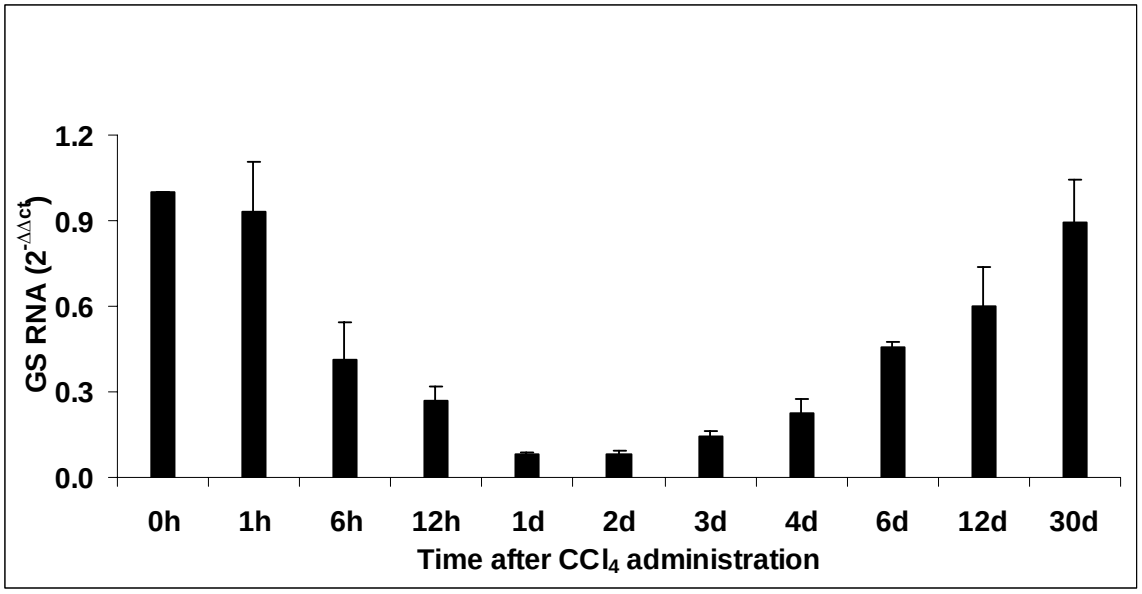

Fig. 3.35: Relative RNA expression of glutamine synthetase (GS) in a time course after injection of 1.6 g/kg CCl_4, showing transient down regulation. One month after CCl_4 intoxication, GS expression was similar to controls. Data are mean ± S.D. of three mice per time point.

This was also confirmed at the protein level by the GS activity assay. GS activity was almost completely lost from day two up to day four post injection. By day six, GS activity began to recover, whereas full recovery was reached only after one month following CCl_4 injection (Fig. 3.36). In addition, immunostaining of GS showed the normal pericentral localization of GS in the control mice. After CCl_4 intoxication, GS staining was lost in a time dependent manner. At day four post injection, the liver stained completely negative for GS. By day six, a very faint staining was seen, while after twelve days it became similar to the control situation (Fig. 3.37). From all these data, it is clear that despite the complete recovery of the damaged tissue by day six after intoxication, the recovery of GS activity was delayed up to one month after CCl_4 administration.

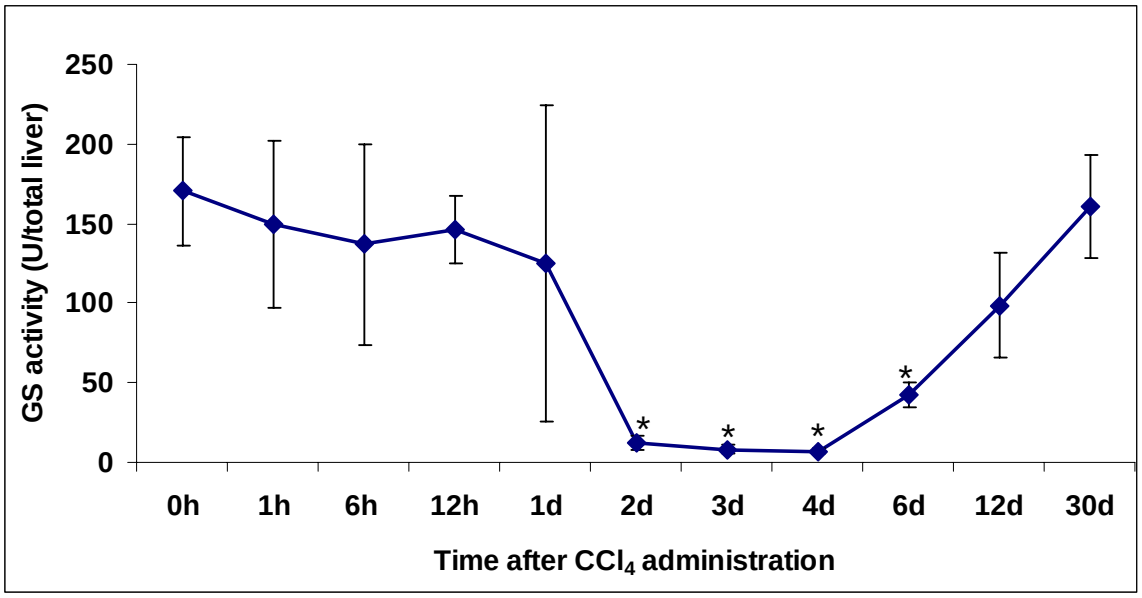

Fig. 3.36: GS activity assay at different time intervals after administration of 1.6 g/kg CCl_4. Glutamine synthetase (GS) activity was almost completely lost between days two and four after intoxication. By day six it began to recover. Full recovery was only reached one month after CCl_4 injection. Data are mean ± S.D. of three mice per time point. * P< 0.05 compared to controls (0h).

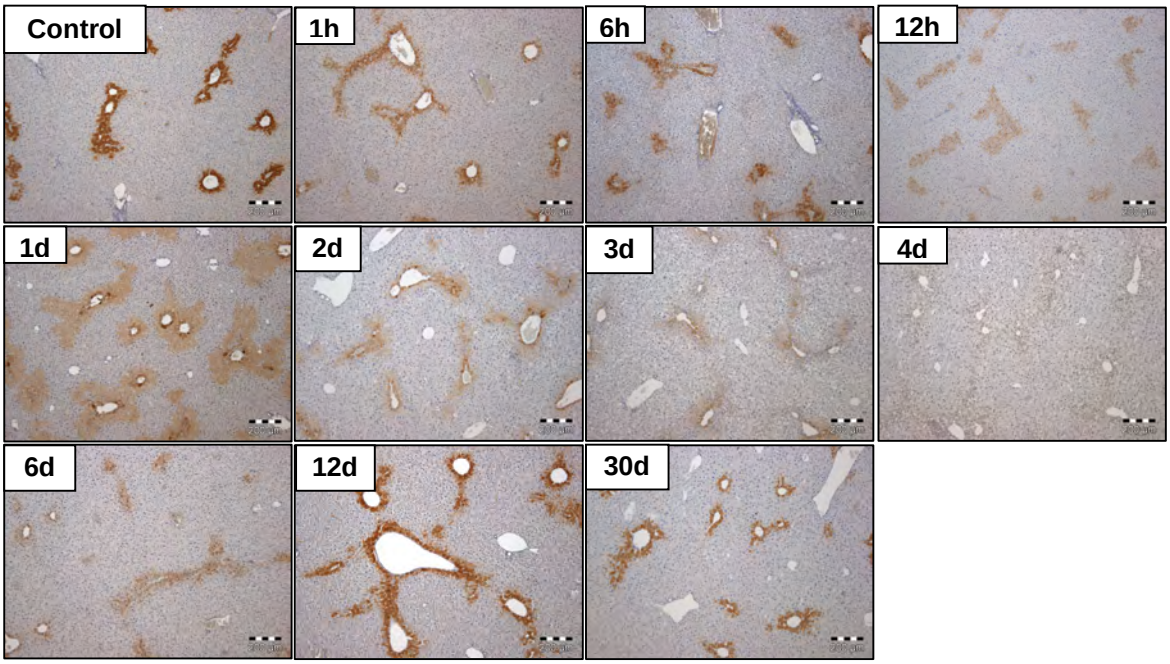

Fig. 3.37: Immunostaining of GS at different time intervals after administration of 1.6 g/kg CCl_4. The control liver shows the normal pericentral zonation of glutamine synthetase (GS). After CCl_4 intoxication, GS protein was lost in a time-dependent manner. On day four, GS staining was completely negative. A very faint staining was observed on day six post injection. After twelve days, GS staining was similar to the control. Scale bars: 200µm.

3.2.4 Influence of the delayed recovery of glutamine synthetase

In a next step, the delayed recovery of GS activity was included into the model. Inclusion of these data into the model helped to reduce the deviation between the measured and simulated glutamine, particularly on days four, six and twelve post CCl_4 intoxication (Fig. 3.38). On the other hand, the delayed regeneration of GS activity led to the prediction of higher ammonia output particularly on days four, six and twelve (Fig. 3.39). In conclusion, by considering the delayed recovery of GS activity, glutamine output was correctly predicted while the discrepancy of ammonia prediction became even worse.

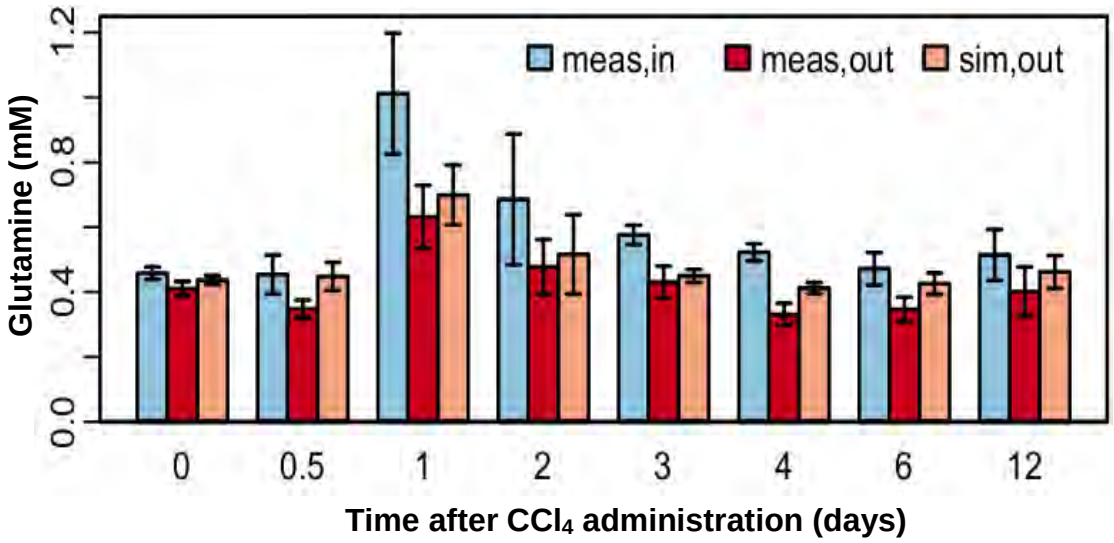

Fig. 3.38: The measured (red) and simulated (orange) glutamine output (in hepatic vein) after CCl_4 intoxication. Consideration of the delayed recovery of GS allowed a correct prediction of glutamine. Data are mean ± S.D. of three mice per time point.

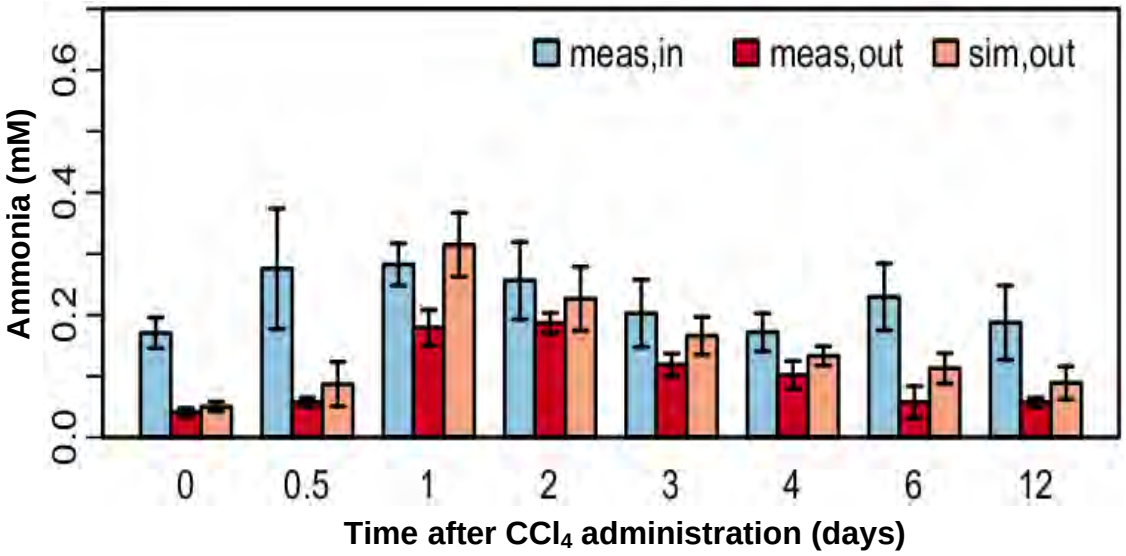

Fig. 3.39: The measured (red) and simulated (orange) ammonia output (in hepatic vein) after CCl_4 intoxication. Consideration of the delayed recovery of GS led to the prediction of more ammonia particularly on day six after CCl_4 intoxication. Data are mean ± S.D. of three mice per time point.

3.2.5 Over expression of CPS1 during liver regeneration

Because the pericentral compartment is almost completely lost after CCl_4 intoxication, the following studies will focus on the periportal compartment of the liver lobule, with the aim to study if a compensatory mechanism for ammonia detoxification during liver damage takes place. Carbamoyl phosphate synthetase1 is well known to be the rate limiting enzyme of the urea cycle. One hypothesis is that the delayed recovery of GS is compensated for by over expression of CPS1 in the PP compartment. To study this hypothesis, formalin fixed paraffin embedded sections of liver tissue were immunostained using antibodies against CPS1 in control, as well as in days four, six and twelve after CCl_4 intoxication. The control liver showed a restricted periportal zonation of CPS1, whereas on days four and six after CCl_4 intoxication, CPS1 was expressed throughout the whole liver lobule (periportal-like liver). By day twelve after injection, CPS1 expression returned to the normal periportal zonation (Fig. 3.40).

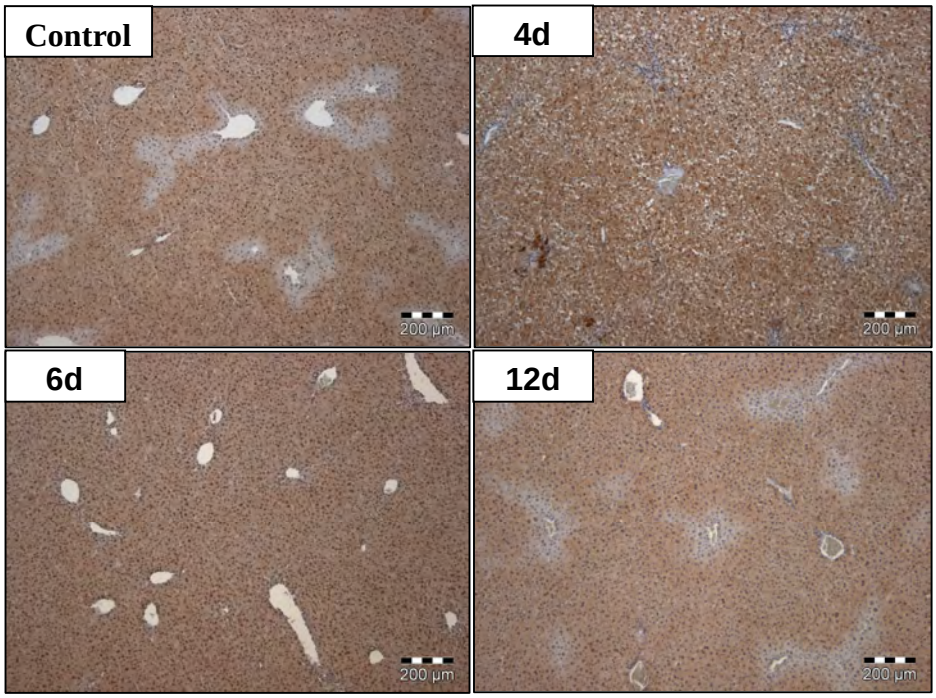

Fig. 3.40: CPS1 immunostaining in liver tissue at control as well as days four, six and twelve after CCl_4 intoxication. The control liver shows restricted periportal zonation of CPS1. On day four and six; CPS1 covers the whole liver parenchyma. Twelve days after CCl_4 injection, normal periportal zonation of CPS1 was observed. Scale bar: 200µm.

3.2.6 Influence of CPS1 over expression during liver regeneration

To simulate the influence of the altered expression patterns of CPS1 the corresponding data were included into the model. This allowed the fitting between the experimental data and simulation results of ammonia output on days four and six post CCl_4 intoxication (Fig. 3.41). In conclusion, the loss of GS activity during liver regeneration was compensated for by the over expression of CPS1.

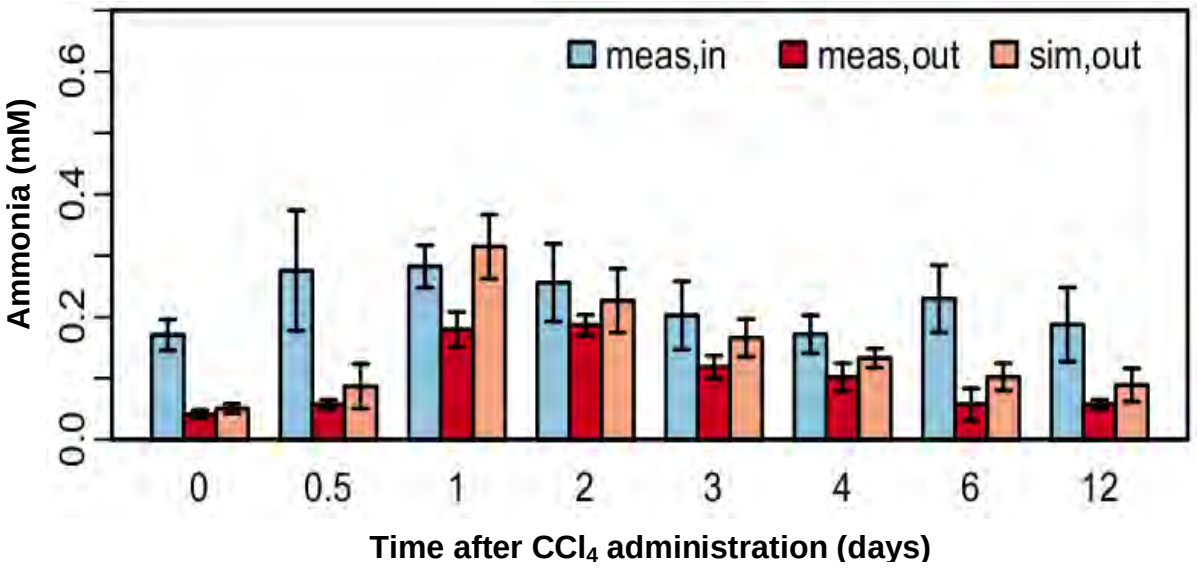

Fig. 3.41: Influence of carbamoyl phosphate synthetase1 (CPS1) Over expression. Over expression of CPS1 corrected the prediction of ammonia during liver regeneration. Consideration of the over expression of carbamoyl phosphate synthetase1 during liver regeneration led to better prediction of ammonia (orange) on day six. Data are mean ± S.D. of three mice per time point.

3.2.7 Expression of urea cycle enzymes after induction of liver damage by CCl_4

3.2.7.1 Down regulation of urea cycle enzymes after CCl_4 intoxication

Despite the model improvement, the measured and the predicted ammonia are still not fitting together, particularly at the time period of maximal liver damage (12h, days one and two after CCl_4 injection). One hypothesis is that the capacity of the urea cycle to detoxify ammonia is altered after damage of the pericentral compartment of the liver lobule by CCl_4. To investigate this, RNA was isolated from frozen liver tissue specimens after CCl_4 intoxication and all urea cycle enzymes were analyzed by qPCR. Out of arginase1, all other urea cycle enzymes, including carbamoyl phosphate synthetase1 (CPS1), argininosuccinate synthetase1 (ASS1) and argininosuccinate lyas1 (ASL), were down regulated 12h up to day three after CCl_4 intoxication. On days four and six, both CPS1 and ASS1 showed slight up regulation and became similar to control levels one month after CCl_4 injection (Fig. 3.42; 3.43; 3.44).

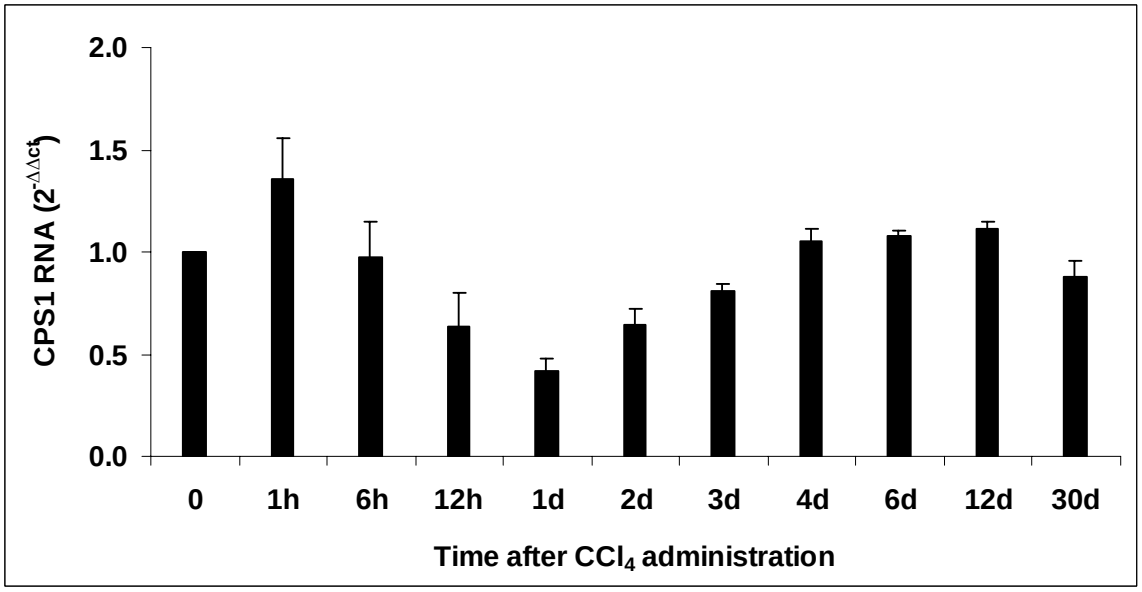

Fig. 3.42: Carbamoyl phosphate synthetase1 (CPS1) RNA expression at different time intervals after CCl_4 intoxication. CPS1 down regulated between 12h up to day three after CCl_4 injection. Data were normalized to the control and expressed as mean ± S.D. of three mice per time point.

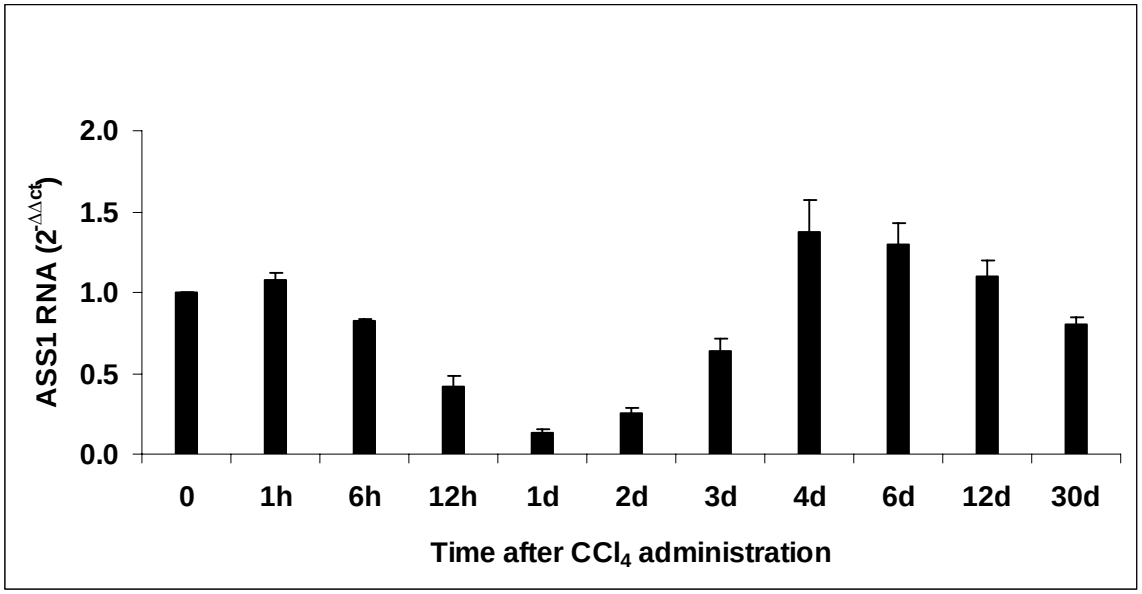

Fig. 3.43: Argininosuccinate synthetase1 (ASS1) RNA expression at different time intervals after CCl_4 intoxication. ASS1 down regulated between 12h up to day three after CCl_4 injection. Data were normalized to the control and expressed as mean ± S.D. of three mice per time point.

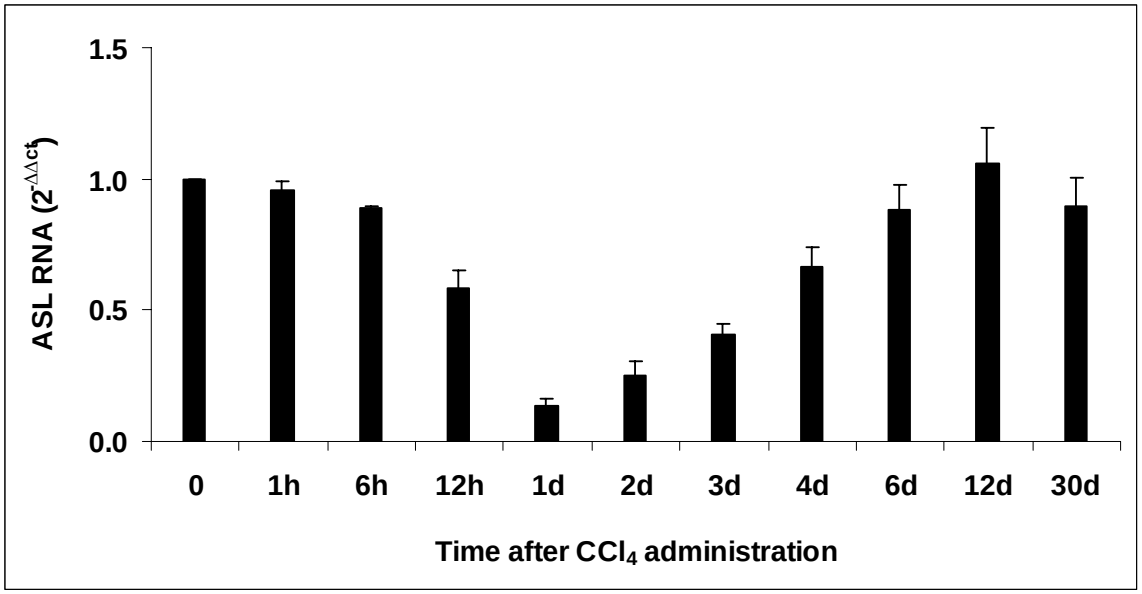

Fig. 3.44: Argininosuccinate lyase (ASL) RNA expression at different time intervals after CCl_4 intoxication. ASL down regulated between 12h up to day four after CCl_4 injection. Data were normalized to the control and expressed as mean ± S.D. of three mice per time point.

Moreover, immunostaining of CPS1 after CCl_4 intoxication showed also a decrease of its signal in the periportal compartment of the liver lobule (Fig. 3.45). In conclusion, CCl_4 intoxication resulted in more than 50% reduction in urea cycle capacity for ammonia detoxification.

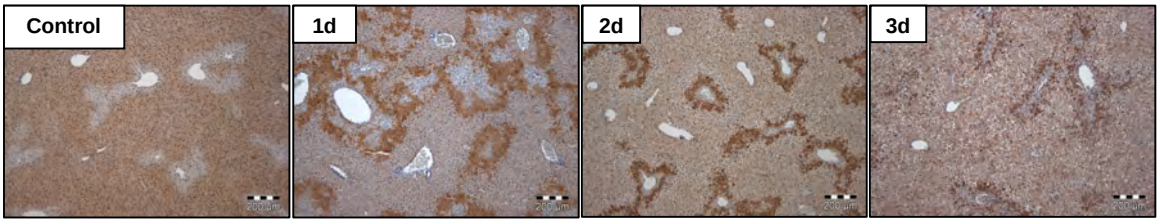

Fig. 3.45: Carbamoyl phosphate synthetase1 (CPS1) immunostaining in liver tissue of controls as well as days one, two and three after CCl_4 intoxication. The control liver shows restricted periportal zonation of CPS1. CCl_4 intoxication decreases the CPS1 signal in the periportal compartment of the liver lobule. Scale bars: 200µm.

3.2.7.2 Arginine loss after CCl_4 intoxication

Arginine is the final substrate of the urea cycle. It metabolized by arginase1 forming urea and ornithine. Despite the alterations of urea cycle enzymes, the urea concentration in the blood was not highly altered. To study whether this was due to over consumption of arginine, the plasma level of arginine was measured. For this purpose, blood samples were collected from the portal vein, hepatic vein and from the right heart chamber at different time intervals after intoxication by 1.6 g/kg CCl_4. In control mice the highest concentration of arginine was measured in the blood of the portal vein, while the concentration was low in the blood of the hepatic vein and the heart. CCl_4 intoxication caused almost a complete depletion of arginine between 12h up to day two after injection (Fig. 3.46). By day three, arginine was even higher compared to control mice at all analized positions of the vascular system. Arginine returned to the basal levels by day twelve after intoxication.

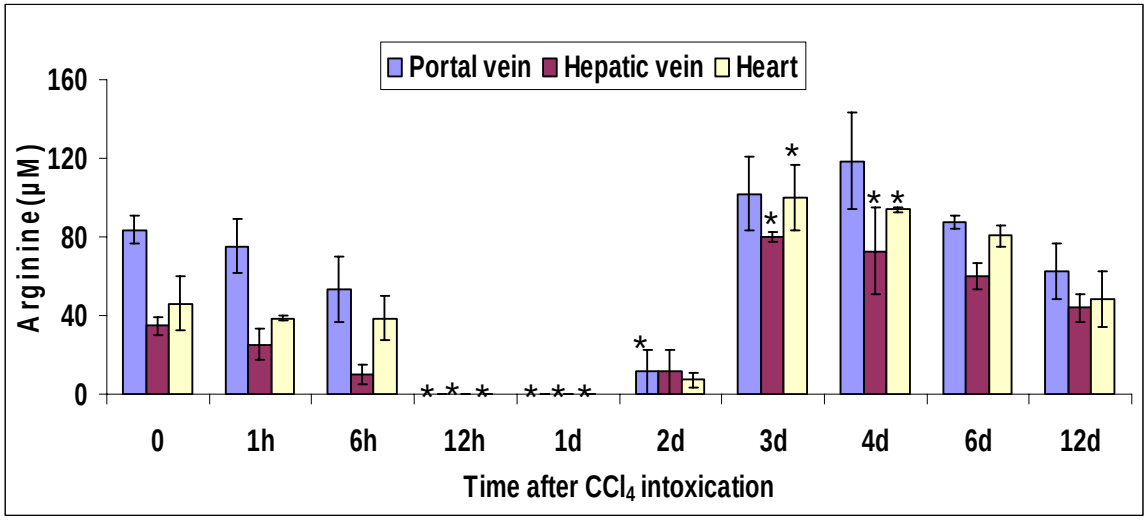

Fig. 3.46: Concentration of arginine (µM) in plasma obtained from three positions in mice at different time intervals after injection of 1.6 g/kg CCl_4, showing a marked loss of arginine at all measured positions of the vascular system between 12h up to day two post injection. Data are mean ± S.D. of three mice per time point. * P< 0.05 compared to the corresponding control (0h).

To explain such a drastic decrease in arginine concentration, arginase1 (the enzyme which metabolizes arginine to urea and ornithine) was analyzed by

qPCR after isolation of RNA from frozen liver tissue. Arginase1 RNA expression showed a slight down regulation between six hours and day six after CCl_4 intoxication, and returned to the control levels by day twelve (Fig. 3.47).

To investigate whether such modest down regulation has affected the protein level, arginase1 was also detected by immunostaining in formaline fixed paraffin embedded sections using antibodies againest arginase1. Arginase1 staining showed the typical periportal zonation in the control liver. After CCl_4 intoxication, arginase1 was similar to the control at all tested time points (Fig. 3.48).

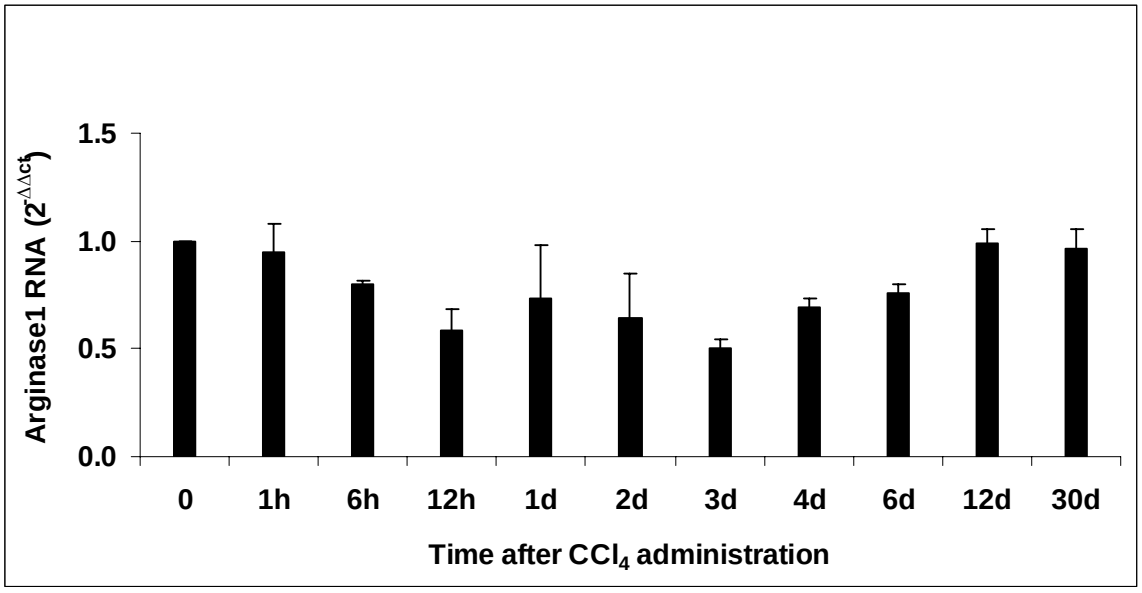

Fig. 3.47: Arginase1 RNA expression at different time intervals after CCl_4 intoxication, showing a slight down regulation between six hours up to day six after CCl_4 injection. Data were obtained from three mice per time point, normalized to the control and expressed as mean ± S.D.

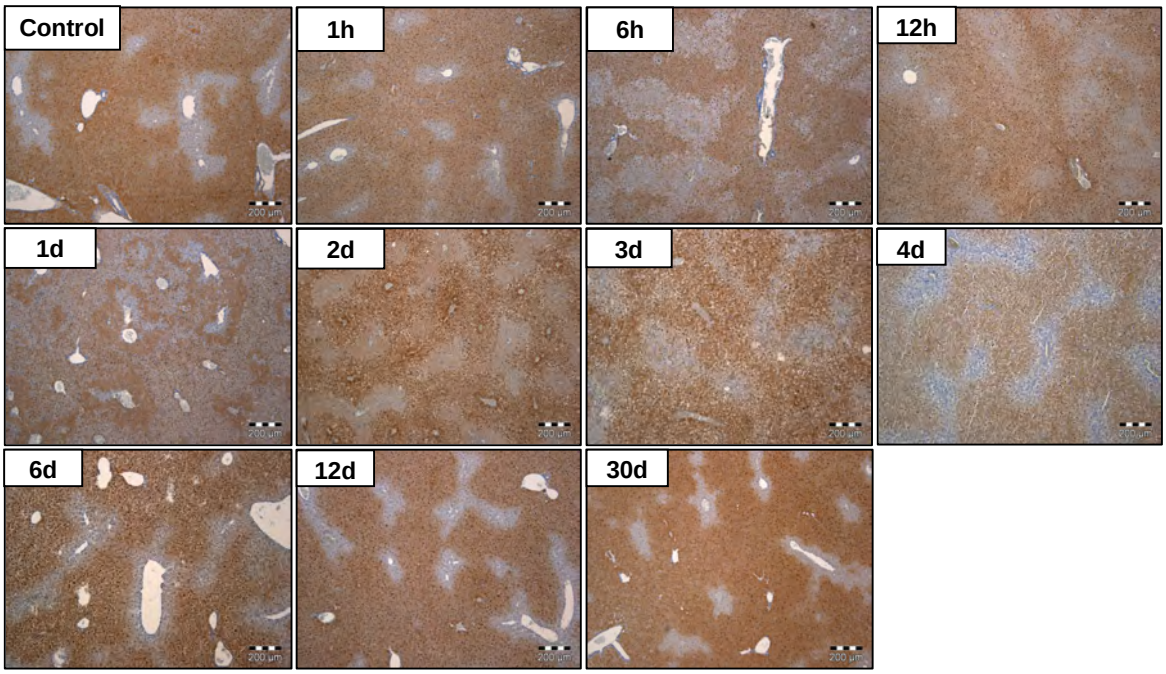

Fig. 3.48: Immunostaining of arginase1 in formalin fixed paraffin embedded sections of mouse liver at different time intervals after CCl_4 intoxication. The control liver showed the typical periportal zonation of arginase1. After CCl_4 intoxication, arginase1 was similar to the control at all tested time points. Scale bars: 200µm.

3.2.8 Influence of urea cycle alterations

CPS1 is well known to be the rate limiting enzyme of the urea cycle. The qPCR data and immunostaining suggested more than 50% impairment of this enzyme after CCl_4 intoxication. By integerating this information into the model, the discrepancy between the simulated and the measured ammonia output became even worse. The discrepancy increased particularly at 12h and day one after CCl_4 intoxication (Fig. 3.49). From all these data, it can be concluded that the known mechanisms of ammonia detoxification are not sufficient to explain the metabolite concentrations after induction of liver damage. Further mechanisms that detoxify ammonia must be activated.

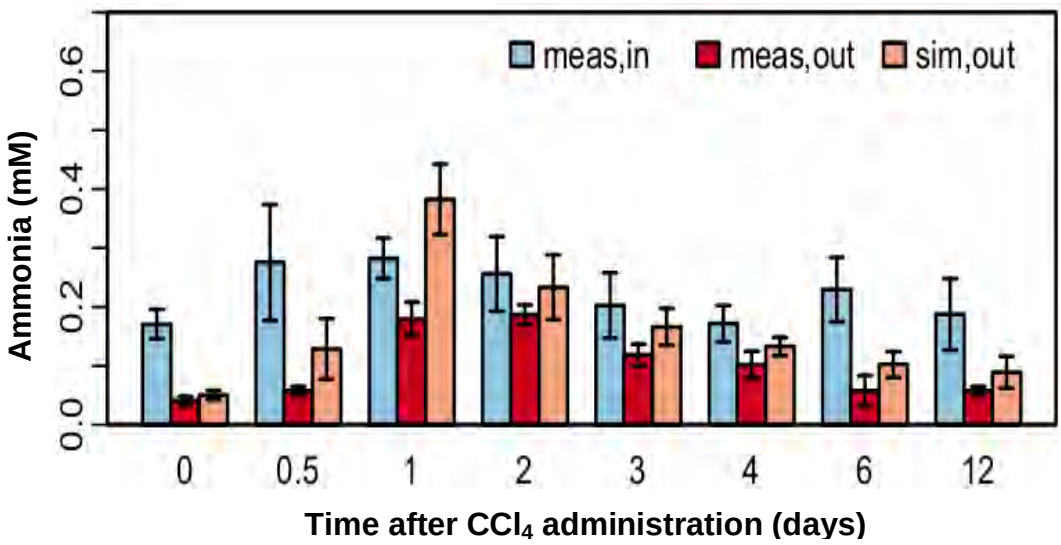

Fig. 3.49: Influence of urea cycle alteration. Alteration of CPS1 after CCl_4 intoxication (particularly between 12h and day one) led to a higher ammonia output prediction. The discrepancy between the predicted and the experimentally obtained data became even worse. Data are mean ± S.D. of three mice per time point.

3.2.9 Identification of a novel mechanism by mathematical modelling

3.2.9.1 The glutamate dehydrogenase switch hypothesis

It is well known that glutamate dehydrogenase (GDH) generates ammonia in the periportal compartment of the liver lobule (Boon et al., 1999). It catalizes the oxidative deamination of glutamate into ammonia and alpha-ketoglutarate (α-KG). Ammonia then enter the urea cycle where it is permenantly detoxified in the form of urea.

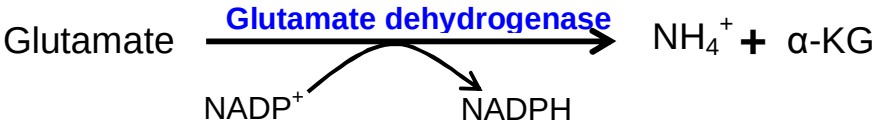

After alteration of urea cycle enzymes in the periportal compartment of the liver lobule, it became important to focus on the GDH reaction and the involved metabolites.

As shown previously, the measured ammonia was lower compared to the model prediction (Fig. 3.49). Moreover, glutamate concentrations were elevated at all three analyzed positions of the vascular system after induction of liver damage (Fig. 3.8). To analyze α-KG, blood samples were collected from the portal vein, hepatic vein and heart of mice in a time-dependent manner after injection of 1.6 g/kg CCl_4. The concentration of α-KG in control mice was highest in the portal vein (approximately 30µM) and was lowest in the hepatic vein (approximately 19µM) with a slight elevation in heart blood (approximately 22µM). CCl_4 intoxication resulted in a drastic decrease of α-KG at all analyzed positions of the vascular system between 12h up to day two after injection. On day three, α-KG was higher compared to controls in the portal and in the hepatic vein blood. By day four after CCl_4 injection α-KG returned to control levels at all analyzed positions (Fig. 3.50). In conclusion, after induction of liver damage, the concentration of glutamate was increased while the concentration of α-KG was strongly decreased.

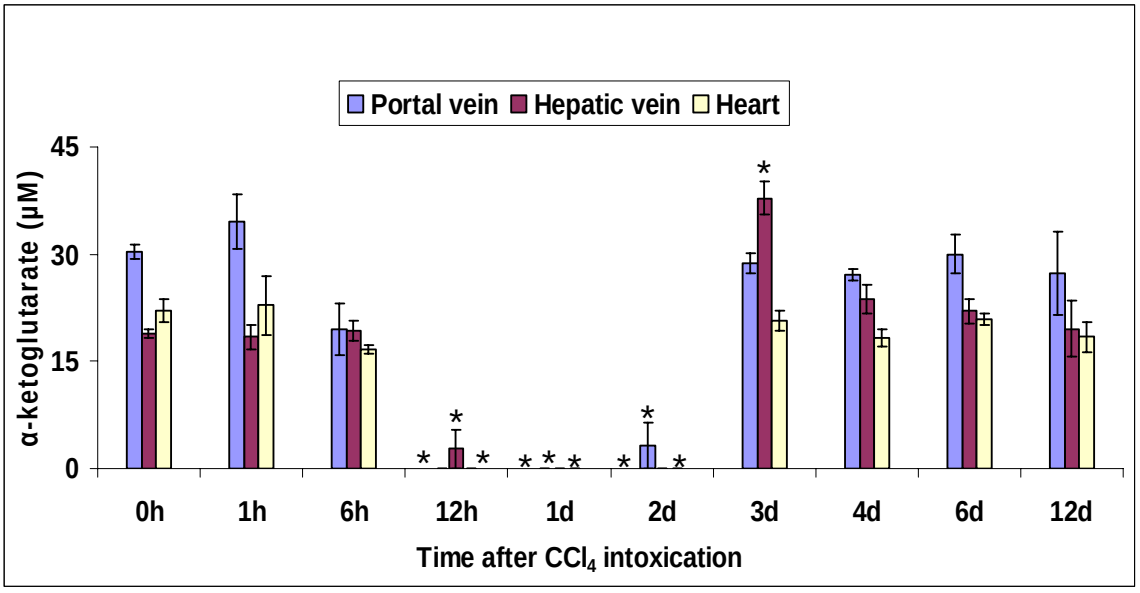

Fig. 3.50: Concentration of alpha ketoglutarate (µM) in plasma obtained from the portal vein, hepatic vein and heart of mice at different time intervals after injection of 1.6 g/kg CCl_4. alpha ketoglutarate decreased to almost undetectable levels between 12h up to day two after CCl_4 injection. Data are mean ± S.E. of three mice per time point. * P< 0.05 compared to the corresponding control (0h).

To study whether the depletion of α-KG was due to the decreased expression of GDH, analysis of the RNA expression of GDH was performed. For this purpose mice were injected with 1.6 g/kg CCl_4. Liver tissue samples were collected and snap frozen in a time-dependent manner after injection. RNA was isolated from frozen liver tissue and the RNA expression of GDH was measured by qPCR. In addition, a GDH activity assay was performed in liver homogenate extracted from the frozen liver tissue. qPCR analysis of GDH expression revealed a slight up regulation after CCl_4 intoxication compared to control levels (Fig. 3.51). This was also confirmed at the protein level by the enzyme activity assay. The activity of GDH was slightly elevated in liver tissue after CCl_4 intoxication compared to control levels. The GDH activity returned to basal levels one month after CCl_4 intoxication (Fig. 3.52). In conclusion, CCl_4 intoxication failed to alter the activity of GDH in liver tissue.

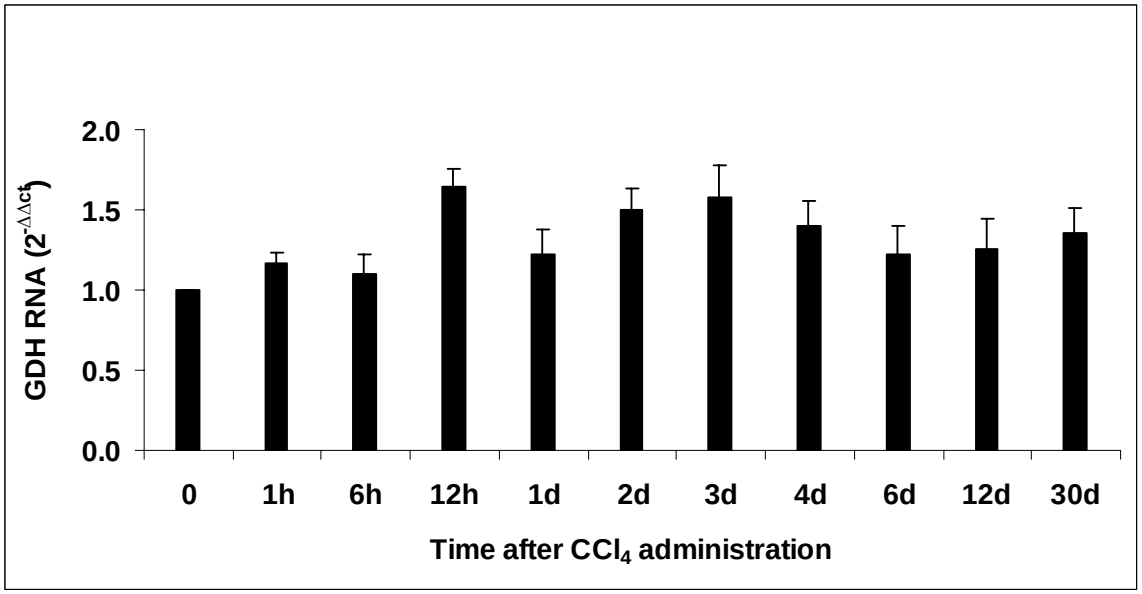

Fig. 3.51: Relative RNA expression of GDH in liver tissue at different time intervals after injection of 1.6 g/kg CCl_4 showing a slight up regulation particularly between 12h and day three after CCl_4 intoxication. Data were normalized to the control and expressed as mean ± S.D. of three mice per time point.

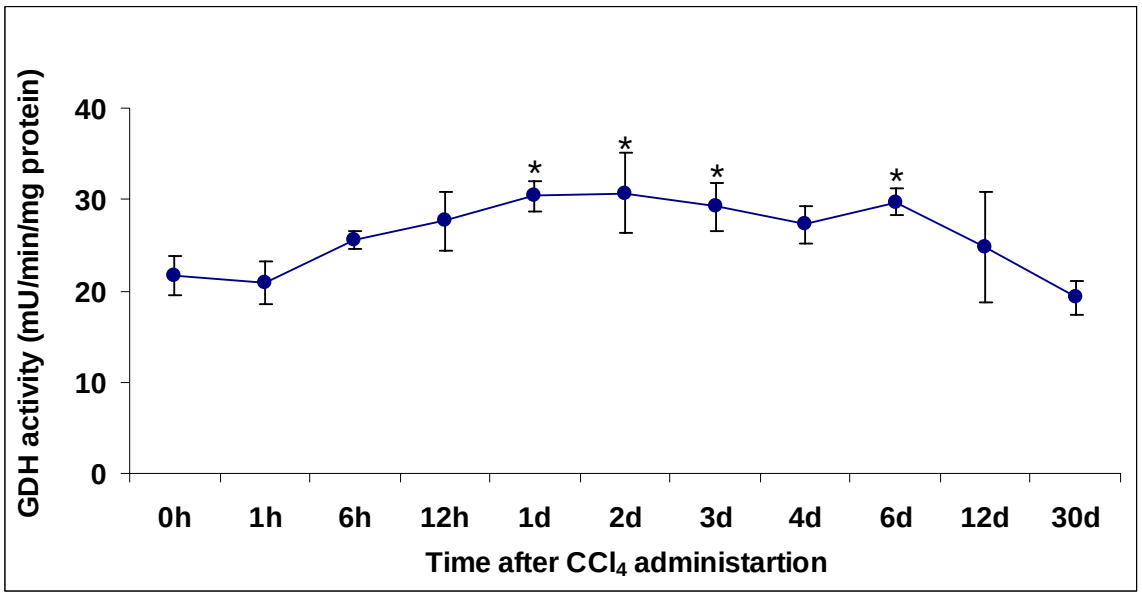

Fig. 3.52: GDH activity assay in liver tissue at different time intervals after injection of 1.6 g/kg CCl_4 showing a slight elevation after CCl_4 intoxication. Data are mean ± S.D. of three mice per time point. * P< 0.05 compared to controls (0h).

All these data allowed to raise the hypothesis that under the condition of liver damage a GDH switch from ammonia production to ammonia consumption occurs as a compensatory mechanism as suggested by the red dotted arrow in the schedule below.

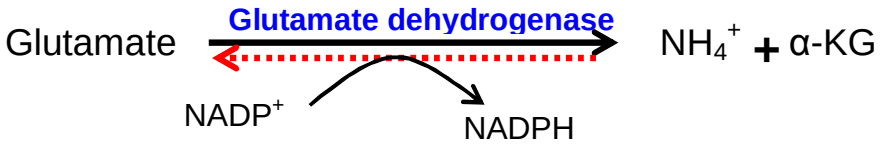

3.2.9.2 Confirmation of the glutamate dehydrogenase switch hypothesis

3.2.9.2.1 The switch of the GDH reaction in cultivated hepatocytes

The aim of this experiment is to investigate whether the cultivated hepatocytes can be used to study ammonia detoxification. For this purpose, mouse hepatocytes were isolated and cultivated in a collagen sandwich using conditions where the cells reached confluency. Various concentrations of ammonium chloride (NH_4Cl) (0, 200, 1800, 16200µM) were added to the hepatocytes culture and to the media control. 1h and 24h following the onset of NH_4Cl, ammonia was measured in the culture supernatant. After 1h, there were no obvious changes of ammonia concentrations. However, after 24h a clear ammonia detoxification was observed in the hepatocytes culture compared to the negative control (without hepatocytes) (Fig. 3.53). This experiment confirms that the in vitro system is useful to study ammonia metabolism.

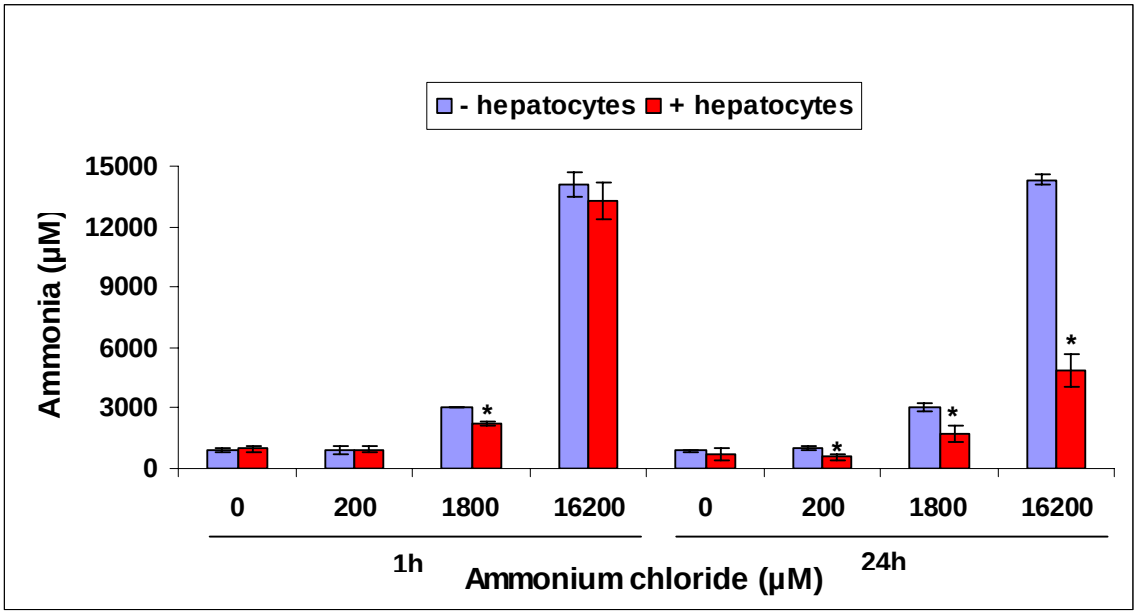

Fig. 3.53: Ammonia concentrations in the culture medium of cultivated mouse hepatocytes (collagen sandwich). 1h after incubation with NH_4Cl, there were no clear changes in ammonia concentrations. However, after 24h there was an obvious ammonia detoxification by hepatocytes (red) compared to the negative control (blue). Data are mean ± S.D. of three independent experiments. * $P< 0.05$ compared to the corresponding control (- hepatocytes).

To study the role of GDH in ammonia metabolism, a GDH inhibitor was used. Mouse hepatocytes were isolated and cultivated as a collagen sandwich and incubated with various concentrations of NH_4Cl in presence or absence of 2,6-pyridinedicarboxylic acid (PDAC), a GDH inhibitor. After 24h, ammonia was measured in the culture supernatant whereas glutamate and GDH activity were analyzed in the cellular extracts (Fig. 3.54).

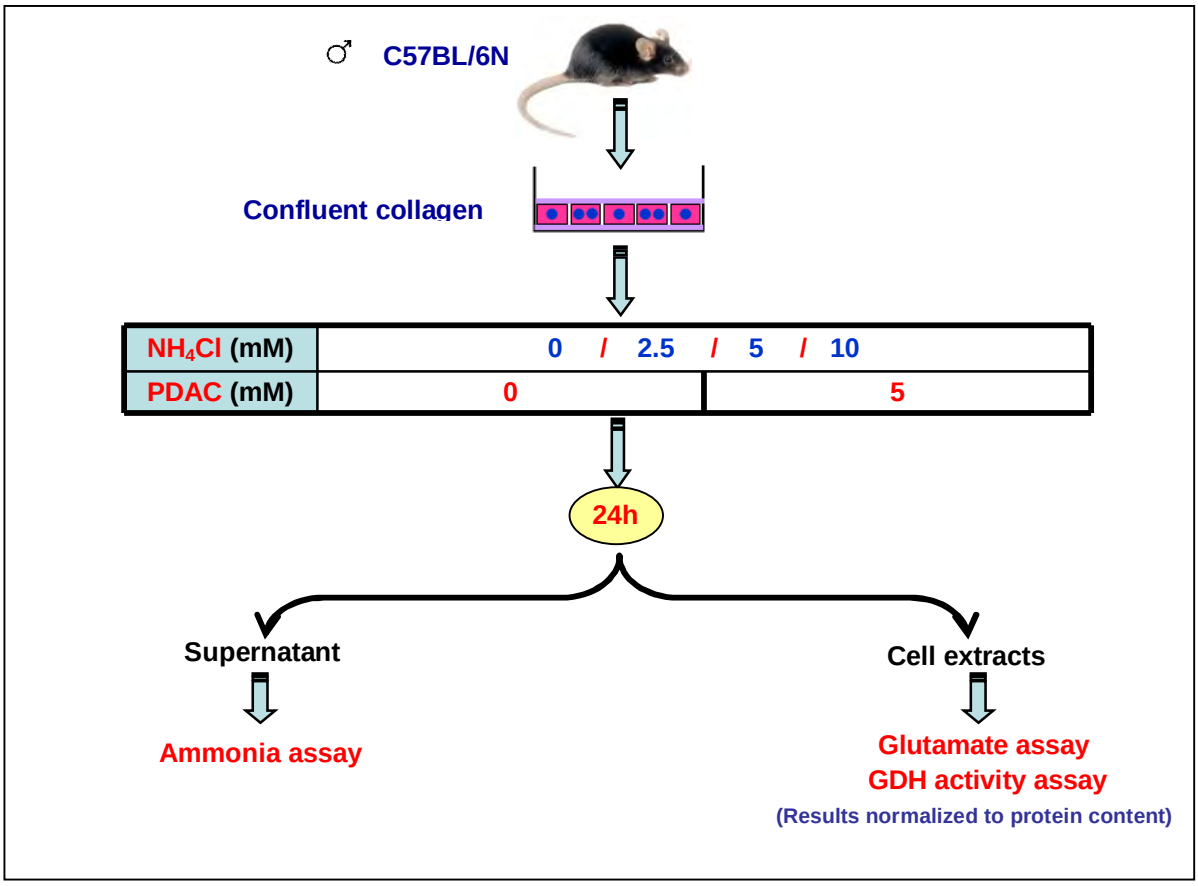

Fig. 3.54: Identification of the glutamate dehydrogenase (GDH) switch in cultivated mouse hepatocytes. Hepatocytes were isolated from C57BL/6N mice and cultivated on six well plates as a collagen sandwich using conditions where cells reach the confluency. The cultivated hepatocytes wrere incubated with various concentrations of ammonium chloride (0, 2.5, 5 and 10mM) ± 5mM 2,6-Pyridinedicarboxylic acid (PDAC, a GDH inhibitor). After 24h, ammonia was measured in the culture supernatant whereas glutamate and GDH activity were measured in cellular extracts and the results normalized to the protein content.

Incubation with 5mM PDAC inhibited the activity of GDH enzyme by approximately 50% compared to control levels (Fig. 3.55).

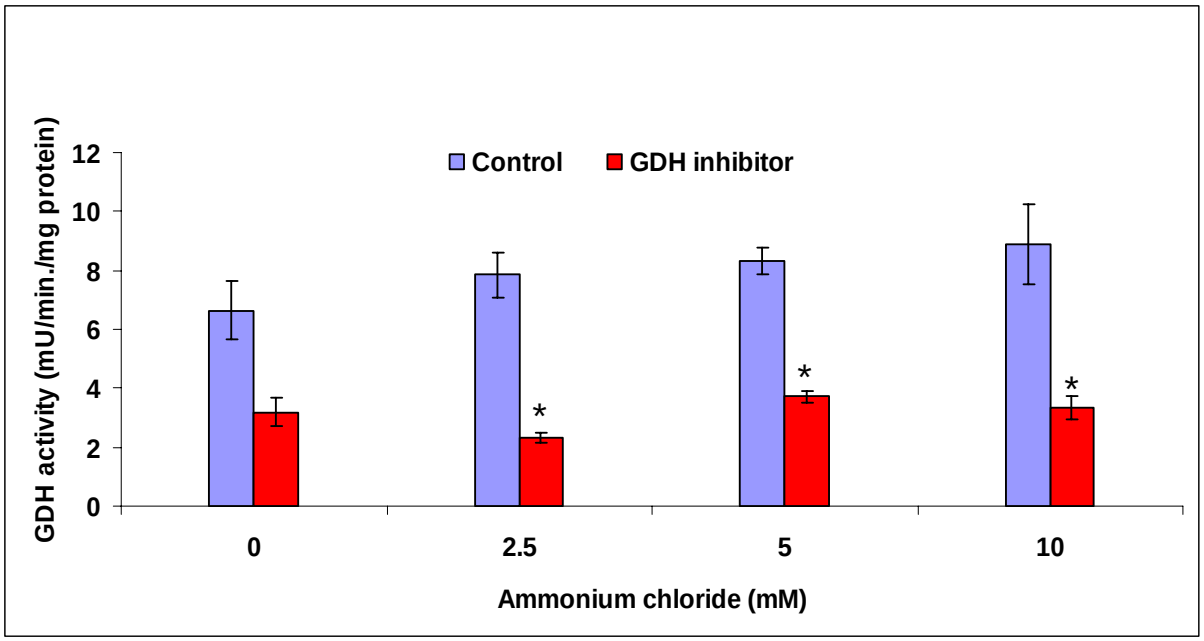

Fig. 3.55: Inhibition of GDH activity in cultivated mouse hepatocytes. Exposure to 5mM 2,6-Pyridinedicarboxylic acid caused approximately 50% inhibition (red) of GDH activity compared to the control (blue). Data are mean ± S.D. of 3 independent experiments. * P< 0.05 compared to the corresponding control.

Using the phase contrast microscopy, the hepatocyte morphology appeared normal in absence of the GDH inhibitor even with the highest concentration of NH_4Cl (10mM). However, after inhibition of the GDH, hepatocytes were completely killed by 5mM NH_4Cl and higher concentration (Fig. 3.56). In absence of NH_4Cl, inhibition of the GDH resulted in decreased ammonia concentrations in the culture media of cultivated hepatocytes. However, after incubation with high concentrations of NH_4Cl, inhibition of the GDH resulted in increased ammonia concentrations in the culture media (Fig. 3.57). In contrast, the concentration of glutamate was reduced in the hepatocyte cultures after inhibition of the GDH and exposure to high concentrations of NH_4Cl (Fig. 3.58). All these data confirm that GDH can switch from ammonia production to ammonia consumption after exposure to high concentrations of ammonia.

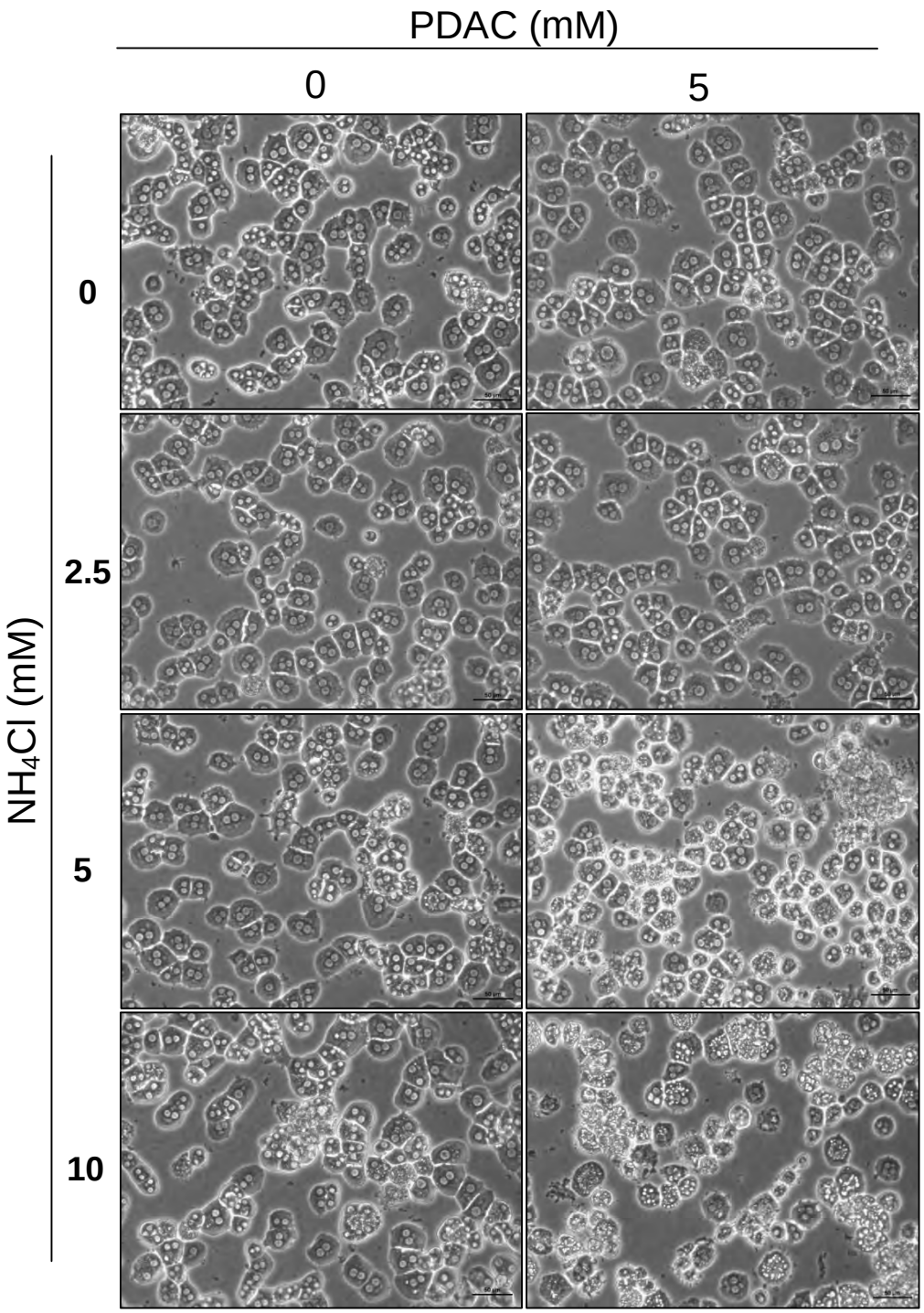

Fig. 3.56: Morphology of cultivated mouse hepatocytes after exposure to various concentrations of ammonium chloride (NH_4Cl) ± the GDH inhibitor. In absence of the GDH inhibitor the hepatocyte morphology looked normal even at the highest concentration of NH_4Cl, whereas after inhibition of GDH hepatocytes were completely killed by 5mM NH_4Cl or at higher concentrations. Scale bars: 50µm.

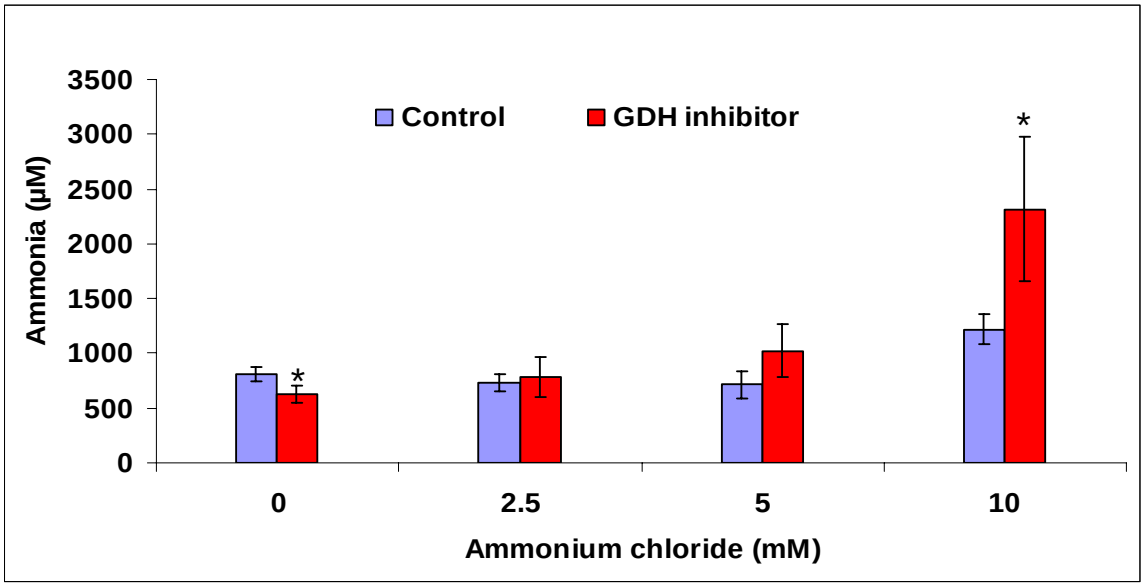

Fig. 3.57: Ammonia concentrations in the culture medium of cultivated mouse hepatocytes after exposure to various concentrations of ammonium chloride (NH_4Cl) ± the glutamate dehydrogenase (GDH) inhibitor. After exposure to high concentrations of NH_4Cl, inhibition of the GDH activity resulted in increased ammonia concentrations in the culture media of cultivated hepatocytes. Data are mean ± S.D. of three independent experiments. * P< 0.05 compared to the corresponding control.

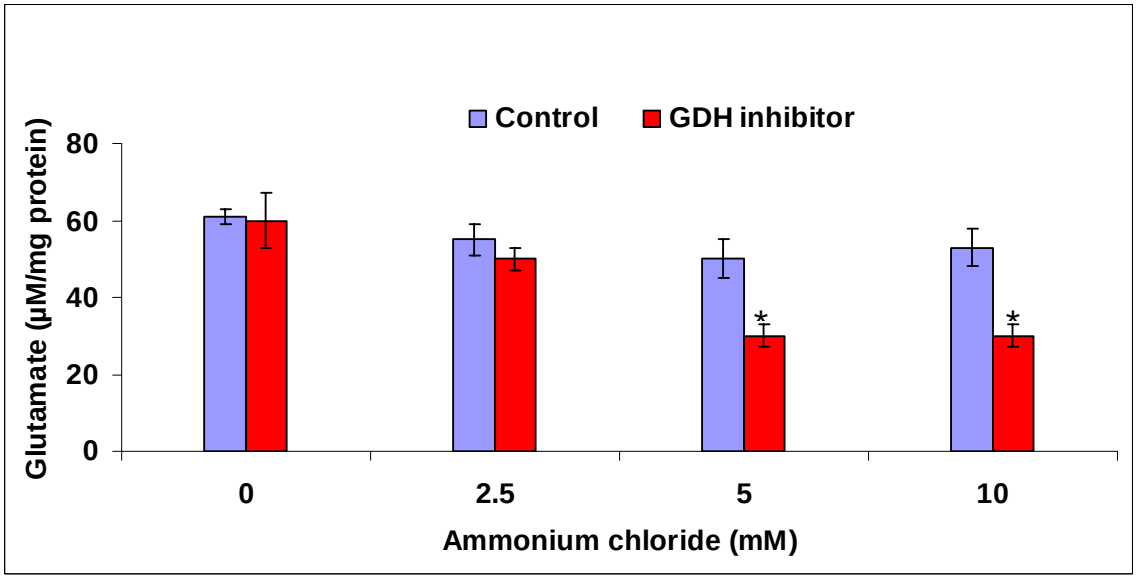

Fig. 3.58: Glutamate concentrations in the culture medium of cultivated mouse hepatocytes after exposure to various concentrations of ammonium chloride (NH_4Cl) ± the glutamate dehydrogenase (GDH) inhibitor. After exposure to high concentrations of NH_4Cl, inhibition of the GDH activity resulted in decreased glutamate concentrations in the culture media of cultivated hepatocytes. Data are mean ± S.D. of three independent experiments. * P< 0.05 compared to the corresponding control.

3.2.9.2.2 Alpha-ketoglutarate substitution provides systemic protection against ammonia in acute liver damage

The previous experiments confirmed that GDH can detoxify ammonia in vitro in response to high concentrations of ammonia. A next question of interest is whether this effect can happen in vivo after liver damage. To get a closer system to the in vivo situation, the switch of the GDH was studied in mouse plasma. In order to investigate the level of GDH in blood after induction of liver damage, mice received an intraperitoneal injection of 1.6 g/kg CCl_4. At day one after injection, the time point of maximal liver damage, blood samples were collected from the portal vein, hepatic vein and heart. Subsequently, the activity of the GDH was measured in plasma. The GDH activity assay revealed an obvious increase after CCl_4 intoxication at all of the three measured positions of the vascular system compared to controls (Fig. 3.59).

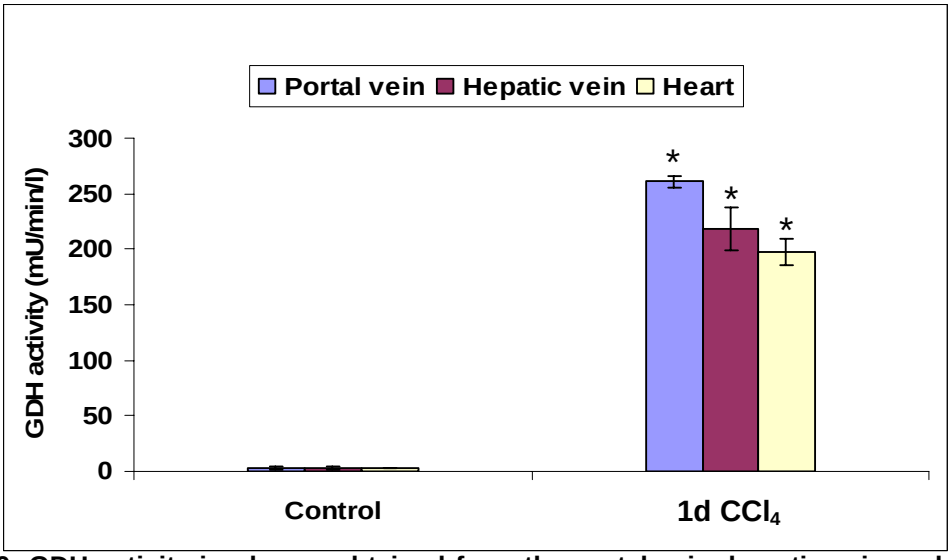

Fig. 3.59: GDH activity in plasma obtained from the portal vein, hepatic vein and heart of mice at day one after injection of 1.6 g/kg CCl_4 . The GDH activity sharply increased at all of the three measured positions of the vascular system after CCl_4 intoxication compared to controls. Data are mean± S.D. of three mice. * P< 0.05 compared to the corresponding control.

A next question of interest is whether the increase of the plasma GDH activity after induction of liver damage can play a role in ammonia detoxification. To study this, a group of C57BL/6N mice received an intraperitoneal injection of 1.6 g/kg CCl_4. After 24h, blood samples were collected from the three previously

mentioned positions of the vascular system (portal vein, hepatic vein and heart). Plasma was separated and the concentration of ammonia was measured (control). To investigate the ability of the GDH to detoxify ammonia, the collected plasma was incubated with either NH_4Cl only or NH_4Cl plus α-KG or NH_4Cl plus α-KG plus the GDH inhibitor. After 1h incubation at 37°C, ammoia, glutamate and GDH activity were measured (Fig. 3.60).

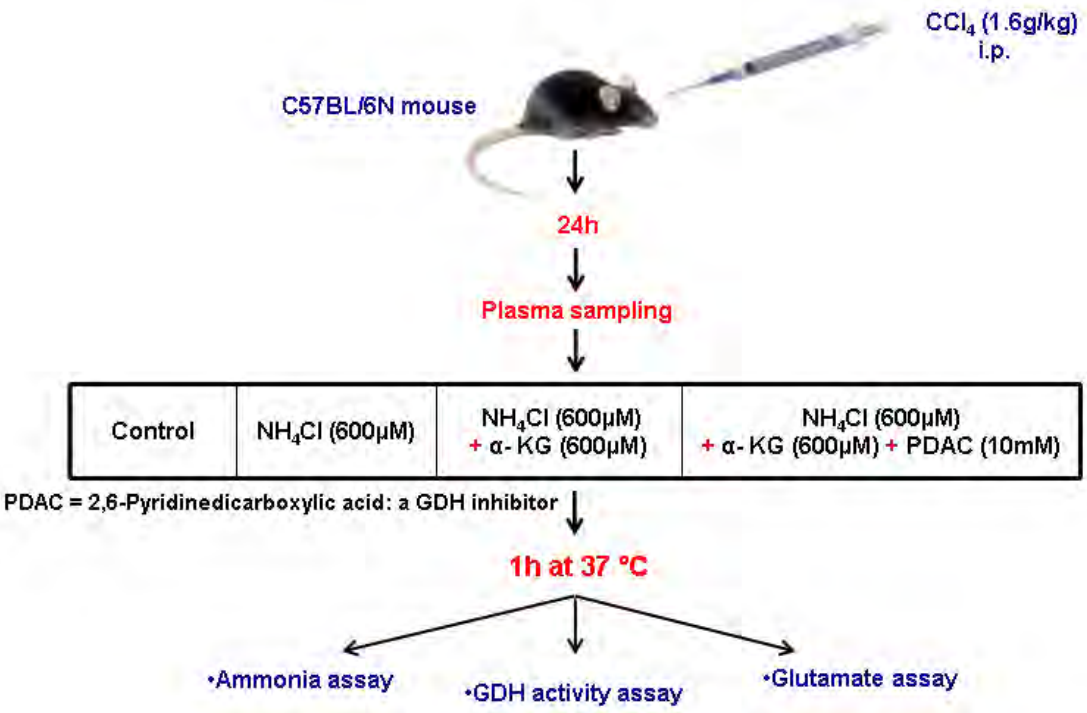

Fig. 3.60: Identification of the GDH switch in mice plasma. Blood samples were collected from the portal vein, hepatic vein and heart of mice on day one after injection of 1.6 g/kg CCl_4. The plasma was separated and the concentration of ammonia was measured (control). Then the plasma was incubated with either ammonium chloride (NH_4Cl) only or NH_4Cl plus alpha ketoglutarate (α-KG) or NH_4Cl plus α-KG plus a glutamate dehydrogenase (GDH) inhibitor. After 1h incubation at 37°C, ammonia, glutamate and GDH activity were measured. Three mice were used.

Incubation with 10mM PDAC led to 90% inhibition of the plasma GDH activity compared to controls (Fig. 3.61). In the absence of α-KG, the added ammonia was not metabolized. Whereas, addition of α-KG led to ammonia detoxification. This effect was blocked by the GDH inhibitor (Fig. 3.62). Moreover, glutamate was produced only when α- KG was added. Inhibition of GDH blocked the production of glutamate (Fig. 3.63). a clinically relevant conclusion is that the GDH can systemically detoxify ammonia if α-KG is supplemented.

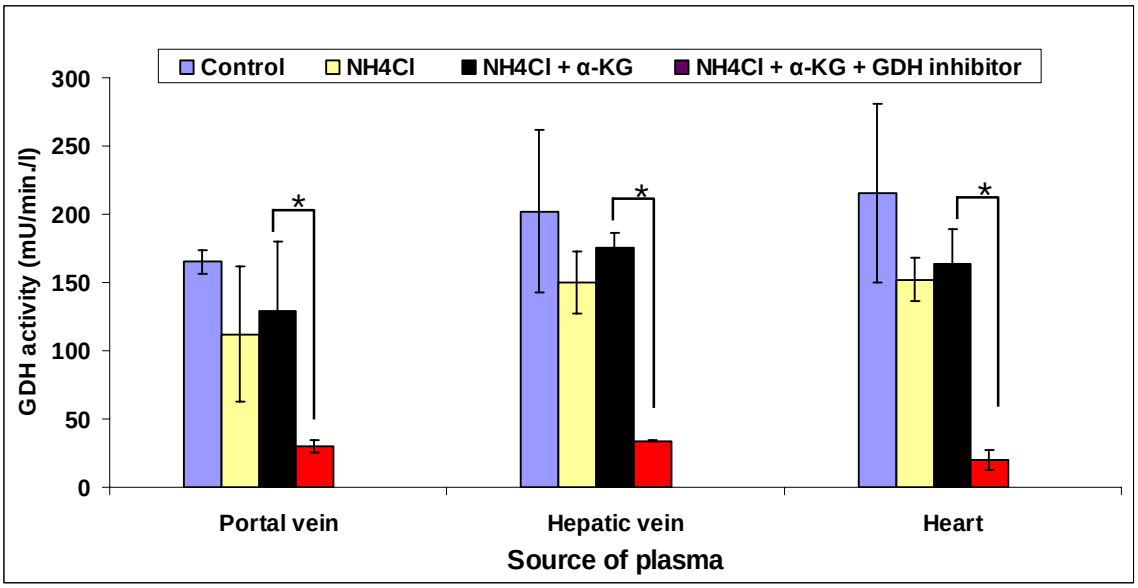

Fig. 3.61: Inhibition of GDH activity by PDAC. Plasma was separated from Blood samples collected from the portal vein, hepatic vein and heart of mice on day one after injection of 1.6 g/kg CCl_4. Plasma was incubated with 10mM 2,6 pyridinedicarboxylic acid (PDAC) for 1h at 37°C (red bar). Exposure to 10mM PDAC caused 90% inhibition of the GDH activity. Data are mean± S.D. of three mice. * P< 0.05 compared to the corresponding control.

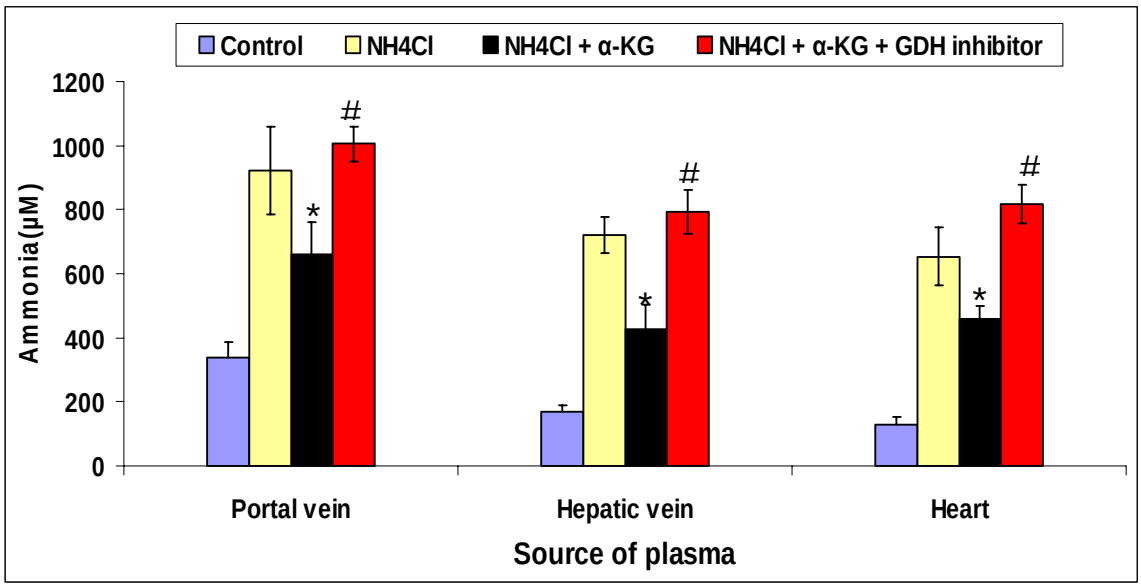

Fig. 3.62: Plasma from mice with acute liver damage consumes ammonia. Blood samples were collected from the portal vein, hepatic vein and heart of mice on day one after injection of 1.6 g/kg CCl_4. The plasma was separated and the concentration of ammonia was measured (control). The plasma was further incubated with either ammonium chloride (NH_4Cl) only, NH_4Cl plus alpha-ketoglutarate (α-KG) or NH_4Cl plus α-KG plus a glutamate dehydrogenase (GDH) inhibitor. After 1h incubation at 37°C, ammonia was measured. The added ammonia was metabolized only when α-KG was added. This effect was blocked by the GDH inhibitor. Data are mean± S.D. of three mice. * P< 0.05 compared to the corresponding NH_4Cl results. # P< 0.05 compared to the corresponding NH_4Cl + α-KG results.

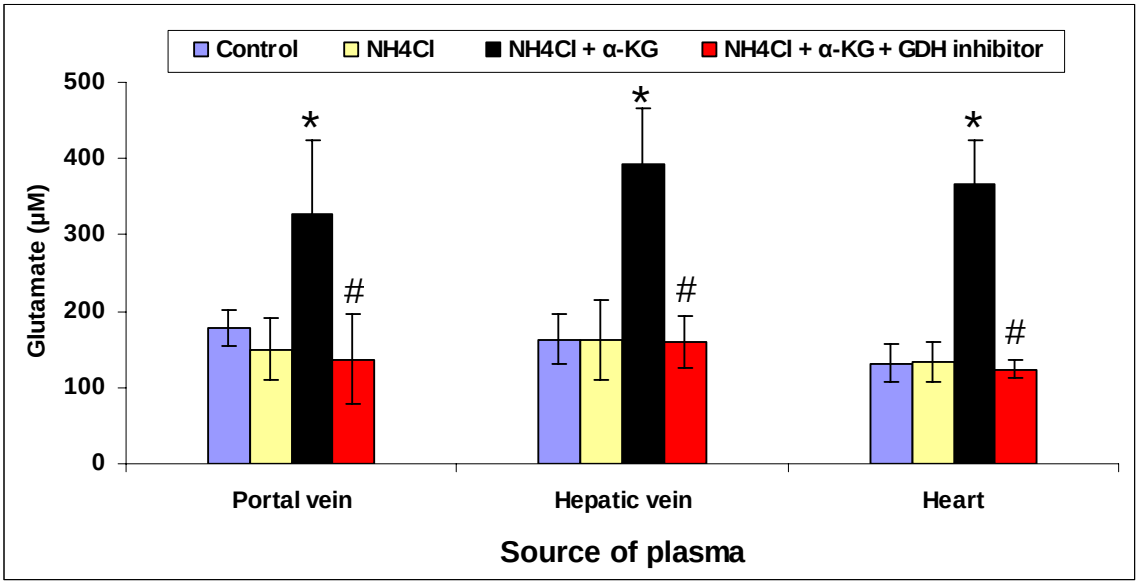

Fig. 3.63: Plasma from mice with acute liver damage produces glutamate. Blood samples were collected from the portal vein, hepatic vein and heart of mice on day one after injection of 1.6 g/kg CCl_4. The plasma was separated and the concentration of glutamate was measured (control). The plasma was further incubated with either ammonium chloride (NH_4Cl) only, NH_4Cl plus alpha ketoglutarate (α-KG) or NH_4Cl plus α-KG plus a glutamate dehydrogenase (GDH) inhibitor. After 1h incubation at 37°C, the concentration of glutamate was measured. Addition of α-KG led to glutamate production. This effect was blocked by the GDH inhibitor. Data are mean± S.D. of three mice.

4 Discussion

4.1 Acutely damaged liver tissue provides systemic protection against ammonia by GDH release

An unexpected and clinically relevant result of this thesis is that the liver upon acute damage provides systemic protection against ammonia. This is due to the release of GDH from damaged hepatocytes (Fig. 4.1). The healthy liver serves as a barrier and prevents the passage of the toxic metabolite ammonia into the systemic circulation. Ammonia is delivered to the periportal hepatocytes via the portal vein. Further ammonia is generated in the periportal hepatocytes through the degradation of glutamine by glutaminase (Haussinger, 1983; Gebhardt et al., 1988). Moreover, GDH provides ammonia in the healthy liver (Christen and Metzler, 1985). Ammonia is then metabolized in the periportal hepatocytes through the urea cycle into urea (Gaasbeek Janzen et al., 1984; Haussinger et al., 1992). Some ammonia that escapes the urea cycle detoxified by GS in the pericentral hepatocytes into glutamine (4.1A) (Haussinger, 1990; Gebhardt et al., 2007). After liver damage, the metabolism of ammonia through these pathways is massively compromised. This results in the escape of the toxic metabolite ammonia into the systemic circulation. A serious complication of hyperammonemia is the risk of hepatic encephalopathy (Fig. 4.1B) (Lemberg and Fernández, 2009; Cash et al., 2010). Interestingly, our model suggests that under conditions of hyperammonemia the GDH reaction switches from ammonia production into ammonia detoxification. This occurs by consumption of ammonia plus α-KG and production of glutamate. Due to the release of GDH from damaged hepatocytes into the systemic circulation, this reaction can systemically detoxify ammonia upon acute liver damage (Fig. 4.1C). By this reaction the organism gets rid of the toxic metabolite ammonia and forms the non toxic glutamate. However, this reaction can only proceed until the α-KG present in the blood is consumed by the GDH reaction (Fig. 4.1D). Subsequently, no further ammonia detoxification by this intravascular GDH reaction is possible (Fig. 3.62).

A clinically relevant conclusion is that α-KG should be substituted in such a scenario (acute liver damage). In the following part the discovery of this novel mechanism will be discussed.

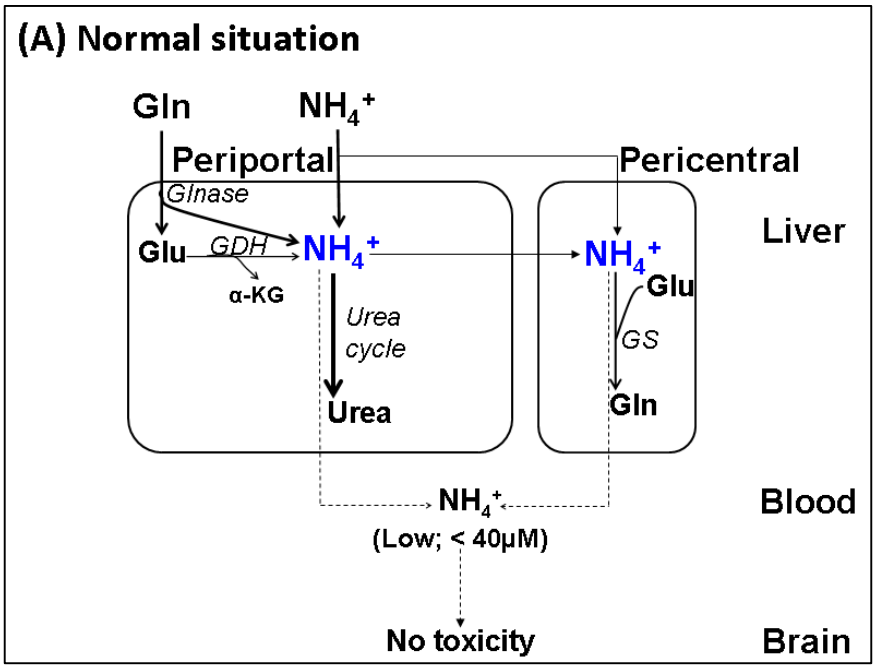

Fig. 4.1A: Pathways of ammonia detoxification in healthy liver. The portal vein guides ammonia and glutamine (Gln) to the periportal compartment (PP) of the liver lobule. Gln is catabolised via glutaminase (Glnase) into ammonia and glutamate. Additional ammonia is formed in the PP of the liver lobule through the deamination of glutamate (Glu) by glutamate dehydrogenase (GDH). Ammonia is then permanently detoxified into urea through the urea cycle. Ammonia that escapes the urea cycle is scavenged through the glutamine synthetase reaction (GS) in the pericentral hepatocytes (PC) generating Gln. These efficient mechanisms prevent the passage of the toxic ammonia into the blood circulation.

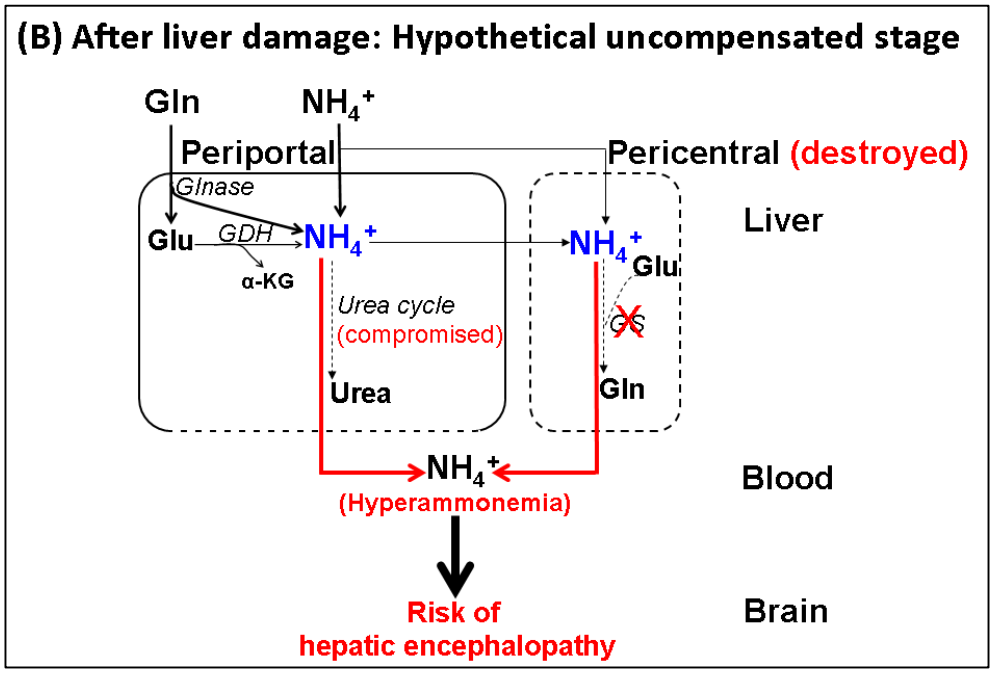

Fig. 4.1B: Alteration of ammonia metabolism after CCl_4 intoxication. After induction of liver damage by CCl_4, the pericentral compartment of the liver lobule is completely destroyed. Also, the activity of the urea cycle is compromised. This results in escape of toxic ammonia into the blood circulation. Hepatic encephalopathy might occur as a consequence of hyperammonemia.

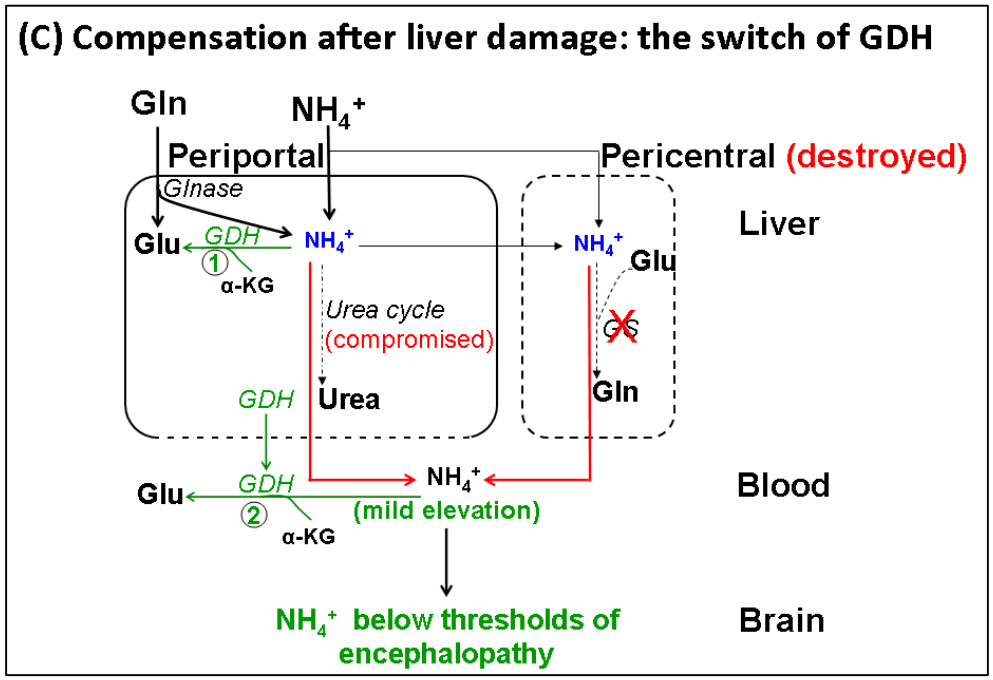

Fig. 4.1C: Acute liver damage provides systemic protection against ammonia by GDH release. After hepatic damage the glutamate dehydrogenase (GDH) reaction switches from ammonia production into glutamate production (1). Moreover, GDH is released from damaged hepatocytes into the systemic circulation leading to systemic detoxification of ammonia (2). The switch of the GDH reaction provides protection for the brain from the risk of encephalopathy.

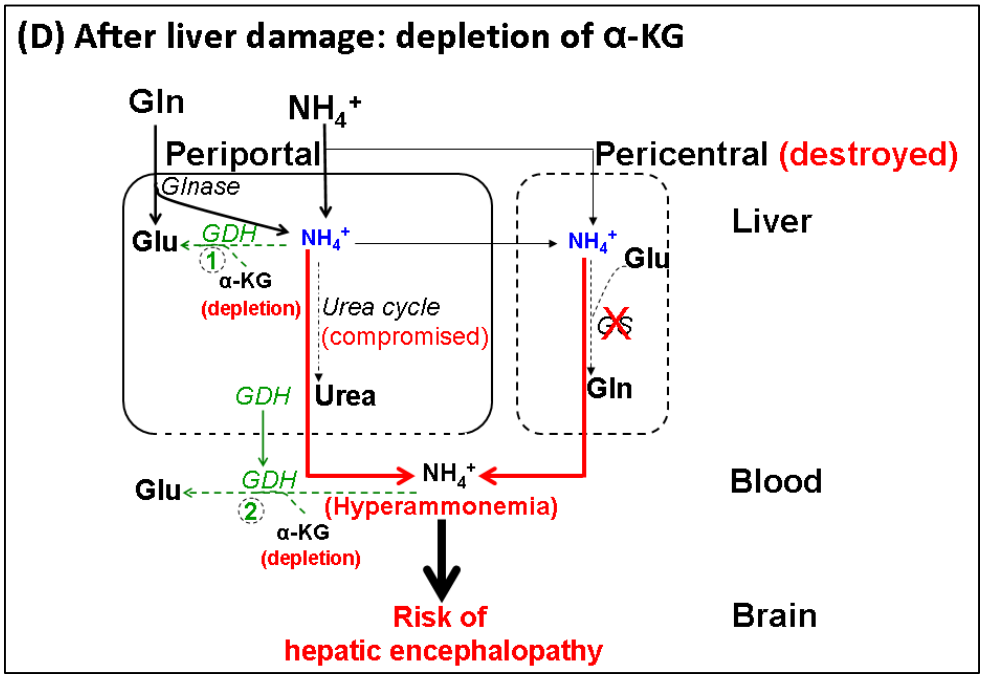

Fig. 4.1D: Depletion of alpha-ketoglutarate (α-KG) due to consumption by the GDH reaction after liver damage. The continuous consumption of α-KG by the glutamate dehydrogenase (GDH) reaction results in systemic depletion of α-KG from the blood. Subsequently, no further ammonia detoxification by the reversed GDH reaction is possible. This results in elevation of ammonia concentration in the blood which might leads to hepatic encephalopathy.

4.2 Compromised ammonia detoxification after CCl_4 intoxication

In healthy mice the portal vein blood has the highest ammonia concentration of the organism. In contrast, much lower ammonia concentrations were measured in the hepatic vein and in the systemic circulation (Fig. 3.7). The portal vein serves as a drainage system leading ammonia generated in the intestinal tract into the liver (Lemberg and Fernandez, 2009). The liver is efficiently detoxifying ammonia through the urea cycle and the GS reaction in the periportal and pericentral hepatocytes, respectively (Haussinger, 1990; Olde Dominik et al., 2002). Thus, the liver acts as a filter that prevents the passage of toxic ammonia into the systemic circulation.

CCl_4 intoxication specifically damages the pericentral hepatocytes (Hoehme et al., 2007; 2010). This is due to the restricted zonation of the

metabolizing enzyme CYP2E1 to the pericentral compartment of the liver lobule (Braeuning et al., 2006). A consequence of CCl_4 induced liver damage is systemic hyperammonemia. Although ammonia was elevated at all measured positions of the vascular system, the heart blood showed lower ammonia concentrations compared to the hepatic and portal vein values. This can be explained by the extra-hepatic contribution from other organs that also express GS. In addition to the pericentral hepatocytes, GS is also expressed in the skeletal muscles, brain (astrocytes) and lungs (Chatauret and Butterworth, 2004; Ytrebø et al., 2006). GS allows the temporary detoxification of ammonia through glutamine formation. Ammonia can again be released from glutamine upon catabolism by the glutaminase enzyme (Haussinger, 1983; Gebhardt et al; 1988).

4.3 Mathematical modelling of ammonia detoxification leads to wrong predictions

As a starting point, a model of ammonia detoxification was established (Fig. 3.32). The model is an extension of Hoehme et al. (2010). The model involves urea and glutamine synthesis which are the major pathways of ammonia detoxification. Based on these pathways the model predicts the hepatic output of ammonia, urea and glutamine before and after CCl_4 intoxication (Fig. 4.2). In a next step, experiments were performed to validate the model predictions. Mice received a single dose of 1.6 g/kg CCl_4 and then ammonia, urea and glutamine were measured in the portal vein (liver inflow) and in the hepatic vein (liver outflow) in a time dependent manner. Interestingly, a transient discrepancy between the predicted and the experimentally obtained data was identified. Predictions of both ammonia and glutamine were higher than the experimental data. This was most obvious on day one for ammonia and on days four and six for glutamine (Fig. 3.33; 3.34). Therefore, the following set of experiments was designed to identify explanations for this discrepancy (4.4; 4.5; 4.6).

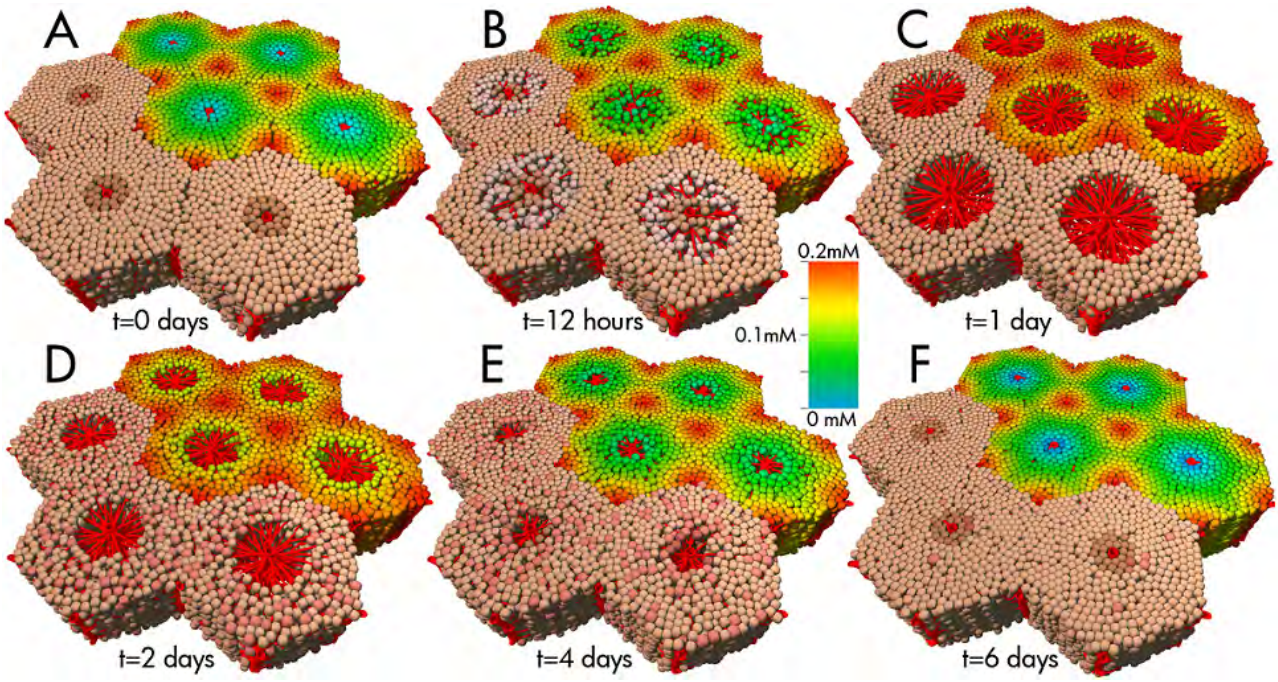

Fig. 4.2: Spatial-temporal modelling of ammonia detoxification during liver damage and regeneration on the level of the individual cell (A-F). The three frontal left lobules show the destruction and the regeneration process following CCl_4 intoxication. The red colored shade indicates hepatocytes proliferation. The other four liver lobules show the alteration of ammonia metabolism during liver damage and regeneration on each individual hepatocyte. The highest concentration of ammonia is in the periportal region (red color), whereas minimal ammonia concentration is in the pericentral region (blue color). Time points where images were taken are (T= 0, 12h, 1d, 2d, 4d and 6d days after injection of 1.6 g/kg CCl_4).

4.4 Disturbance of metabolic zonation during liver regeneration

GS is a well known pericentral marker of the liver lobule restricted to 1-3 layers of hepatocytes surrounding central veins (Fig. 4.3) (Gebhardt and Mecke, 1983). Although complete regeneration of liver architecture was reached six days after CCl_4 intoxication, the recovery of GS activity took at least 12 days. Possibly this was due to the periportal origin of the newly formed hepatocytes. These cells may need a period of contact to the endothelial cells of central veins until they become reprogrammed to express the pericentral signal. The theory of this sinusoidal cell-hepatocyte interaction was previously reported by Kuo et al. (1991) and Gebhardt (1992a). These findings allowed correcting the prediction of

glutamine during liver regeneration. However, the delayed recovery of GS led to even worse ammonia prediction.

In contrast to GS, CPS1 is expressed in the periportal hepatocytes occupying 93% of the liver parenchyma (Gebhardt, 1992b). CPS1 is well known to be the rate limiting enzyme of the urea cycle (Gaasbeek Janzen et al., 1984; Gebhardt, 1992b). Immunohistochemical analysis of CPS1 during liver regeneration showed unexpected results. The territory of CPS1 was extended to cover the whole liver parenchyma on days four and six after CCl_4 administration (Fig. 4.3). By including these data into the model, ammonia was correctly predicted during liver regeneration.

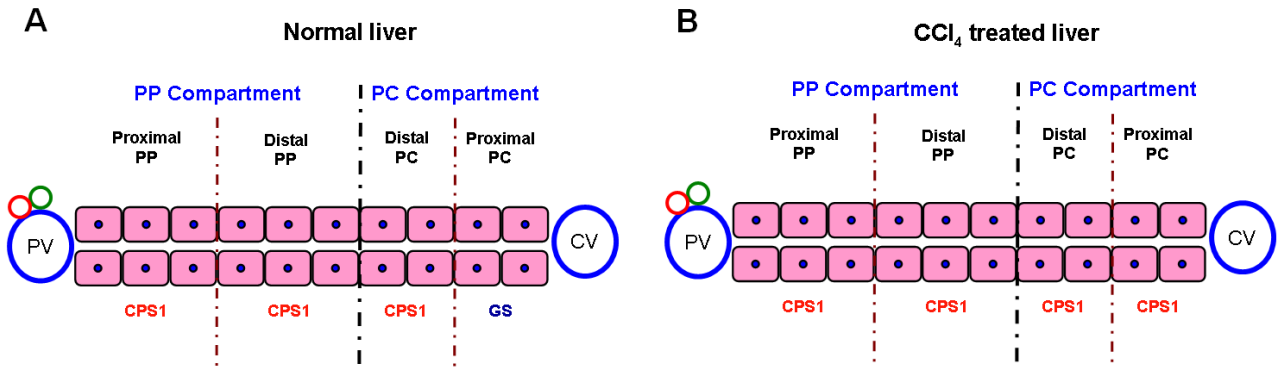

Fig. 4.3: Illustration of the disturbed zonation of glutamine synthetase (GS) and carbamoyl phosphate synthetase1 (CPS1) during liver regeneration. The liver lobule is divided into two metabolic compartments: the periportal (PP) and the pericentral (PC) compartment. Both of which are subdivided into proximal and distal part. (A) In normal liver the expression of GS is restricted to the proximal PC of the liver lobule. In contrast, CPS1 is expressed in the whole PP and in the distal PC of the liver lobule. (B) During liver regeneration after CCl_4 intoxication the territory of CPS1 is extends to cover the whole liver parenchyma (periportal like liver). PV: portal vein; CV: central vein.

4.5 Reduction of the urea cycle capacity after CCl_4 intoxication

Based on image analysis, CCl_4 intoxication destroyed maximally 32% of the periportal compartment of the liver lobule. However, the urea cycle capacity was reduced by approximately 60% after CCl_4 intoxication. These findings were in agreement with Haussinger and Gerok (1984); Gebhardt et al. (1988). When

these results were included into the model, the prediction of ammonia became even worse. The model predicted too high ammonia concentrations in comparison to the experimentally obtained data. This was most obvious on day one after CCl_4 administration (Fig. 3.49).

Although the capacity of the urea cycle was reduced after CCl_4 intoxication, the blood urea concentration was slightly or almost unaltered. A possible explanation for this is the release of arginase from damaged hepatocytes. Arginase catalyzes the hydrolysis of arginine into urea and ornithine. This resulted in systemic depletion of arginine (Fig. 3.46). Arginine consumption was previously reported in similar scenarios of acute liver damage (Reid et al., 2007; Murayama et al., 2008; Jeyabalan et al, 2008).

4.6 The reversibility of GDH and systemic protection against hyperammonemia

GDH is homogeneously expressed in the liver parenchyma (Wimmer and Pette, 1979; Lamers et al., 1988; Boon et al., 1999). However, the function and the activity of GDH show a spatial heterogeneity. Lamers et al. (1988) reported a “U-shaped” activity profile of GDH: medium/high activity in the periportal hepatocytes, high activity in the pericentral hepatocytes and low activity in the mid-zonal area. The periportal GDH serves as a source of ammonia in the liver. It catalyzes the deamination of glutamate into ammonia and α-KG. In contrast, the pericentral GDH is ammonia consumer. It catalyzes the formation of glutamate from ammonia and α-KG. Glutamate is then consumed by the GS reaction to form glutamine (Haussinger, 1990; Meijer et al., 1990; Maly and Sasse, 1991; Boon et al., 1999). This is due to the spatial difference of the affinity of GDH to glutamate (Jonker et al., 1996).

A key observation in this study is the systemic depletion of α-KG after induction of liver damage by CCl_4 (Fig. 3.50). This was accompanied with systemic elevation of glutamate concentrations. Moreover, the activity of GDH

was also increased after CCl_4 intoxication. These data suggest that under conditions of liver damage the GDH reaction switches from ammonia production to ammonia detoxification. Priesnitz et al. (2012) investigated the switch of the GDH reaction toward glutamate production in a brain cell line exposed to high concentrations of ammonium chloride. Moreover, several studies have reported glutamate production after administration of high concentrations of ammonia in experimental animals (Brosnan and Williamson, 1974; Cooper et al., 1987; Nissim et al., 2003; Dadsetan et al., 2011).

4.6.1 Confirmation of the GDH switch in cultivated hepatocytes

In order to investigate the role of the GDH in ammonia metabolism a GDH inhibitor was used. Inhibition of GDH in cultivated hepatocytes resulted in decreased ammonia concentrations in the culture media (Fig. 3.57). These findings confirm that under normal conditions GDH works in the direction of ammonia production. In contrast, inhibition of the GDH in hepatocyte cultures exposed to high concentrations of ammonium chloride resulted in elevation of ammonia concentrations in the culture media. Inhibition of GDH under these conditions caused cytotoxic effects in the cultivated hepatocytes (Fig. 3.56). These findings suggest that GDH acts as an ammonia scavenger under conditions of high ammonia concentrations.

In addition, the intracellular glutamate concentration decreased after inhibition of the GDH in cultivated hepatocytes exposed to high concentrations of ammonium chloride. This confirms the switch of the GDH reaction toward glutamate production under conditions of high ammonia concentrations. However, in absence of the GDH inhibitor there was no obvious increase in glutamate concentrations, even after exposure to high concentrations of ammonium chloride. It should be considered that glutamate interacts with many biochemical pathways in hepatocytes (Fig. 4.4). Glutamate which is generated by the switch of the GDH reaction might be consumed by these pathways.

The switch of the GDH reaction from ammonia production to ammonia detoxification was observed only after incubation with high concentrations of

ammonium chloride. This might be because all mechanisms of ammonia detoxification (urea cycle, GS) are functioning in cultivated hepatocytes. These mechanisms might be sufficient to detoxify the relatively low concentrations of ammonia.

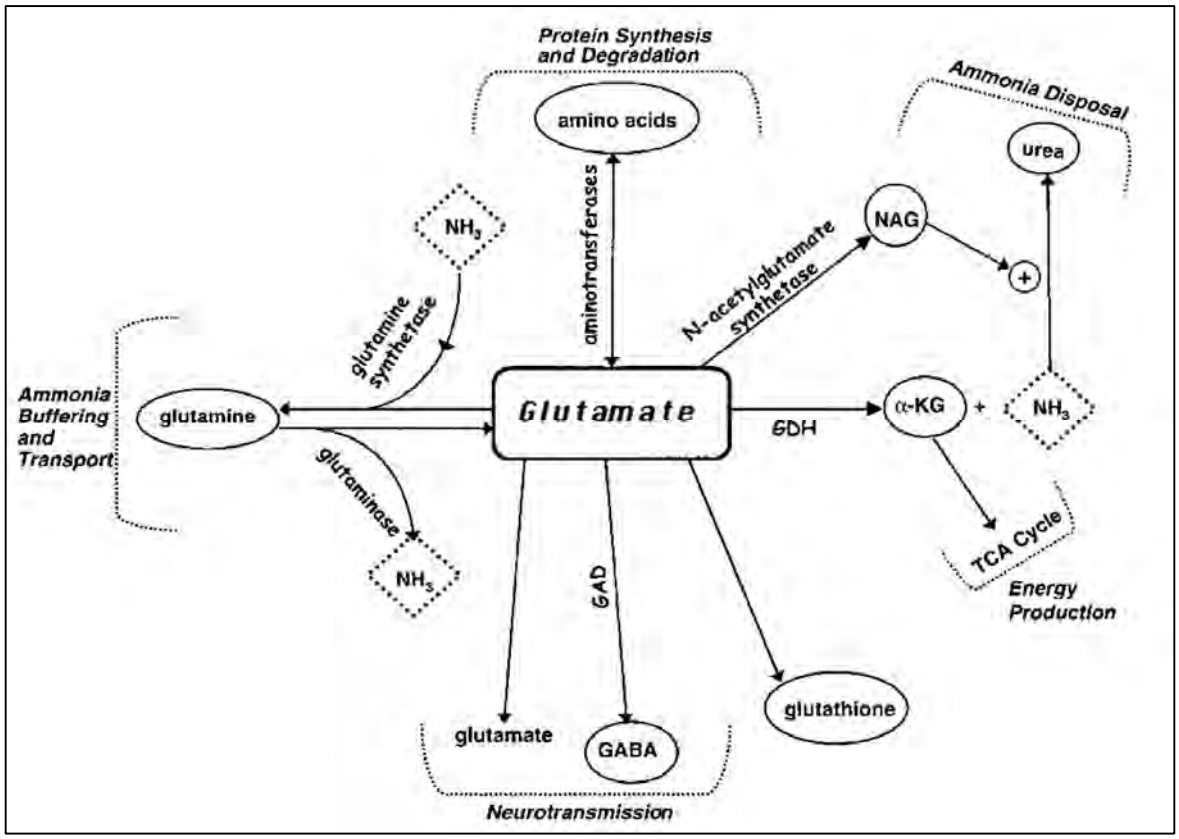

Fig. 4.4: Pathways of glutamate metabolism. In addition to the glutamate dehydrogenase (GDH) reaction, glutamate can be further metabolized by many metabolic pathways in the liver: (i) Aminotransferases reactions to form other amino acids. (ii) Glutamine synthetase reaction to form glutamine. (iii) N-acetyl glutamate (NAG)-synthetase to form NAG. (IV) Cysteine and glycine to form glutathione (source: Kelly and Stanley, 2001)

4.6.2 Identification of a novel mechanism of systemic protection against ammonia

Induction of liver damage by CCl_4 resulted in systemic elevation of the GDH activity (Fig. 3.59). This was due to the release of GDH from damaged hepatocytes. Analysis of the plasma GDH activity is routinely used as a marker of hepatic necrosis (O'Brien et al., 2002).

In order to test whether the released GDH can detoxify ammonia, plasma was collected from the portal vein, hepatic vein and heart of mice after induction of acute liver damage by CCl_4. The plasma was incubated with a certain concentration of ammonium chloride in presence or absence of α-KG. Interestingly, the results showed obvious ammonia consumption and glutamate production only when α-KG had been added (Fig.3.62). This is because that the released GDH catalyzes the conversion of ammonia and α-KG into glutamate and thereby consumes the α-KG available in the plasma. This suggests that supplementation of α-KG in case of acute liver damage should reestablish systemic detoxification of ammonia through the reversed GDH reaction. This unique hitherto unrecognized mechanism can provide systemic protection against hyperammonemia in patients with acute liver damage. A clinically relevant implication of these results is that α-KG should be supplemented in patients with acute liver damage.

5 Summary

The liver is responsible for maintaining the metabolic homeostasis throughout the body. Therefore, acute liver failure is life threatening. Only little is known about how the complex metabolic function of the liver is restored after liver injury. The goals of this thesis were to 1) study the metabolic alterations during liver damage and regeneration, 2) model ammonia detoxification during liver damage and regeneration, 3) study the alterations of metabolic zonation and to 4) identify possible compensatory mechanisms for ammonia detoxification during liver damage and regeneration. For this purpose I used a mouse system where the hepatotoxic agent CCl_4 was injected to induce acute liver damage. Metabolic parameters relevant for ammonia and carbohydrate metabolism were quantified in a time and in a dose-dependent manner after CCl_4 intoxication including ammonia, urea, glutamine, glutamate, glucose, lactate, pyruvate, alanine, arginine and alpha-ketoglutarate. The measurement was done in blood collected from the portal vein “representing the liver inflow”, the hepatic vein “representing the liver outflow” and from the heart “representing the mixed venous blood”.

For deeper understanding of ammonia metabolism during liver damage and regeneration, a model of ammonia detoxification was established. Model predictions and experimental data were compared. After iterative cycles of modeling and experiments the following so far unknown mechanism was identified. Upon acute liver damage hepatocytes release glutamate dehydrogenase (GDH) (together with further liver enzymes) into the systemic circulation. As soon as blood ammonia concentrations increase, the GDH reaction takes place in a reversed manner. This means that GDH uses ammonia and alpha-ketoglutarate (α-KG) as substrates to form glutamate. By this reaction the toxic ammonia is detoxified to form the non-toxic glutamate. Interestingly, this reaction is not limited to the liver itself but upon release of GDH from damaged hepatocytes protection against ammonia is provided systemically in blood. However, this protection lasts only as long as α-KG is present in the blood. It can

not continue when α-KG has been consumed by the GDH reaction. This observation is of clinical relevance since it might be possible to therapeutically substitute α-KG after induction of acute liver damage. This mechanism was discovered in experiments with plasma of mice and in vitro with cultivated hepatocytes. After administration of CCl_4 a transient increase of plasma GDH was observed which was accompanied by a decrease in α-KG. When plasma was taken from such mice detoxification of ammonia to glutamate was only observed when α-KG was added. Ammonia detoxification as well as glutamate production were both blocked by addition of the GDH inhibitor 2,6-pyridinedicarboxylic acid (PDAC). In cultivated hepatocytes PDAC increased ammonia cytotoxicity. Interestingly, hepatocytes decreased the ammonia concentrations in the culture medium at high ammonia concentrations. In contrast, hepatocytes released ammonia if its concentrations in the culture medium were relatively low. This fits to the mechanism that GDH switches from ammonia production to ammonia detoxification if the concentrations of ammonia increase.

Studying the metabolic zonation after CCl_4 intoxication showed a transient disturbance of metabolic zonation during liver regeneration. This included the delayed recovery of the pericentral marker glutamine synthetase. In contrast, the territory of the periportal marker carbamoyl phosphate synthetase1 is extended to cover the whole liver parenchyma on days four and six after CCl_4 intoxication. When these findings were included into the model, the predictions of both ammonia and glutamine were in a good accordance with the experimentally obtained data.

In conclusion, the acutely damaged liver provides systemic protection against hyperammonemia by the release of GDH into the blood. As soon as plasma α-KG is consumed by the GDH reaction it should be therapeutically substituted.

6 Zusammenfassung

Die Leber spielt eine zentrale Rolle bei der Aufrechterhaltung des metabolischen Gleichgewichts. Akutes Leberversagen ist daher lebensbedrohlich. Relativ wenig ist bekannt, wie metabolische Funktionen während und nach Leberschädigung aufrechterhalten werden. Die Ziele dieser Arbeit waren daher 1) metabolische Veränderungen der Leber der Maus während Leberschädigung- und Regeneration zu untersuchen, 2) die Ammoniak-Entgiftung zu modellieren, 3) die Veränderungen der metabolischen Zonierung des Leberläppchens während Leberschädigung und Regeneration zu berücksichtigen, 4) mögliche Kompensationsmechanismen während der Schädigungs- und Regenerationsphase zu identifizieren. Für diese Untersuchungen wurden Mäuse eingesetzt, denen Tetrachlorkohlenstoff (CCl_4) zur Verursachung eines akuten Leberschadens injiziert wurde. Für den Ammoniakstoffwechsel relevante Parameter wurden Zeit- und Dosisabhängig nach Injektion von CCl_4 erfasst: Ammoniak, Harnstoff, Glutamin, Glutamat, Glucose, Laktat, Pyruvat, Alanin, und alpha-Ketoglutarat. Diese Analysen wurden durchgeführt in Blut aus a) der Portalvene, welche den „Lebereingang“ repräsentiert, b) der Lebervene als „Leberausfluss“ und c) der rechten Herzkammer, um auch gemischt venöses Blut zu erfassen.

Um die komplexen Vorgänge des Ammoniakstoffwechsels quantitativ erfassen zu können, wurde ein metabolisches Modell eingesetzt. Vorhersagen dieses metabolischen Modells (welches alle zur Zeit wesentlichen Prozesse des Ammoniakstoffwechsels einschließt) wurden mit den experimentellen Daten verglichen. Nach mehreren Zyklen von Experimenten und Modellierung wurde hierbei gezeigt, dass die bisher bekannten Mechanismen nicht ausreichen, den Ammoniakstoffwechsel während Leberschädigung quantitativ zu beschreiben. Vielmehr wurde der folgende Mechanismus identifiziert, welcher für das Verständnis der gesamten Situation wesentlich ist: nach Leberschädigung setzen geschädigte Hepatozyten neben zahlreichen weiteren Proteinen Glutamatdehydrogenase (GDH) in dem systemischen Blutkreislauf frei. Sobald

die Ammoniakkonzentrationen im Blut ansteigen, findet eine GDH-Reaktion in umgekehrter Richtung statt. Bei dieser Reaktion wird der toxische Ammoniak dadurch entgiftet, dass er mit Ammoniak zum relativ untoxischen Glutamat verbunden wird. Ein neuer Aspekt ist hierbei, dass Ammoniakentgiftung in Folge der GDH-Freisetzung nicht nur in der Leber, sondern auch systemisch im Blut stattfindet. Allerdings kann diese entgiftende Reaktion im Blut nur so lange stattfinden, bis das dort vorhandene alpha-Ketoglutarat durch die GDH-Reaktion verbraucht wurde. Diese Beobachtung ist möglicherweise von klinischer Relevanz. Denn sobald die alpha-Ketoglutarat Konzentration in der Leber als Folge der GDH-Reaktion absinkt, könnte es therapeutisch substituiert werden. Dieser Mechanismus der reversen GDH-Reaktion wurde bei Experimenten mit Plasma von Mäuse und mit kultivierten Hepatozyten der Maus beobachtet. Nach Verabreichung von CCl_4 an Mäusen wurde eine transiente Zunahme von GDH im Plasma beobachtet. Dies ging einher mit einer sehr starken Abnahme des alpha-Ketoglutarat. Falls Plasma in diesem Zustand Mäusen entnommen wurde, konnte Ammoniak-Entgiftung zu Glutatmat nur dann beobachtet werden, nachdem alpha-Ketoglutarat zugesetzt worden war. Weiterhin konnten im Plasma sowohl die Ammoniakentgiftung, als auch die Bildung von Glutamat durch den GDH-Inhibitor 2,6 Pyridine dicarboxylsäure (PDAC) gehemmt werden. In kultivierten Hepatozyten steigerte PDAC die Toxizität des Ammoniaks. Bemerkenswert ist, dass kultivierte Hepatozyten nur bei hohen Ammoniakkonzentrationen im Kulturmedium Ammoniak zu Glutamat entgifteten. Bei niedrigen Konzentrationen gaben Hepatozyten sogar noch Ammoniak in das Kulturmedium ab. Auch diese Beobachtung passt zur Hypothese des „GDH switch“, wobei GDH bei niedrigen Ammoniakkonzentrationen Ammoniak produziert, hingegen bei hohen Konzentrationen konsumiert.

Leberschädigung mit CCl_4 verursachte eine transiente Störung der metabolischen Zonierung des Läppchens. Zum Beispiel wurde eine verzögerte Erholung des perizentralen Markers Glutaminsynthetase beobachtet. Im Gegensatz hierzu dehnte das normalerweise auf die periportale Region begrenzte Enzym Carbamoylphosphat-Synthetase sein Territorium auf das

gesamte Leberläppchen aus. Dies wurde zwischen Tag 4 und 6 nach Intoxikation mit CCl_4 beobachtet. Nachdem sämtliche neue Mechanismen im Modell berücksichtigt wurden, ergab sich eine gute Übereinstimmung zwischen der Modellsimulation und den experimentellen Daten.

Zusammenfassend kann festgestellt werden, dass die Leber nach akuter Schädigung einen systemischen Schutz gegen Hyperammonämie durch Freisetzung von GDH vermittelt. Eine mögliche klinische Relevanz dieser Beobachtung besteht darin, dass alpha-Ketoglutarat im Plasma therapeutisch substituiert werden könnte, sobald es durch die GDH Reaktion verbraucht worden ist.

7 References

Apte U, Singh S, Zeng G, Cieply B, Virji MA, Wu T, Monga SP (2009): Beta-catenin activation promotes liver regeneration after acetaminophen-induced injury. Am J Pathol; 175(3):1056-1065.

Benhamouche S, Decaens T, Godard C, Chambrey R, Rickman DS, Moinard C, Vasseur-Cognet M, Kuo CJ, Kahn A, Perret C, Colnot S (2006). Dev Cell; 10(6):759-770.

Bergmeyer HU, Beutler HO (1985). Methods of Enzymatic Analysis, 3rd Edition, vol. VIII, Bergmeyer, H. U., ed., Academic Press; New York: 454-461.

Bioulac-Sage P, Lafon ME, Saric J, Balabaud C (1990). Nerves and peri-sinusoidal cells in human liver. J. Hepatol.; 10: 105-112.

Böhm F, Köhler UA, Speicher T, Werner S (2010). Regulation of liver regeneration by growth factors and cytokines. EMBO Mol Med; 2(8):294-305.

Bondar RJ, Mead DC (1974). Evaluation of glucose-6-phosphate dehydrogenase from Leuconostoc mesenteroides in the hexokinase method for determining glucose in serum. Clin Chem; 20(5):586-590.

Boon L, Geerts WJ, Jonker A, Lamers WH, Van Noorden CJ (1999). High protein diet induces pericentral glutamate dehydrogenase and ornithine aminotransferase to provide sufficient glutamate for pericentral detoxification of ammonia in rat liver lobules. Histochem Cell Biol; 111(6):445-452.

Bouwens L, Baekeland M, De Zanger R, Wlsse E (1986). Quantitation, tissue distribution and proliferation kinetics of Kupffer cells in normal rat liver. Hepatology; 6: 718-722.

Braeuning A, Ittrich C, Kohle C, Hailfinger S, Bonin M, Buchmann A (2006). Differential gene expression in periportal and perivenous mouse hepatocytes. FEBS J; 273:5051-5061.

Brosnan JT, Williamson DH (1974). Mechanisms for the formation of alanine and aspartate on rat liver in vivo after administration of ammonium chloride. Biochem J; 138(3):453-462.

Burt AD (1999). Pathobiology of hepatic stellate cells. J. Gastroenterol.; 34: 299-304.

Cadoret A, Ovejero C, Terris B, Souil E, Levy L, Lamers WH, Kitajewski J, Kahn A, Perret C (2002). New targets of beta-catenin signaling in the liver are involved in the glutamine metabolism. Oncogene; 21:8293– 8301.

Campbell JS, Prichard L, Schaper F, Schmitz J, Stephenson-Famy A, Rosenfeld ME, Argast GM, Heinrich PC, Fausto N (2001). Expression of suppressors of cytokine signaling during liver regeneration. J Clin Invest; 107(10):1285-1292.

Cardell EL, Cardell RR (1997). Structure and function of hepatic parenchymal cells. In: McCuskey RS, Earnest DL, eds. Comprehensive toxicology. Vol. 9. Hepatic and gastrointestinal toxicology. Oxford: Elsevier Science: 11–34.

Cash WJ, McConville P, McDermott E, McCormick PA, Callender ME, McDougall NI (2010). Current concepts in the assessment and treatment of hepatic encephalopathy. QJM; 3(1):9-16.

Chatauret N, Butterworth RF (2004). Inter-organ ammonia trafficking in liver failure. Journal of Gastroenterology and Hepatology; 19: 219–223.

Chomczynski P, Sacchi N (1987). Single-step method of RNA isolation by acid guanidinium thiocyanate-phenol-chloroform extraction. Anal Biochem.; 162(1):156-159.

Christen P and Metzler DE (1985). Transaminases, Wiley-Interscience, Inc., New York: 365-451.

Colnot S and Perret C (2011). Liver zonation. In: Molecular pathology of liver diseases. S.P.S. Monga (ed.), Molecular pathology library 5: 7-16.

Connor HD, Thurman RG, Galiz MD, Mason RP (1986). The formation of a novel free radical metabolite from CCl_4 in the perfused rat liver and in vivo. J. Biol. Chem.; 261: 4542-4548.

Cooper AJ, Nieves E, Coleman AE, Filc-DeRicco S, Gelbard AS (1987). Short-term metabolic fate of [13N]ammonia in rat liver in vivo. J Biol Chem; 262(3):1073-1080.

Dadsetan S, Bak LK, Sørensen M, Keiding S, Vilstrup H, Ott P, Leke R, Schousboe A, Waagepetersen HS (2011). Inhibition of glutamine synthesis induces glutamate dehydrogenase-dependent ammonia fixation into alanine in co-cultures of astrocytes and neurons. Neurochem Int; 59(4):482-488.

Desmet V (2001). Organizational principles in the liver. In: Arias IM, Boyer JL, Chisari FV et al. (eds) The Liver: Biology and Pathobiology, 4th edn. New York: Raven Press: 3–15.

Drochmans P, Wanson J C, Mosselmans R (1975). Isolation and sub-fractionation on Ficoll gradients of adult rat hepatocytes. J. Cell Biol.; 66: 1-22.

Fausto N, Webber E M (1994). In the Liver Biology and Pathobiology: Arias I M, Boyer J L, Fausto N, Jacoby WB, Schachter D, Shafritz D A(eds); Raven Press Ltd, New York, USA.: 53–68.

Fausto N, Campbell JS, Riehle KJ (2006). Liver regeneration. Hepatology; 43: 45–53.

Flecknell P(1996). Laboratory animal anaesthesia. A practical introduction for research workers and technicians. Academic Press London, 2. ed.

Gaasbeek Janzen JW, Lamers WH, Moorman AF, DE Graaf A, Los JA and Charles R (1984). Immunohistochemical localization of carbamoyl-phosphate synthetase (ammonia) in adult rat liver: evidence for a heterogeneous distribution. J. Histochem. Cytochem.; 32: 557-564.

Gebhardt R (1992a). Cell-cell interactions: clues to hepatocyte heterogeneity and beyond? Hepatology; 16: 843– 845.

Gebhardt R (1992b). Metabolic zonation of the liver: regulation and implications for liver function. Pharmac. Ther.; 53: 275-354.

Gebhardt R, Baldysiak-Figiel A, Krugel V, Ueberham E, Gaunitz F (2007). Hepatocellular expression of glutamine synthetase: an indicator of morphogen actions as master regulators of zonation in adult liver. Prog Histochem Cytochem.; 41(4):201–266.

Gebhardt R, Burger HJ, Heini H, Schreiber KL, Mecke D (1988). Alterations of hepatic enzyme levels and of the acinar distribution of glutamine synthetase in response to experimental liver injury in the rat. Hepatology; 8(4): 822-830.

Gebhardt R, Gaunitz F (1997). Cell-cell interactions in the regulation of the expression of hepatic enzymes. Cell Biology and Toxicology; 13: 263-273.

Gebhardt R, Mecke D (1983). Heterogeneous distribution of glutamine synthetase among rat liver parenchymal cells in situ and in primary culture. EMBO J; 2:567-570.

Gebhardt R, Williams GM (1986). Amino acid transport in established adult rat liver epithelial cell lines. Cell Biol Toxicol;2: 9-20.

Glasel J (1995). Validity of nucleic acid purities monitored by 260/280 absorbance ratios. BioTechniques; 18 (1): 62–63.

Gruebele A, Zawaski K, Kaplan D, Novak RF (1996). Cytochrome P450 2E1 and cytochrome P4502B1/2B2 catalyzed carbon tetrachloride metabolism: effects on signal transduction as demonstrated by altered immediate-early (c-Fos and c-Jun) gene expression and nuclear AP-1 and NFκB transcription factor levels. Drug. Metabol. Disp.; 24:15–22.

Häussinger D (1990). Nitrogen metabolism in liver: structural and functional organization and physiological relevance. Biochem J; 267: 281–290.

Häussinger D, Gerok W (1984). Hepatocyte heterogeneity in ammonia metabolism-Impairment of glutamine synthesis in CCl_4-induced liver cell necrosis with no effect on urea synthesis. Chem Biol Interact; 48: 191-194.

Häussinger D (1983). Hepatocyte heterogeneity in glutamine and ammonia metabolism and the role of an intracellular glutamine cycle during ureagenesis in perfused rat liver. Fur. J. Biochem.; 133: 269-275.

Häussinger D, Gerok W (1983). Hepatocyte heterogeneity in glutamine uptake by isolated perfused rat liver. Eur. J. Biochem.; 136: 421-425.

Häussinger D, Lamers WH, Moorman AFM (1992). Hepatocyte heterogeneity in the metabolism of amino acids and ammonia. Enzyme; 46 (1–3): 72–93.

Higgins GM, Anderson RM (1931). Experimental pathology of the liver. Arch Pathol; 12: 186-202.

Hoehme S, Brulport M, Bauer A, Bedawy E, Schormann W, Hermes M, Puppe V, Gebhardt R, Zellmer S, Schwarz M, Bockamp E, Timmel T, Hengstler JG, Drasdo D (2010). Prediction and validation of cell alignment along microvessels as order principle to restore tissue architecture in liver regeneration. Proc Natl Acad Sci. USA;107(23):10371-10376.

Hoehme S, Hengstler JG, Brulport M, Schäfer M, Bauer A, Gebhardt R, Drasdo D (2007). Mathematical modelling of liver regeneration after intoxication with CCl_4. Chem Biol Interact; 168(1):74-93.

Jeyabalan G, Klune JR, Nakao A, Martik N, Wu G, Tsung A, Geller DA (2008). Arginase blockade protects against hepatic damage in warm ischemia-reperfusion. Nitric Oxide; 19(1):29-35.

Jonker A, Geerts WJC, Charles R, Lamers WH, Van Noorden CJF (1996). The dynamics of local kinetic parameters of glutamate dehydrogenase in rat liver. Histochem Cell Biol; 106: 437–443.

Jungermann K, Kietzmann T (1996). Zonation of parenchymal and non parenchymal metabolism in liver. Annu Rev Nutr.; 16:179–203.

Jungermann K, Katz N (1989). Functional specialization of different hepatocyte populations. Physiol Rev; 69 (3): 708–764.

Jungermann K (1986). Functional heterogeneity of periportal and perivenous hepatocytes. Enzyme; 35:161-180.

Katz N, Teutsch HF, Jungermann K, Sasse D (1977). Heterogeneous reciprocal localization of fructose-1, 6-bisphosphatase and of glucokinase in microdissected periportal and perivenous rat liver tissue. FEBS Lett.; 83(2): 272–276.

Kelly A, Stanley CA (2001). Disorders of glutamate metabolism. Ment Retard Dev Disabil Res Rev; 7(4):287-95.

Kera Y, Sippel HW, Penttilä KE, Lindros KO (1987). Acinar distribution of glutathione-dependent detoxifying enzymes. Low glutathione peroxidase activity in perivenous hepatocytes. Biochem Pharmacol; 36(12):2003-2006.

Kessler R, Fanestil D (1986). Interference by lipids in the determination of protein using bicinchoninic acid. Anal. Biochem.; 159: 138 -142.

Kietzmann T, Jungermann K (1997). Modulation by oxygen of zonal gene expression in liver studied in primary rat hepatocyte cultures. Cell Biology and Toxicology; 13: 243-255.

Klingmüller U, Bauer A, Bohl S, Nickel PJ, Breitkopf K, Dooley S, Zellmer S, Kern C, Merfort I, Sparna T, Donauer J, Walz G, Geyer M, Kreutz C, Hermes M, Götschel F, Hecht A, Walter D, Egger L, Neubert K, Borner C, Brulport M, Schormann W, Sauer C, Baumann F, Preiss R, MacNelly S, Godoy P, Wiercinska E, Ciuclan L, Edelmann J, Zeilinger K, Heinrich M, Zanger UM, Gebhardt R, Maiwald T, Heinrich R, Timmer J, von Weizsäcker F, Hengstler JG (2006). Primary mouse hepatocytes for systems biology approaches: a standardized in vitro system for modelling of signal transduction pathways. Syst Biol (Stevenage); 153(6):433-47.

Kuntz E, Kuntz H (2006). Hepatology principles and practice 2nd edition Springer Medizin Verlag Heidelberg: 1-27.

Kuo FC, Hwu WL, Valle D, Damell JE Jr (1991). Co-localization in pericentral hepatocytes in adult mice and similarity in developmental expression pattern of ornithine aminotransferase and glutamine synthetase mRNA. Proc Natl Acad Sci. USA; 88: 9468-9472.

Lamers WH, Janzen JW, Moorman AF, Charles R, Knecht E, Martínez-Ramón A, Hernández-Yago J, Grisolía S (1988). Immunohistochemical localization of glutamate dehydrogenase in rat liver: plasticity of distribution during development and with hormone treatment. J Histochem Cytochem; 36(1):41-47.

Lemberg A, Fernandez MA (2009). Hepatic encephalopathy, ammonia, glutamate, glutamine and oxidative stress. Annals of Hepatology; 8 (2):95-102.

Levesque R (2007). SPSS programming and data management: A guide for SPSS and SAS users, Fourth Edition, SPSS Inc., Chicago Ill.

Levintow L (1954). The glutamyltransferase activity of normal and neoplastic tissues. J. Natl. Cancer; 15:347-352.

Livak KJ, Schmittgen TD (2001). Analysis of relative gene expression data using real-time quantitative PCR and the 2(-Delta Delta C(T)) Method. Methods; 25(4):402-408.

Loeppen S, Schneider D, Gaunitz F, Gebhardt R, Kurek R, Buchmann A, Schwarz M (2002). Over expression of glutamine synthetase is associated with beta-catenin-mutations in mouse liver tumors during promotion of hepatocarcinogenesis by phenobarbital. Cancer Res; 62:5685–5688.

Lough J, Rosenthall L, Arzoumanian A, Goresky CA (1987). Kupffer cell depletion associated with capillarization of liver sinusoids in carbon tetrachloride-induced rat liver cirrhosis. J. Hepatol.; 5: 190-198.

Lutz WD, Weber Boll M, Stampfl A (2003). Hepatotoxicity and Mechanism of Action of Haloalkanes: Carbon Tetrachloride as a Toxicological Model. Critical Reviews in Toxicology; 33(2):105–136.

MacSween RNM, Scothorne RJ (1994). Developmental anatomy and normal structure. In: MacSween RNM, Anthony PP, Scheuer PJ et al. (eds) Pathology of the Liver. Edinburgh: Churchill Livingstone: 1–49.

Maly IP, Sasse D (1991). Micro-quantitative analysis of the intra-acinar profiles of glutamate dehydrogenase in rat liver. J Histochem Cytochem; 39(8): 1121-1124.

Meijer AJ, Lamers WH, Chamuleau RA (1990). Nitrogen metabolism and ornithine cycle function. Physiol Rev 70:701–748.

Michalopoulos GK (2007). Liver regeneration. J Cell Physiol; 213(2):286-300.

Michalopoulos GK, DeFrances M (2005). Liver regeneration. Adv Biochem Eng Biotechnol.; 93: 101–134.

Michalopoulos GK, DeFrances M, (1997). Liver regeneration. Science; 276:60–66.

Murayama H, Ikemoto M, Fukuda Y, Nagata A (2008). Superiority of serum type-I arginase and ornithine carbamyltransferase in the detection of toxicant-induced acute hepatic injury in rats. Clin Chim Acta; 391(1-2):31-35.

Nakatani K, Kaneda K, Seki S, Nakajima Y (2004). Pit cells as liver-associated natural killer cells: morphology and function. Med Electron Microsc; 37(1):29-36.

Nicholes K, Guillet S, Tomlinson E, Hillan K, Wright B, Frantz GD, Pham TA, Dillard-Telm L, Tsai SP, Stephan JP, Stin-son J, Stewart T, French DM (2002). A mouse model of hepato-cellular carcinoma: ectopic expression of fibroblast growth factor 19 in skeletal muscle of transgenic mice. Am J Pathol; 160: 2295–2307.

Nissim I, Horyn O, Luhovyy B, Lazarow A, Daikhin Y, Nissim I, Yudkoff M (2003). Role of the glutamate dehydrogenase reaction in furnishing aspartate nitrogen for urea synthesis: studies in perfused rat liver with 15N. Biochem J; 15:179-188.

O'Brien PJ, Slaughter MR, Polley SR, Kramer K (2002). Advantages of glutamate dehydrogenase as a blood biomarker of acute hepatic injury in rats. Lab Anim; 36(3):313-321.

Olde Damink SW, Deutz NE, Dejong CH, Soeters PB, Jalan R (2002). Inter-organ ammonia metabolism in liver failure. Neurochem. Int.; 41: 177–188.

Park BK, Kitteringham NR, Maggs JL, Pirmohamed M, Williams DP (2005). The role of metabolic activation in drug-induced hepatotoxicity. Annu Rev Pharmacol Toxicol; 45:177-202.

Parkinson A, Ogilvie BW (2008). Biotransformation of Xenobiotics. In: Klaassen CD, editor. Casarett and Doull's toxicology: the basic science of poisons. 7th ed. New York: McGraw-Hill: 161–304.

Piper MT, Suzanne MD (2012). Comparative Anatomy and Histology: A Mouse and Human Atlas. First edition: 193-199.

Priesnitz C, Niklas J, Rose T, Sandig V, Heinzle E (2012). Metabolic flux rearrangement in the amino acid metabolism reduces ammonia stress in the α1-antitrypsin producing human AGE1.HN cell line. Metab Eng; 14(2):128-137.

Ramos-Vara JA (2005). Technical Aspects of Immunohistochemistry. Vet Pathol; 42 (4): 405–426.

Recknagel RO, Glende EA (1973). Carbone tetrachloride hepatotoxicity: an example of lethal cleavage. CRC Crit. Rev. Toxicol.; 2: 263-297.

Recknagel RO, Glende EA, Dolak JA, Waller RL (1989). Mechanisms of carbon tetrachloride toxicity. Pharmacol Ther; 43: 139 – 154.

Reid KM, Tsung A, Kaizu T, Jeyabalan G, Ikeda A, Shao L, Wu G, Murase N, Geller DA (2007). Liver I/R injury is improved by the arginase inhibitor, N(omega)-hydroxy-nor-L-arginine (nor-NOHA). Am J Physiol Gastrointest Liver Physiol; 292(2):512-517.

Rodés J, Benhamou J, Andres T, Blei RJ, Rizzetto M, (2007). Text book of Hepatology from Basic Science to Clinical Practice, 3rd edition by Blackwell Publishing Ltd: 1-43.

Rodriguez-Soto J, Warnke RA, Rouse RV (1997). Endogenous avidin binding activity revealed by microwave treatment of sections. Appl. Immunohistochem. 5, 59-62.

Saxena R, Theise N (2004). Canals of Hering: recent insights and current knowledge. Semin Liver Dis; 24: 43–48.

Schneeberger CP, Speiser F, Kury Zeillinger R (1995). Quantitative detection of reverse transcriptase-PCR products by means of a novel and sensitive DNA stain. PCR Methods Appl.; 4:234-238.

Schuppan D, Schmid M, Somasundaram R, Ackermann R, Ruehl M, Nakamura T, Riecken EO (1998). Collagens in the liver extracellular matrix bind hepatocyte growth factor. Gastroenterology; 114(1):139-52.

Seglen PO (1972). Preparation of rat liver cells: I. Effect of $Ca2^{+}$ on enzymatic dispersion of isolated, perfused liver. Exp Cell Res; 74(2):450-454.

Shi SR, Cote RJ, Chaiwun B, Young LL, Shi Y, Hawes D, Chen T, et al. (1998). Standardization of immunohistochemistry based on antigen retrieval technique for routine formalin-fixed tissue sections. Appl Immunohistochem; 6:89–96.

Slater RF (1966). Necrogenic action of carbon tetrachloride in the rat: speculative mechanism based on action. Nature; 209: 36-40.

Stockert RJ, Wolkoff AW (2001). Cellular and molecular biology of the liver. Curr. Opin. Gastroenterol.; 17: 205-210.

Taub R (2004). Liver regeneration: From myth to mechanism. Nat Rev Mol Cell Biol; 5:836–847.

Te Koppele JM, Thurman RG (1990). Phagocytosis by Kupffer cells predominates in pericentral regions of the liver lobule. Am J Physiol; 259:814-821.

Thoolen B, Maronpot RR, Harada T, Nyska A, Rousseaux C, Nolte T, Malarkey DE, Kaufmann W, Küttler K, Deschl U, Nakae D, Gregson R, Vinlove MP, Brix AE, Singh B, Belpoggi F, Ward JM (2010). Proliferative and nonproliferative lesions of the rat and mouse hepatobiliary system. Toxicol Pathol; 38(7 Suppl):5S-81S.

Torre C, Perret C, Colnot S (2011). Transcription dynamics in a physiological process: β-catenin signaling directs liver metabolic zonation. Int J Biochem Cell Biol; 43(2):271-278.

Ugele B, Kempen HJ, Kempen JM, Gebhardt R, Meijer P, Burger HJ, Princen HM (1991). Heterogeneity of rat liver parenchyma in cholesterol 7 alpha-hydroxylase and bile acid synthesis. Biochem J; 15; 276 (Pt 1):73-7.

Ullrich D, Fischer G, Katz N, Bock KW (1984). Intralobular distribution of UDP-glucuronosyltransferase in livers from untreated, 3-methylcholanthrene- and phenobarbital-treated rats. Chem Biol Interact; 48 (2), 181–190.

Vidal-Vanaclocha F, Barbera-Guillem E (1985). Fenestration patterns in endothelial cells of rat liver sinusoids. J Ultrastruct Res; 90:115–123.

Vollmer B, Menger MD (2009). The Hepatic Microcirculation: Mechanistic Contributions and therapeutic Targets in Liver Injury and Repair. Physiol Rev; 89: 1269 –1339.

Wake K (1974). Development of vitamin A-rich lipid droplets in multivesicular bodies of rat liver stellate cells. J Cell Biol; 63:683–691.

Weibel ER, Staubli W, Gnagi HR, Hess FA (1969). Correlated morphometric and biochemical studies on the liver cell. J Cell Biol; 42, 68–90.

Williams JA, Hurst SI, Bauman J, Jones BC, Hyland R, Gibbs JP, Obach RS, Ball SE (2003). Reaction phenotyping in drug discovery: moving forward with confidence? Curr Drug Metab; 4(6):527-534.

Wimmer M, Pette D (1979). Microphotometric studies of intra-acinar enzyme distribution in rat liver. Histochemistry; 64 (1):23-33.

Wisse E, De Zanger RB, Charels K, Van Der Smissen P, McCuskey RS (1985). The liver sieve: considerations concerning the structure and function of endothelial fenestrae, the sinusoidal wall and the space of Disse. Hepatology; 5(4):683-692.

Ytrebø LM, Sen S, Rose C, Ten Have GA, Davies NA, Hodges S, Nedredal GI, Romero-Gomez M, Williams R, Revhaug A, Jalan R, Deutz NE (2006). Interorgan ammonia, glutamate, and glutamine trafficking in pigs with acute liverfailure. Am J Physiol Gastrointest Liver Physiol; 291:373–381.

8 Erklärung

Ich erkläre:

Ich habe die vorgelegte Dissertation selbständig, ohne unerlaubte fremde Hilfe und nur mit den Hilfen angefertigt, die ich in der Dissertation angegeben habe. Alle Textstellen, die wörtlich oder sinngemäß aus veröffentlichten oder nicht veröffentlichten Schriften entnommen sind, und alle Angaben, die auf mündlichen Auskünften beruhen, sind als solche kenntlich gemacht. Bei den von mir durchgeführten und in der Dissertation erwähnten Untersuchungen habe ich die Grundsätze guter wissenschaftlicher Praxis, wie sie in der „Satzung der Justus-Liebig-Universität Gießen zur Sicherung guter wissenschaftlicher Praxis“ niedergelegt sind, eingehalten.

Ahmed M. Ghallab

Acknowledgments

I am very grateful to **Prof. Dr. med. Jan G. Hengstler** for giving me the chance to do my PhD at IfADo. Thank you very much for your supervision, personal kindness, guidance and your continuous support. I learn a lot from you.

I would like to express my deepest gratitude to **Prof. Dr. Joachim Geyer** for his guidance and professional supervision throughout all my work.

Everlasting thanks to **Prof. Dr. Abdel latif Shaker Seddek** for his continuous support, guidance and personal kindness.

I wish to express my deepest gratitude to Prof. Dr. Rolf Gebhardt for the continuous fruitful discussion and support.

I am greatly indebted to Prof. Dr. Dirk Drasdo, Dr. Stefan Hoehme, Dr. Dominik Driesch, Dr. Sebastian Henkel and Dr. Lars Kuepfer for the helpful discussion and the great help in mathematical modelling.

I would like to thank Ms. Silke Hankinson for her help and support in all administrative things.

I am very grateful to Dr. Rosemarie Marchan (for her support and English correction), Dr. Patricio Godoy, Dr. Raymond Reif, Dr. Iris von Recklinghausen and Dr. Cristina Cadenas for the continuous helpful discussion and support.

Special thanks to Ms. Georgia Günther for the daily help and encouragement. Really I received a lot of help from you.

I would also like to thank Ms. Brigitte Begher-Tibbe for her help in preparation of the histopathological samples.

Many thanks to Dr. Silvia Seliniski for her great help in statistical analysis

Thank you very much to my colleagues at the Leibniz-Institut für Arbeitsforschung an der TU Dortmund (IfADo): Alshimaa Adawy, Jakia Amin, Regina Stober, Michaela Lesjak, Esmina Mjumjunov, Gisela Campos, Sonia Vossbeck, Dennis Frankenstein, Agata Widera, Katharina Rochlitz and Doreen Werchau. Thank you all for the nice working environment.

My special thanks should go to my dear parents and brothers. Thank you very much for praying, support and encouragement throughout all these years.

My heartfelt thanks are to my wife Reham Hassan Elkashef for her patience, support and encouragement. This work was only possible because of your support.

List of publications

Heise T, Schug M, Storm D, Ellinger-Ziegelbauer H, Ahr HJ, Hellwig B, Rahnenfuhrer J, **Ghallab AM**, Guenther G, Sisnaiske J, Reif R, Godoy P, Mielke H, Gundert-Remy U, Lampen A, Oberemm A, Hengstler JG (2012). In vitro - in vivo correlation of gene expression alterations induced by liver carcinogens. *Curr Med Chem*; 19(11):1721-1730.

Schliess F*, Hoehme S*, Henkel S*, **Ghallab AM***, Driesch D, Böttger J, Guthke R, Pfaff M, Hengstler J, Gebhardt R, Häussinger D, Drasdo D, Zellmer S. Integrated metabolic-spatial-temporal models for prediction of ammonia metabolism during liver damage and regeneration. (in submission *** indicates equal contribution)**

Ghallab AM, Henkel S, Driesch D, Hoehme S, Kuepfer L, Zellmer S, Drasdo D, Gebhardt R, Hengstler JG. Integrated spatial-temporal and metabolic modelling identifies the necessity of alpha-ketoglutarate substitution upon acute liver damage. (In preparation)